Novel synthetic strategies towards atomically precise cationized Au cluster compounds

原子精度カチオン性金クラスター化合物の新規合成手法の確立

Kunihiro Narita

Graduate School of Engineering

Hokkaido University

March 2022

Novel synthetic strategies towards atomically precise cationized Au cluster compounds

原子精度カチオン性金クラスター化合物の新規合成手法の確立

Kunihiro Narita

Laboratory of Novel Hybrid Materials Engineering,

Division of Materials Science and Engineering,

Graduate School of Engineering, Hokkaido University

Kita 13 Nishi 8, Kita-ku, Sapporo, Hokkaido 060-8628, Japan.

A dissertation submitted to the Graduate School of Engineering of Hokkaido University in partial fulfilment of the requirements for the degree of Doctor of Philosophy in Materials Science and Engineering

March 2022

CONTENTS

LIST OF ABBREVIATIONS

^{1}H NMR	proton nuclear magnetic resonance
4-PyET	4-pyridineethanethiol
B.C.	before Christ
BF	bright field
BT	butanethiolate
DCM	dichloromethane
DMF	*N*,*N*-dimethylformamide
DMSO	dimethyl sulfoxide
ESI	electrospray ionization
HAADF	high-angle annular dark field
HOMO	highest occupied molecular orbital
HPLC	high-performance liquid chromatography
HSTEA	*N*,*N*,*N*-triethyl(11-undecenylmercapto)ammonium chloride
HT	hexanethiolate
LA-ICP	laser ablation inductively coupled plasma
LEIST	ligand-exchange-induced size/structure transformation
LUMO	lowest unoccupied molecular orbital
MALDI	matrix assisted laser desorption ionization
Me_2SO_4	dimethyl sulfate
Me_3OBF_4	trimethyl oxonium tetrafluoroborate
MeI	iodomethane

MeOH	methanol
MHA	6-mercaptohexanoic acid
MS	mass spectrometry
MUTA	(11-Mercaptoundecyl)-*N*,*N*,*N*-trimethylammonium
NPs	nanoparticles
PAGE	poly acrylamide gel electrophoresis
p-BBT	p-bromobenzenethiol
PET	phenylethanethiol
Ph	phenyl group
p-MBA	p-mercaptobenzoic acid
Py	pyridyl group
QQQ	triple quadripole
ROS	reactive oxygen species
SC12	dodecanethiol
SDS	sodium dodecylsulfate
SG	glutathione
SR	thiolate ligand
SR^+	cationic thiolate ligand
STEM	scanning transmission electron microscope
TBBT	4-tert-butylbenzenethiolate
TC	2-mercaptoethyl-N,N,N-trimethylammonium
TEM	transmission electron microscope
TfOMe	methyl trifluoromethanesulfonate

TGA	thermogravimetric analysis
THF	tetrahydrofuran
TLC	thin layer chromatography
TOAB	tetraoctylammonium bromide
TOF	time of flight
UV-Vis	ultraviolet-visible

Chapter 1

General Introduction

1.1 History of Au clusters with atomic precision

Gold (Au) clusters have been a subject of major interest in nanoscience and nanotechnology, because of their unique optical features, electrochemical behaviors, and catalytic properties, due to the quantum confinement effects,[1-4] and they therefore are well explored, reaching across many areas such as chemistry, physics, and biology.[5-7] The ultra-small Au clusters with a size smaller than 2 nm demonstrate molecular-like electronic transitions between HOMO-LUMO energy levels, according to their discrete electronic structure.[1,2,4,8,9] The Au clusters are composed of fixed numbers of Au atoms and SR ligands, and their numbers are determined by the number of free electron. When the number of free electron, calculated from the following equation, is 2, 8, 18, 34, 58, 92, 138, and so on, the electronic structure becomes closed shell and the cluster obtains extraordinary stability.[10-13] The determined compositions and well-defined molecular structures provide ideal models to establish the structure/function relationships for fundamental study. [8,9,14-16]

$$n = N - M - z$$

(n is the number of free electrons, N is the number of Au atoms, M is the number of SR ligands, and z is the number of charges)

Gold (Au) is one of the most important elements in the human civilization. The history of the use of Au dates far back to the 5th millennium B.C. when the Tutankhamun's

golden mask was made in Egypt (Figure 1.1). The modern scientific research on Au nanoparticles, non-bulk form of Au, was started in the 1800s. In 1857, Faraday reported the formation of deep red solutions of colloidal Au by reduction of an aqueous solution of chloroaurate ($AuCl_4^-$).[17] After more than 100 years of scientific researches on metal nanoparticles, nanoscience and nanotechnology have achieved excellent control of particle size, shape, and properties in many cases.[18-21] In the long time history of the researches on metal nanoparticles, Au is the most studied metal element because of its nontoxic property and high stability.

Figure 1.1 Tutankhamun's golden mask (source: https://en.wikipedia.org/wiki/Tutankhamun)

Although the synthesis technology of metal nanoparticles have developed, the nanoparticles are not atomically precise (the number of constituent atoms are unknown), and they are characterized and discussed based on the particle size. Such drawbacks left many unclear issues, such as the poorly understood in terms of surface layer (including organic stabilizers and the inorganic-organic interface), their structure-property

relationships, the mechanisms for shape-controlled synthesis of nanoparticles, and the evolution of surface and core structures with particle size.[9,22-24] To address all of these fundamentally critical issues, nanoscience and nanotechnology are motivated to pursue atomically precise ultra-small nanoparticles with a size smaller than 2 nm, namely nanoclusters (or clusters).

The synthesis of nanoparticles with a size smaller than 2 nm (its exact composition is still unknown) started to be reported in the 1990s.[25-29] In 1994, Brust *et al.* reported the first report using thiols as surface capping agent for stabilizing Au nanoparticles (so-called Brust-Schiffrin method).[25] The Brust-Schiffrin method involves two steps; (i) the phase transfer of gold salt by using a phase transfer agent (tetraoctyl ammonium bromide, TOAB), and (ii) the reduction of the formed Au(I)–SR precursors by $NaBH_4$ to form nanoparticles. This gold (Au)-thiolate (SR) system will be a model system of the research because of the extraordinary robustness, while there are many types of metal nanoparticles capped by different ligands. Since then, many researchers intensively investigated toward synthesizing atomically precise Au cluster with single composition and controlling its particle size, based on the early works by Whetten,[30] Murray,[31] and Tsukuda[32] groups. From around this time, such nano-compounds started to be called "cluster" in terms of accumulation of several atoms through bottom-up approach.

In 2007, for the first time, Jin group developed a novel synthesis method for synthesizing Au_{25} clusters with atomic precision with high-purity and high-yield,[33] without further isolation techniques such as polyacrylamide gel electrophoresis (PAGE)[32] and high-performance liquid chromatography (HPLC).[34] Based on this research, many works have been reported on the size-controlled synthesis Au clusters with high-purity and high-yield, and revealed a series of magic-numbered clusters which exhibit

extraordinary stabilities, including $Au_{25}(SR)_{18}$, $Au_{38}(SR)_{24}$, $Au_{44}(SR)_{28}$, $Au_{68}(SR)_{34}$, $Au_{102}(SR)_{44}$, $Au_{144}(SR)_{60}$, and so on, where SR represents surface thiolate ligands. Furthermore, their total structures including not only metal core structure, but also the surface structure (the arrangements of ligands and the bonding between the ligands and the metal core), have been investigated.

In 2007, among the various sizes of Au clusters, the structure of the Au_{102}(p-MBA)$_{44}$ clusters (p-MBA: p-mercaptobenzoic acid) was solved by Kornberg group, for the first time (Figure 1.2).[35] Following the elucidation, in 2008, Jin group reported the structure of the $Au_{25}(PET)_{18}$ clusters (PET: phenylethanethiol), which is the hottest and most studied magic number in the series of Au clusters, because of its easy preparation, high stability, and easy utilization for application (Figure 1.3).[36] The structure of $Au_{25}(SR)_{18}$ exhibits an icosahedral Au_{13} kernel, which is further wrapped by six $Au_2(SR)_3$ staple motifs. To date, more than 40 species of atomically precise Au clusters such as Au_{18}, Au_{24}, Au_{25}, Au_{28}, Au_{34}, Au_{36}, Au_{38}, Au_{40}, Au_{42}, Au_{49}, Au_{60}, Au_{92}, Au_{130}, Au_{133}, Au_{144}, Au_{187}, Au_{246}, Au_{279}, Au_{329}, and so on, have been synthesized, and their structures have been revealed (Figure 1.4).[1,37-55] Furthermore, some researches revealed that the transition from bulk-like (plasmonic) to molecule-like behavior happens between Au_{187} and Au_{144} (Figure 1.5).[40,56]

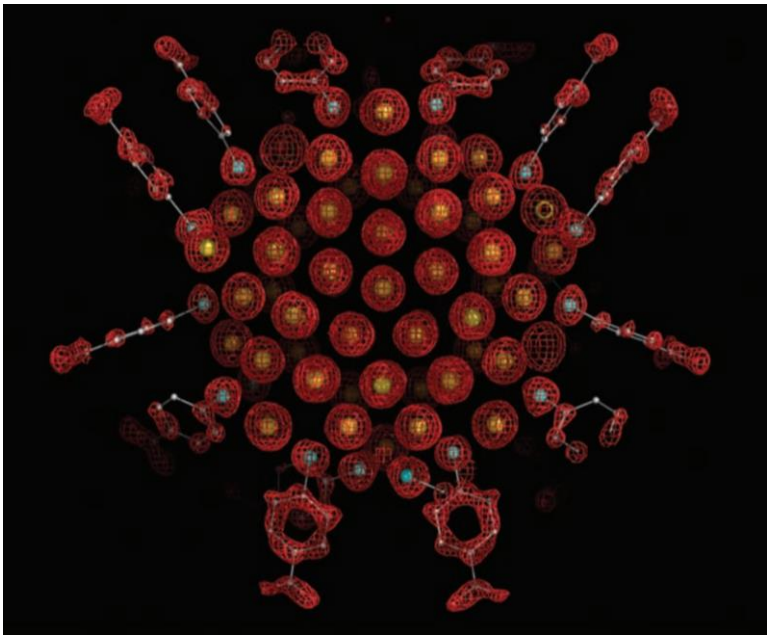

Figure 1.2 Crystal structure of the $Au_{102}(p\text{-}MBA)_{44}$ clusters. Reproduced with permission from ref. (35). Copyright 2018 American Association for the Advancement of Science.

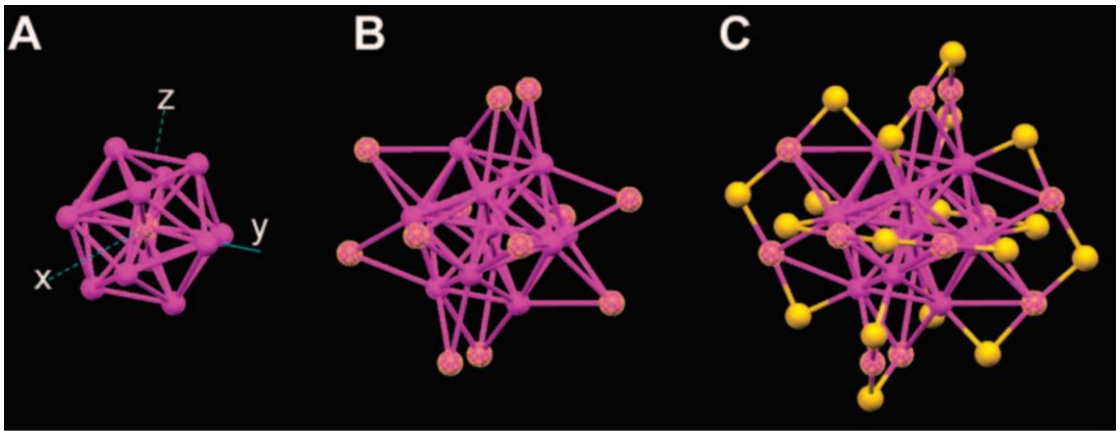

Figure 1.3 Crystal structure of the $Au_{25}(PET)_{18}$ clusters. Reproduced with permission from ref. (36). Copyright 2008 American chemical society.

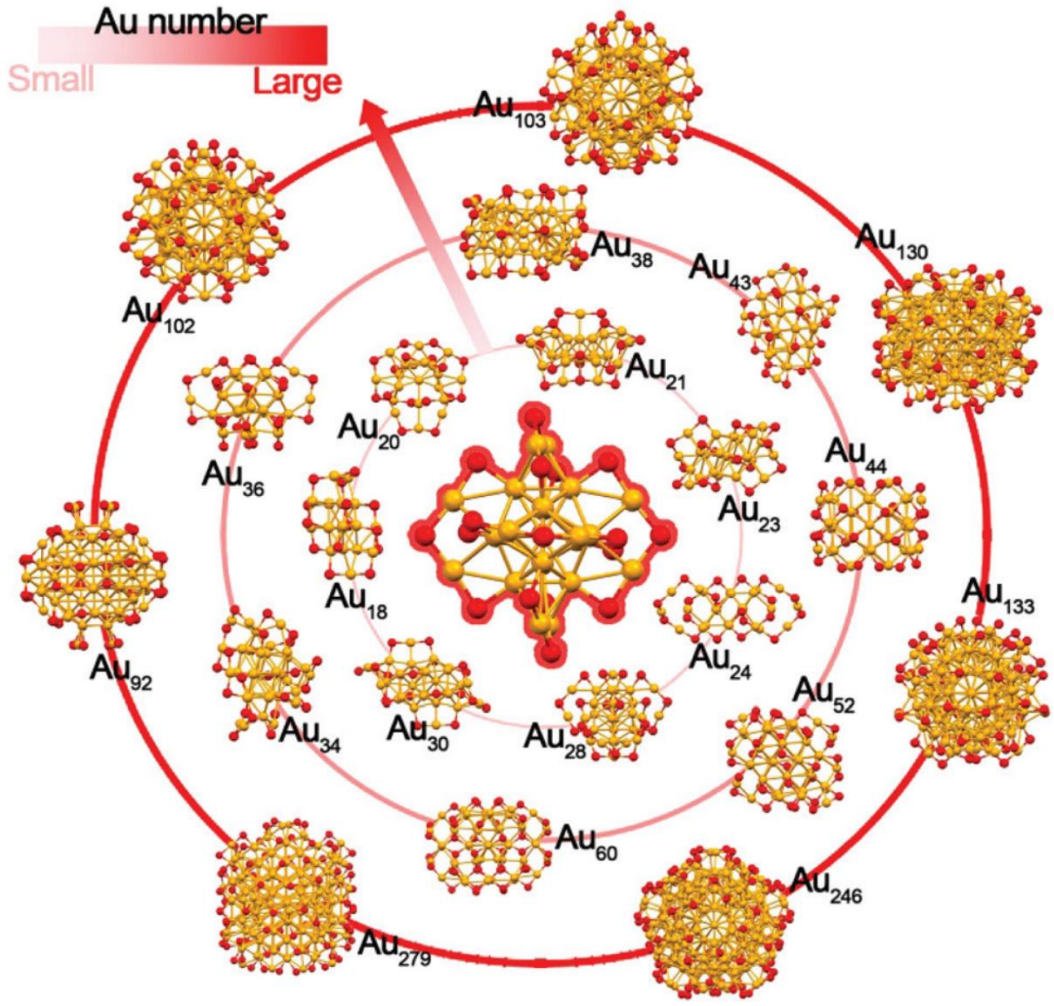

Figure 1.4 Crystal structure of $Au_m(SR)_n$ clusters. Reproduced with permission from ref. (37). Copyright 2018 Royal Society of Chemistry.

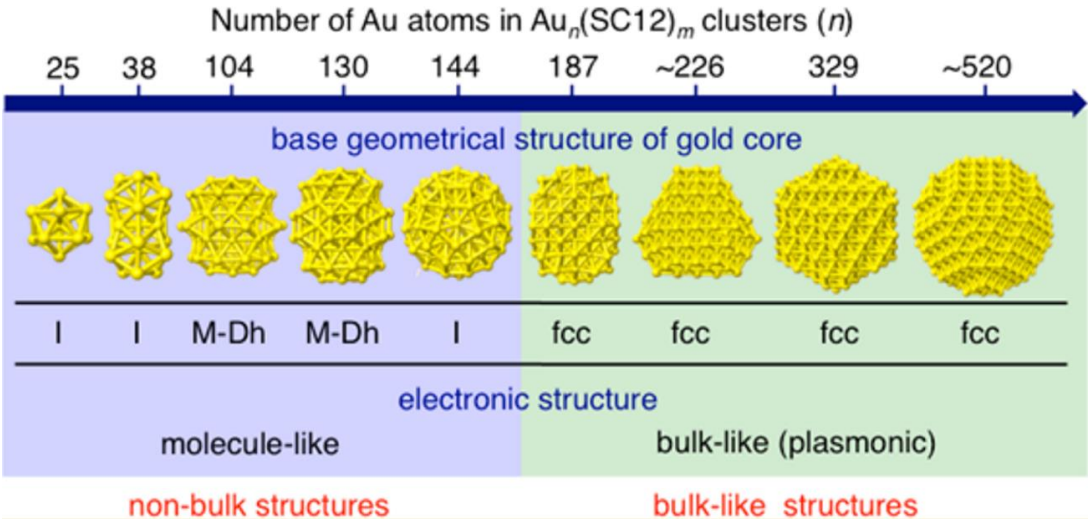

Figure 1.5 The boundary between bulk-like and molecule-like size. Reproduced with permission from ref. (56). Copyright 2014 American Chemical Society.

As described above, a series of Au clusters with various metal core sizes have been prepared through the long time diligent research. The Au clusters are further diversified by using different types of thiolate ligands. The surface ligands not only affect the magic size and structures of the clusters, but also determine the molecular-like characteristics of clusters.[15,57-64] Thus, up-to-date, the Au clusters with various types of surface SR ligands have been synthesized, and the ligands used are summarized in Table 1.1.

Table 1.1 The summary of SR ligands used for the syntheses of atomically precise Au clusters.

	Thiolate ligands (SR)
Neutral	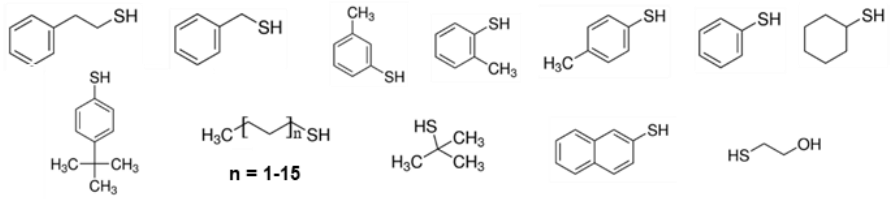
Anionic (or acidic)	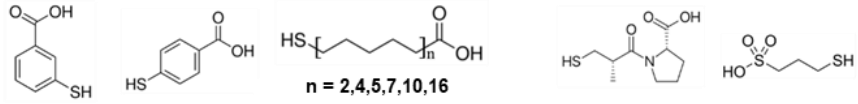
Cationic (or basic)	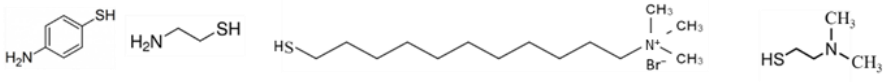

1.2 Synthesis method of Au clusters

To date, major protocols for the preparation of atomically precise Au clusters with various thiolate ligands have been categorized into size-focusing method and ligand-exchange method.

1.2.1 Size-focusing method

The fundamental principle of the size-focusing method lies in the essential stabilities of each $Au_m(SR)_n$ cluster, and their different stabilities lead to the survival of the most robust one, reminiscent of natural selection "survival of the fittest". The key for size-focusing is making a comfortable environment for only one size of the Au clusters, which can simultaneously eliminate other Au cluster species. The size-focusing method is largely relied on the kinetic control, and the important parameters include solvent, reducing agent, reactant ratio, temperature, and so on.

In 2007, Jin group pioneered the size-focusing method on the basis of kinetically controlled strategy (Scheme 1.1), and succeeded in synthesizing atomically pure Au_{25} clusters with high-purity and high-yield.[33] The procedure had two main modifications from the previous Brust-Schiffrin method. (i) During the addition of $HSCH_2CH_2Ph$ (PET) into Au(III)-TOA (TOA = tetraoctylammonium, toluene solution), a very low stirring speed ~30 rpm and a temperature of 0°C (ice bath) were modified for the formation of Au(I)-SR precursors. (ii) The freshly-made $NaBH_4$ aq. solution was immediately injected into above solution under the vigorous stirring (~1100 rpm). These two changes are critical for the formation of monodisperse Au(I)-SR precursors as well as the final $Au_{25}(PET)_{18}$ clusters. The UV-Vis absorption spectrum of the purified product (Figure 1.6) exhibited an obvious peak at 670 nm and two shoulder peaks at 400 and 450 nm,

which correspond well to the characteristic peaks of Au_{25} clusters. This was the first report that $Au_{25}(PET)_{18}$ clusters could be synthesized with high-purity and high-yield (~40%, based on Au atoms).

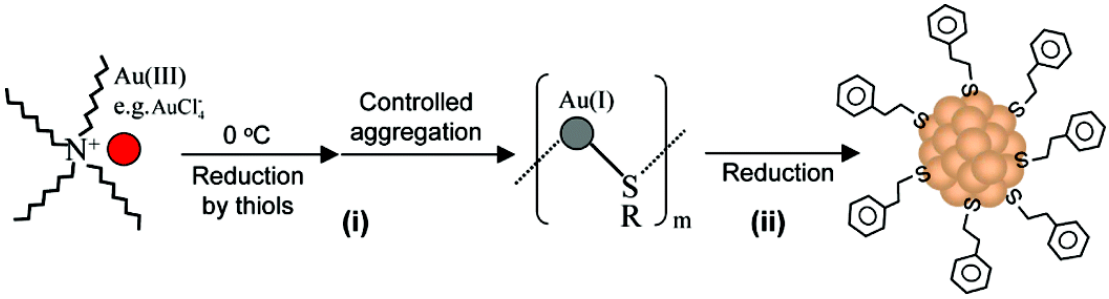

Scheme 1.1 Synthetic scheme of the $Au_{25}(PET)_{18}$ clusters by the kinetically controlled strategy. Reproduced with permission from ref. (33). Copyright 2007 American Chemical Society.

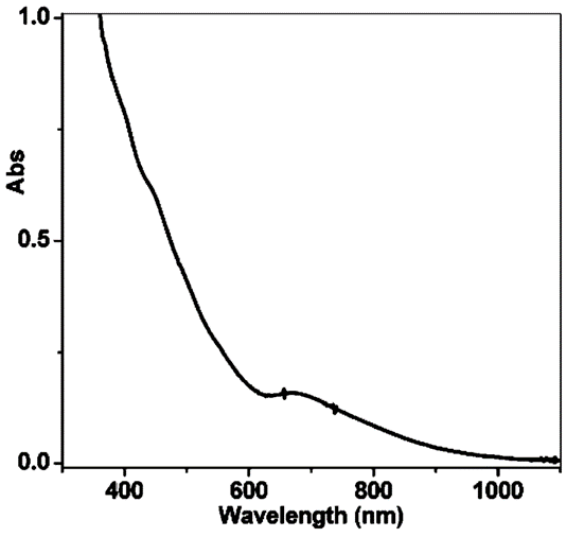

Figure 1.6 UV-Vis absorption spectrum of the obtained $Au_{25}(PET)_{18}$ clusters. Reproduced with permission from ref. (33). Copyright 2007 American Chemical Society.

While the first successful size-focusing method by Jin group was a two-phase liquid–liquid system which includes the phase transfer step, this procedure was further updated to a one-phase system by Murray group in 2010 (Scheme 1.2).[65] In this method, $HAuCl_4$ and TOAB (tetraoctylammonium bromide) were added to the tetrahydrofuran (THF) solvent and stirred for 15 min, followed by the addition of PET at room temperature. The solution was stirred for overnight, and it would become completely transparent. $NaBH_4$ dissolved in ice-cold water and then stirred for 1 hour under 0°C (ice bath). The $NaBH_4$ aq. was rapidly added under the vigorous stirring. The reaction was stirred quietly for more than 48 h, and then the obtained solution was purified to get the pure $[TOA]^+[Au_{25}(PET)_{18}]^-$. The UV-Vis absorption spectrum of the obtained Au cluster (Figure 1.7(A)) showed the characteristic peaks of $Au_{25}(PET)_{18}$ at ~670, 450, and 400 nm regardless of core charge (0 or 1). The MALDI-MS detected only one peak, corresponding to the $Au_{25}(PET)_{18}$ clusters (Figure 1.7 (B)). The synthetic yield could be achieved at ~52% based on Au atom. They also synthesized several other species of Au_{25} clusters capped by different thiols (i.e., $HS(CH_2)_5CH_3$, $HSCH_2CH(CH_3)_2$, and $HS(CH_2)_{11}CH_3$) using the same procedure.

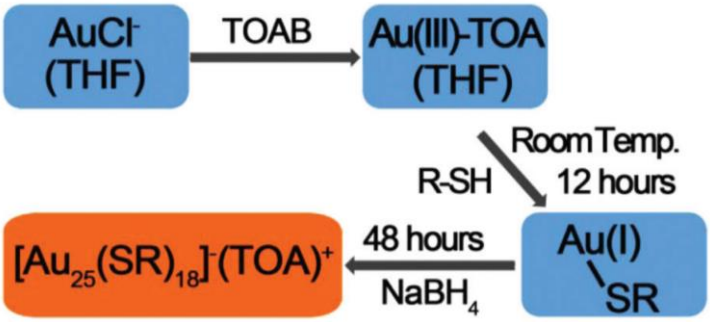

Scheme 1.2 Synthetic scheme of the $Au_{25}(PET)_{18}$ clusters by the one-phase synthetic method. Reproduced with permission from ref. (65). Copyright 2018 Royal Society of

Chemistry.

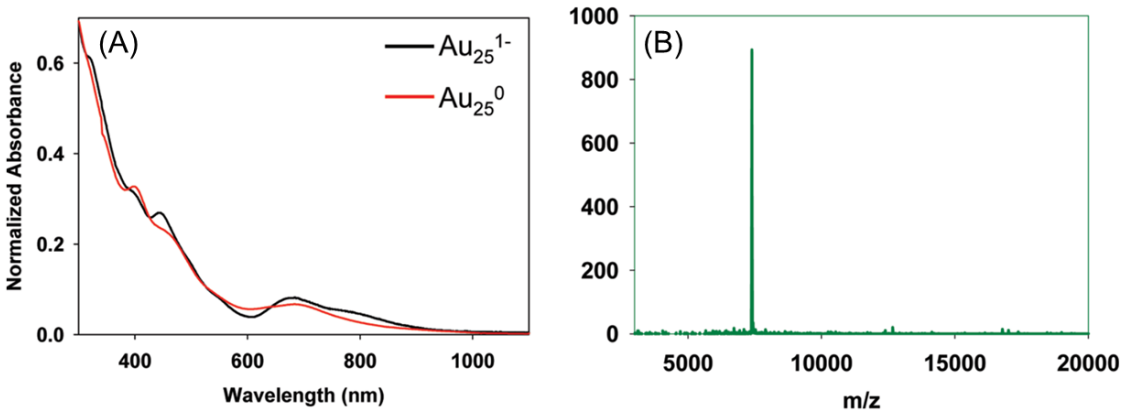

Figure 1.7 (A) UV-Vis absorption spectrum and (B) Matrix-assisted laser desorption ionization (MALDI)-MS of the obtained $Au_{25}(PET)_{18}$ clusters. Reproduced with permission from ref. (65). Copyright 2018 Royal Society of Chemistry.

Besides these two famous examples, recently, Xie group developed a NaOH-mediated $NaBH_4$ reduction method for $Au_{25}(SR)_{18}$ synthesis (Scheme 1.3).[66] In this method, instead of toluene or THF, water was used as a solvent, and NaOH was added to tune the formation kinetics by decreasing the reducing power of $NaBH_4$ and enhancing the etching capability of thiols. Thanks to the effect of NaOH, the etching time shortened to less than 3h.

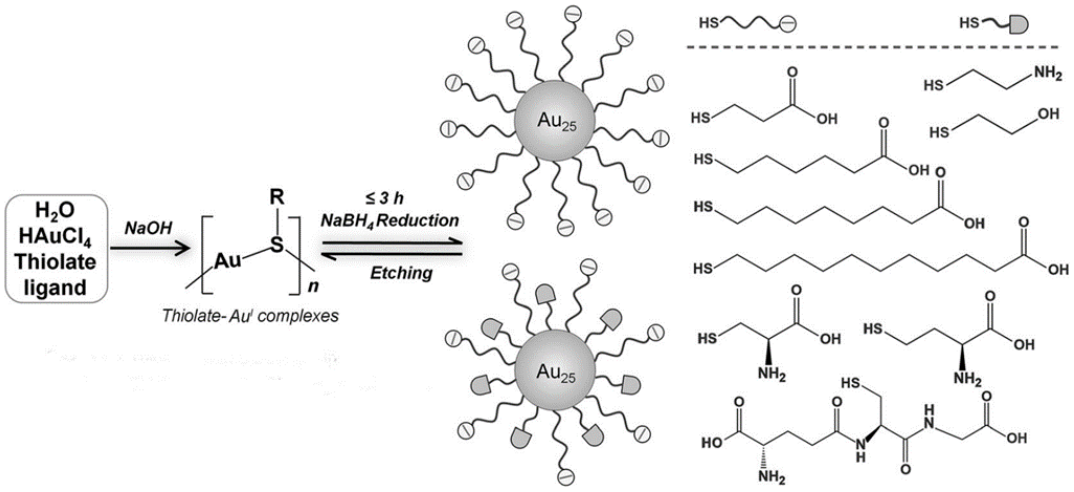

Scheme 1.3 Synthetic scheme of the $Au_{25}(SR)_{18}$ clusters by the NaOH-mediated $NaBH_4$ reduction method. Reproduced with permission from ref. (66). Copyright 2014 Wiley-VCH.

In the past decade, the size-focusing method made a great progress toward the synthesis of atomically pure Au clusters, and various Au cluster species, such as $Au_{38}(SR)_{24}$,[67] $Au_{64}(SR)_{32}$,[68] $Au_{99}(SR)_{42}$,[69] and $Au_{144}(SR)_{60}$,[70] and so on, were successfully synthesized with atomic precision.

1.2.2 Ligand-exchange method

Ligand-exchange method involves the synthesis of Au clusters, followed by the replacement of their initial ligands with the desired ligands. In addition to this simple replacement, ligand-exchange method can produce the Au clusters with bi- (or tri-) thiolate ligands, and the substituent R-group affects the sizes and structures of clusters, which provides an opportunity to create the new Au clusters (which have not yet obtained by the size-focusing method) through a ligand-exchange-induced size/structure transformation (LEIST) process.[33]

In 2007, the Murray group[71,72] reported the ligand-exchange process on the $Au_{25}(PET)_{18}$ clusters with several different thiolate ligands, including −SPh, $-SC_6H_{13}$, and −SPhCOOH ligands. The results suggest that the initial PET ligands were partially exchanged, and thus the bi-thiolate ligands-protected Au_{25} clusters, $Au_{25}(PET)_{18-x}(SR')_x$ (SR′ represents the incoming thiolate ligand), were produced. Moreover, the $-SC_6H_{13}$ ligands can substitute all initial PET ligands on the surface of $Au_{25}(PET)_{18}$ clusters, and the mono-thiolate-protected $Au_{25}(SC_6H_{13})_{18}$ clusters were produced (Figure 1.8 (A)). In 2010, Murray group also ligand-exchanged the $Au_{25}(PET)_{18}$ with toluene-3,4-dithiol ($CH_3Ph(SH)_2$), and the ESI-QQQ mass spectrum revealed the formation of tri-thiolate-protected $Au_{25}(SR)_{18}$ clusters, $Au_{25}(CH_3Ph(S-)_2)_x(CH_3Ph(SH)(S-))_y(PET)_{18-2x-y}$ clusters (Figure 1.8 (B)).[73]

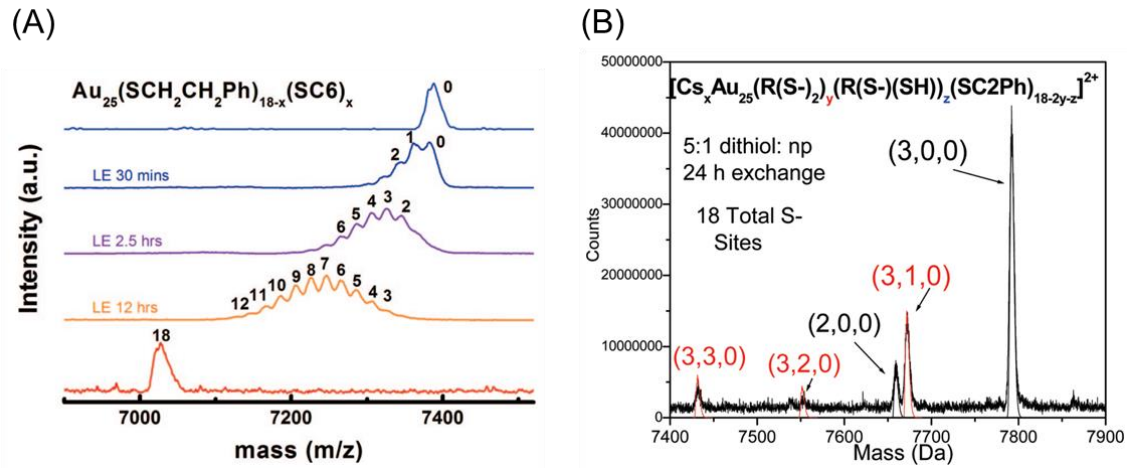

Figure 1.8 (A) MALDI-TOF-MS to detect the number of exchanged $-SC_6H_{13}$ ligands on the surface of $Au_{25}(PET)_{18}$ clusters. Reproduced with permission from ref. (72). Copyright 2008 American Chemical Society. (B) ESI-QQQ-MS to detect the number of exchanged ligands including monothiol and dithiol. Reproduced with permission from ref. (73) Copyright 2010 American Chemical Society.

The aforementioned works indicate that the surface ligands of Au_{25} clusters were difficult to be completely exchanged by the incoming ligand, and each ligand at the different sites should hold different activity in exchange reaction. Indeed, Ackerson group successfully prepared the crystal of $Au_{25}(SC_6H_{12})_{16}(p\text{-}BBT)_2$ by ligand-exchange reaction of $Au_{25}(SC_6H_{12})_{18}$ with p-bromobenzenethiol (p-BBT),[74] and their X-ray crystallography results showed that the surface ligand, that bond to the most solvent -exposed Au atom, is easier to be exchanged by incoming thiols (Figure 1.9).

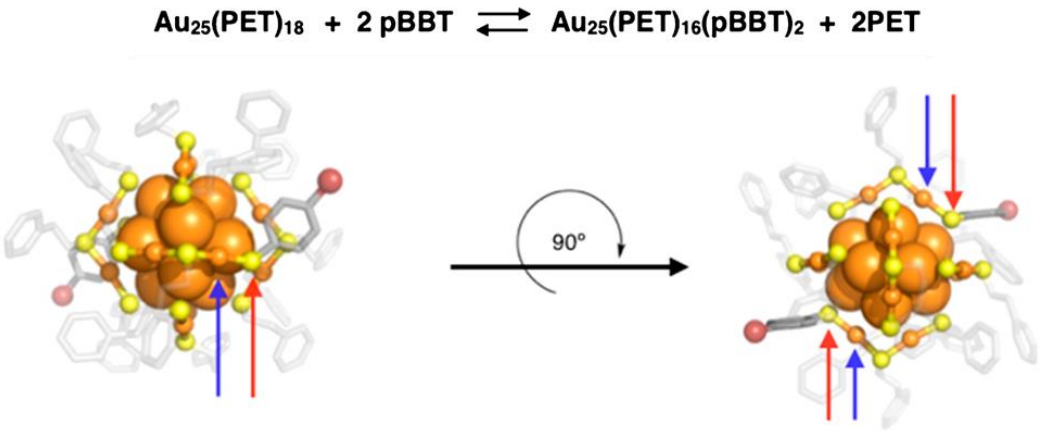

Figure 1.9 Crystal structure of the $Au_{25}(PET)_{16}$(p-BBT)$_2$ clusters. Red arrows point to the S atoms of the p-BBT ligands. Reproduced with permission from ref. (74). Copyright 2014 American Chemical Society.

In the above conventional ligand-exchange reactions, they were typically conducted with low amount ratios of incoming thiol ligands to the surface ligands of clusters at room temperature. Jin group reported that when the ligand-exchange reaction were carried out under the harsh conditions (i.e., a large excess of incoming thiol and high temperature), the ligand exchange process not only lead to the complete exchange of the surface ligands, but also generate a new kind of Au clusters with different size or structure with high-purity and high-yield.[33] They reported four notable examples of the transformations of $Au_{25}(PET)_{18}$ to $Au_{28}(TBBT)_{20}$ or $Au_{20}(TBBT)_{16}$,[42,75] $Au_{38}(PET)_{24}$ to $Au_{36}(TBBT)_{24}$,[76] and $Au_{144}(PET)_{60}$ to $Au_{133}(TBBT)_{52}$,[77] where TBBT is 4-tert-butylbenzenethiolate. For instant, the initial $Au_{38}(PET)_{24}$ clusters were transformed into $Au_{36}(PET)_{24}$, by the ligand-exchange reaction with an excess amount of TBBT at 80 °C. The yield of $Au_{36}(TBBT)_{24}$ clusters were unexpectedly high (90%, based on Au atom) and with high purity (Figure 1.10).[76]

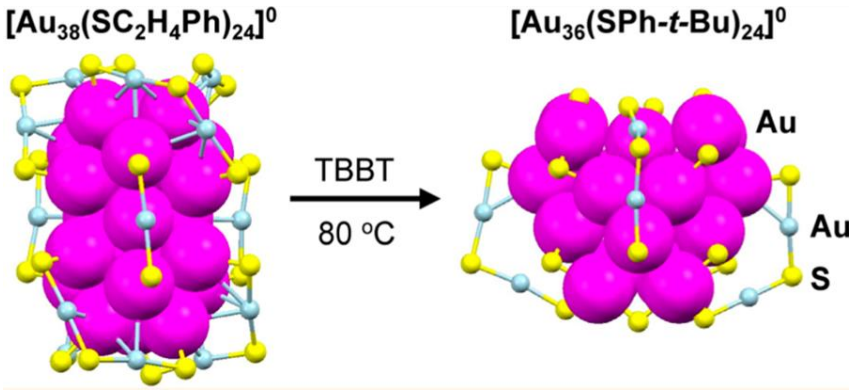

Figure 1.10 Conversion of $Au_{38}(PET)_{24}$ to $Au_{36}(TBBT)_{24}$ clusters. Reproduced with permission from ref. (76). Copyright 2013 American Chemical Society.

The ligand-exchange method not only exchanges the initial surface ligands of Au clusters with the desirable ligands, but also creates a new Au clusters, which could not be obtained by the simple size-focusing method, through the LEIST process. It is an important strategy for synthesizing Au clusters along with the size-focusing method.

1.2.3 Isolation method

Although it is the best that the aimed Au cluster (single size and single composition) is produced by size focusing method or ligand-exchange method one time, mixture of Au clusters including various sized species are often obtained. At such times, isolation method is used to obtain the single composition of the Au clusters. Polyacrylamide gel electrophoresis (PAGE), high performance liquid chromatography (HPLC), and thin layer chromatography (TLC) are the most common method to separate Au clusters.

PAGE was the first isolation method adopted for Au clusters, and started to be used in the early 2000s.[78-80] In 2004, Tsukuda group used PAGE to separate different sized Au clusters.[80] They synthesized the mixture of Au clusters including $Au_{18}(SG)_{11}$, $Au_{21}(SG)_{12}$, $Au_{25\pm1}(SG)_{14\pm1}$,$Au_{28}(SG)_{16}$, $Au_{32}(SG)_{18}$, and $Au_{39}(SG)_{23}$ (SG = glutathione), and successfully isolated into each size of the clusters using PAGE. The Au clusters showed different electrophoretic mobilities, depending on their sizes, molecular waits, and structures in PAGE. The collected gels and ESI-MS characterization are shown in Figure 1.11.

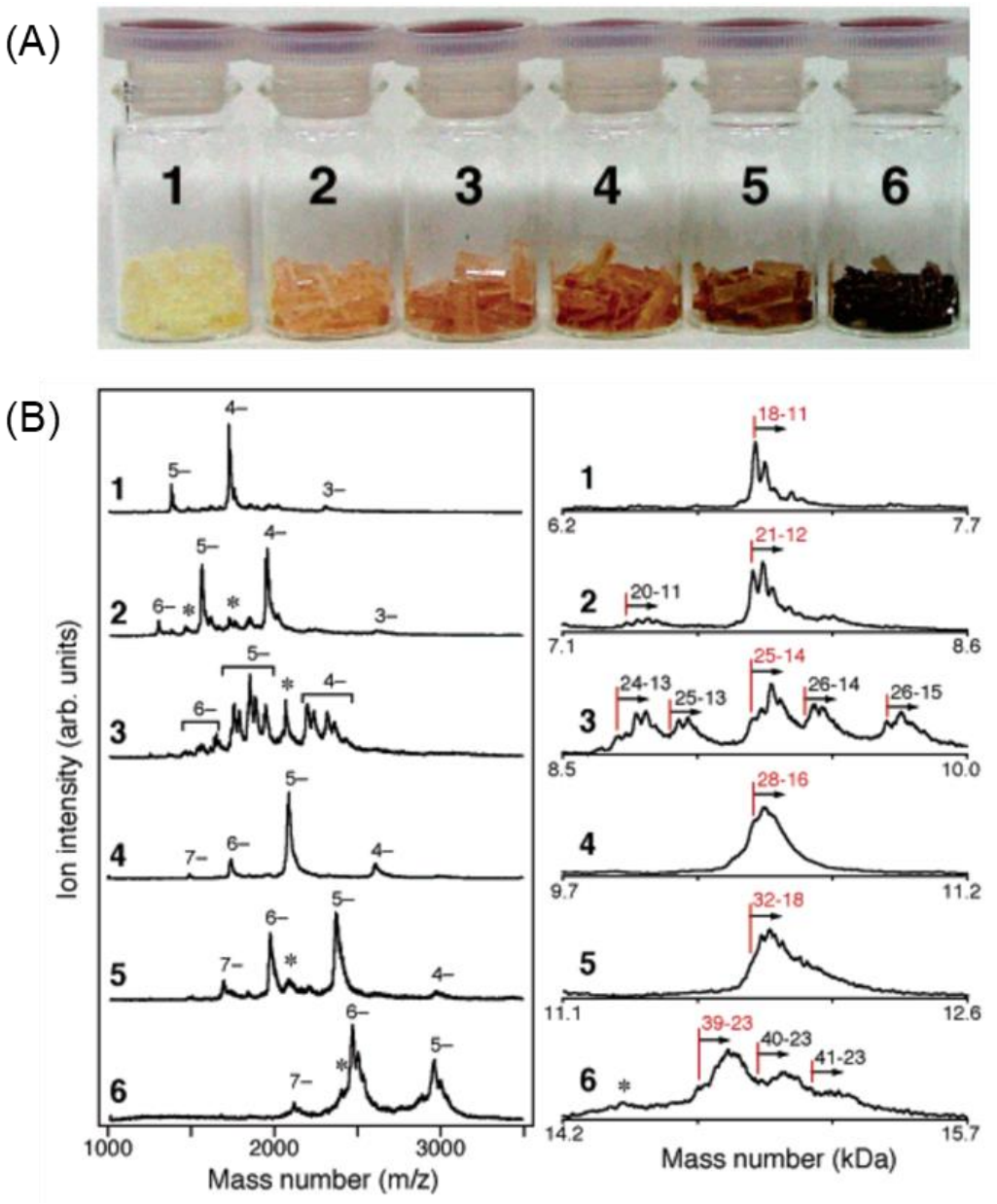

Figure 1.11 (A) Appearance of the gels containing fractionated clusters 1-6 by PAGE, and (B) ESI-MS of the clusters 1-6. The red bars indicate the molecular weights of $Au_n(SG)_m$ clusters with n-m values designated on the envelopes. Reproduced with permission from ref. (80). Copyright 2004 American Chemical Society.

In the 2010s, HPLC and TLC also started to be used. In 2014, Negishi group reported the separation of Au clusters by HPLC. The mixture of various size of the Au clusters including $Au_{38}(SC12)_{24}$, $Au_{104}(SC12)_{45}$, $Au_{144}(SC12)_{60}$, $Au_{187}(SC12)_{68}$, $Au_{226}(SC12)_{76}$, $Au_{253}(SC12)_{90}$, $Au_{329}(SC12)_{84}$, $Au_{356}(SC12)_{112}$, $Au_{520}(SC12)_{130}$ (SC12 = dodecanethiol) were prepared.[56] The prepared Au clusters interacted differently with the adsorbent material in the HPLC column, and were separated into each size of the Au clusters. The separated each clusters were characterized by ESI-MS (Figure 1.12). In 2014, Ghosh *et al.* reported the separation of the Au clusters using conventional TLC.[81] They successfully separated not only the 2 kinds of Au_{25} clusters $Au_{25}(BT)_{18}$ (BT = butanethiolate) and $Au_{25}(PET)_{18}$ (PET = phenylethanethiolate), but also 2 different sized Au clusters $Au_{25}(PET)_{18}$ and $Au_{144}(PET)_{60}$. UV-Vis absorption spectra and MALDI-MS of the separated Au clusters are shown in Figure 1.13.

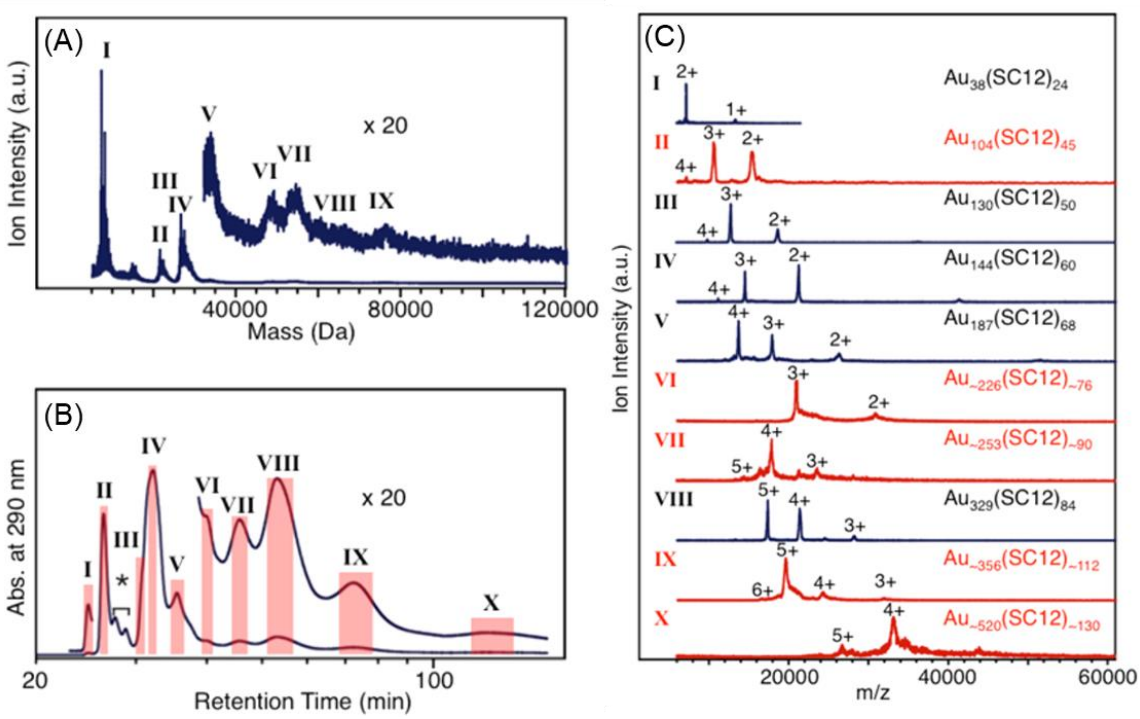

Figure 1.12 (A) Positive-mode LDI MS, (B) reverse-phase HPLC chromatogram of a crude sample of $Au_n(SC12)_m$, and (C) positive-mode ESI-MS of the fractions I−X. Reproduced with permission from ref. (56). Copyright 2014 American Chemical Society.

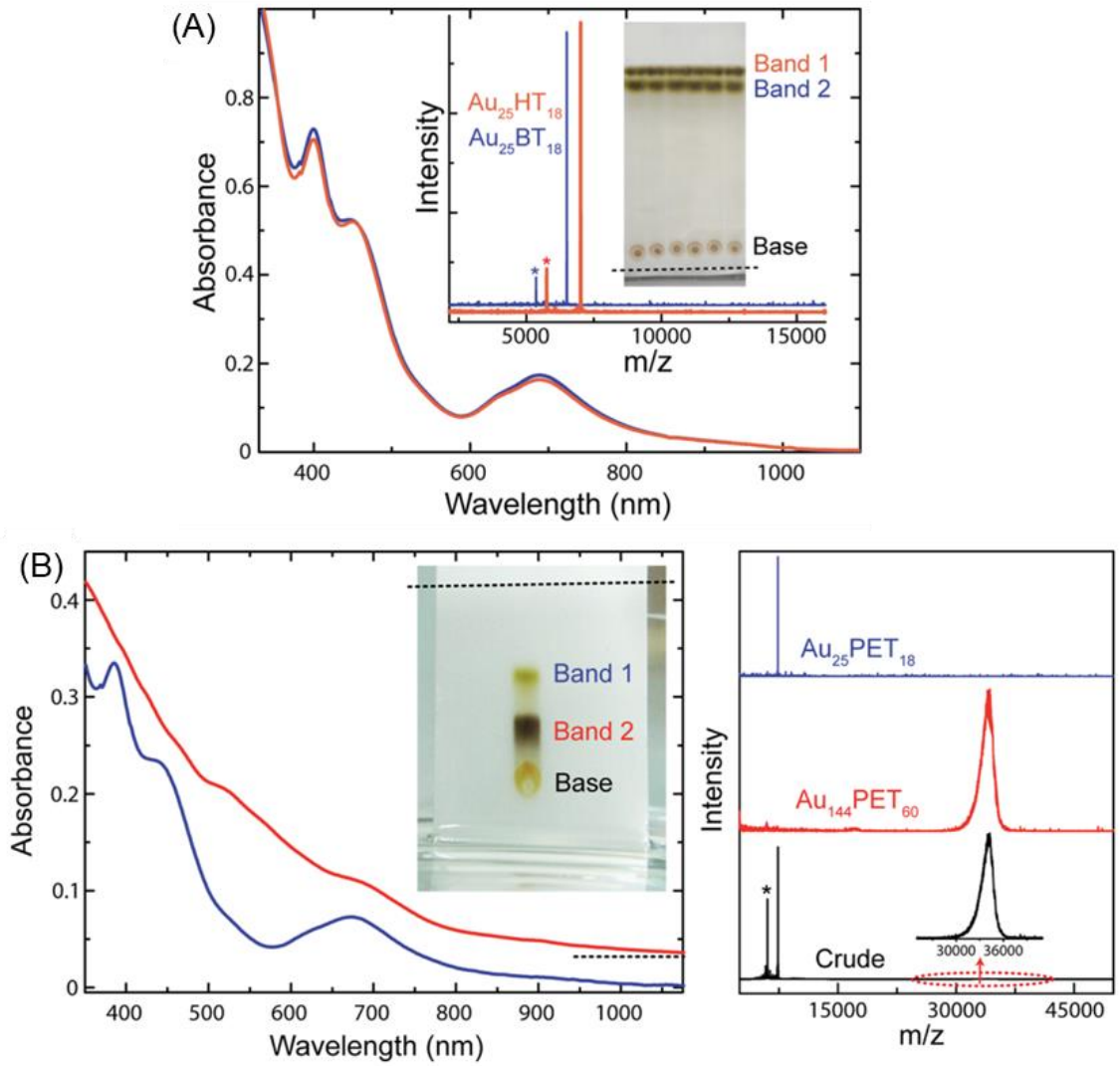

Figure 1.13 (A) The separation of $Au_{25}(HT)_{18}$ and $Au_{25}(BT)_{18}$ by TLC, and (B) The separation of $Au_{25}(PET)_{18}$ and $Au_{144}(PET)_{60}$ by TLC. Reproduced with permission from ref. (81). Copyright 2014 American Chemical Society.

1.3 Towards a synthesis of fully cationized Au clusters

To date, the Au clusters with various types of surface thiolate ligands have been synthesized (Table 1.1). However, the thiolate ligands used for their synthesis were neutral and anionic, and cationic-ligand-protected Au clusters have never been synthesized. In the 2000s, many researchers pursued and made extensive efforts towards the successful synthesis of Au clusters capped by cationic thiols with atomic precision, because the cationized Au clusters widen the application fields especially in bioimaging and sensing applications.

In the early 2000s, the cationized Au nanoparticles (larger than 2 nm) started to be synthesized.[82-85] In 2000, Murray group reported the first successful synthesis of the fully cationized metal nanoparticles, which are soluble in water.[82] They synthesized Au, Ag, and Pd nanoparticles using the chemical reduction method in the same procedure. The metal salt ($HAuCl_4$, $AgNO_3$, or K_2PdCl_4) and the cationic ligand (*N*,*N*-trimethyl (undecylmercapto) ammonium) were mixed in water, followed by addition of $NaBH_4$. After the solution was stirred for 1 h, Au nanoparticles (4.4 ± 1.6 nm), Ag nanoparticles (4.8 ± 2.1 nm), and Pd nanoparticles (2.7 ± 1.1 nm) were obtained, respectively (Figure 1.14). This was the first report of the successful synthesis of metal nanoparticles using cationic thiols as a capping agent.

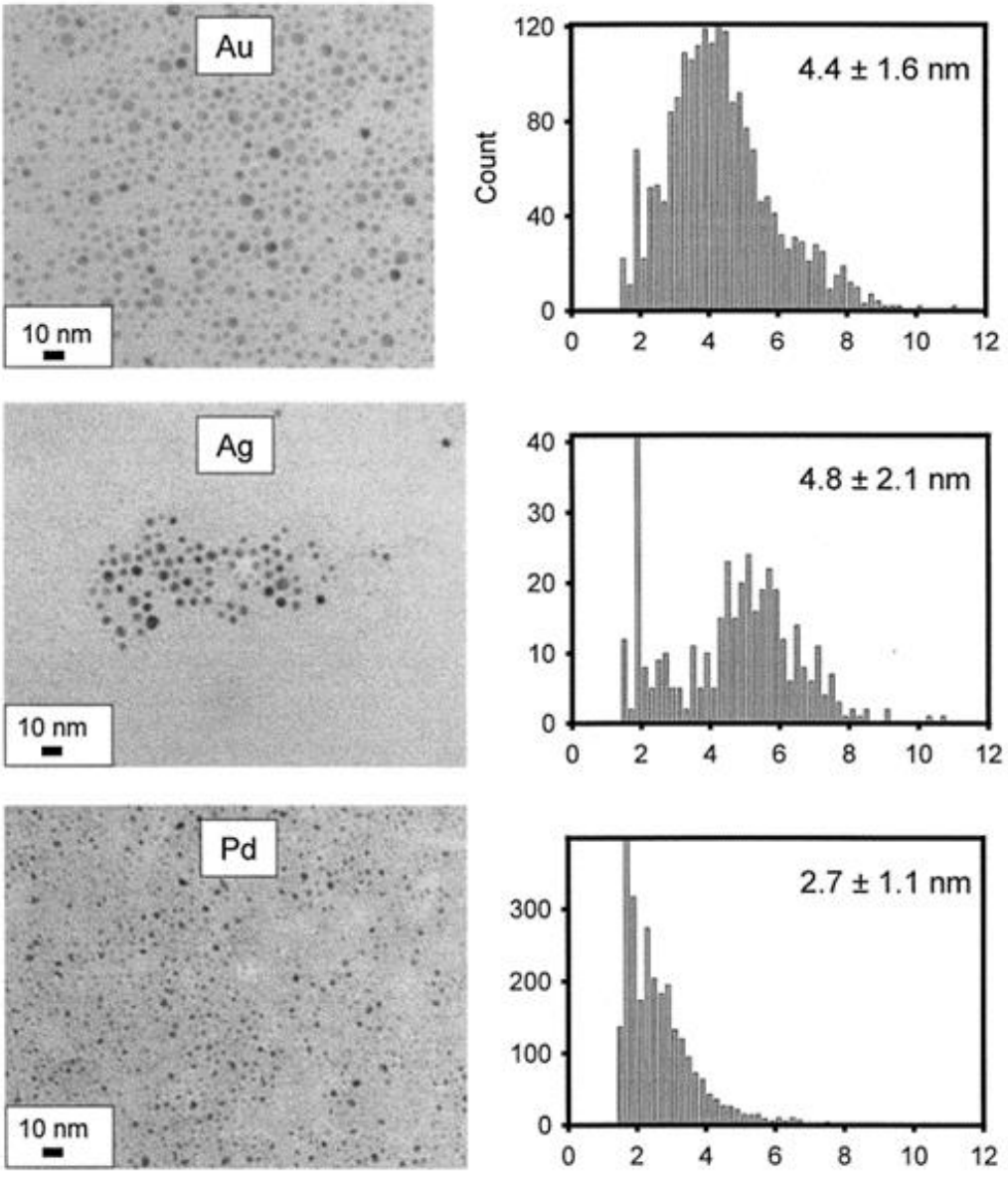

Figure 1.14 TEM images and histograms with average diameters of the obtained cationized Au, Ag, and Pd nanoparticles. Reproduced with permission from ref. (82). Copyright 2000 American Chemical Society.

In the 2010s, some researchers reported the synthesis of Au clusters capped by basic thiols, which can be cationized in acidic condition via protonation reaction.[66,83,86-88] In 2018, Whetten group succeeded in synthesizing series of the captamino ($-S(CH_2)_2N(CH_3)_2$)-capped Au clusters with atom numbers ranging from 25 to 144 (Figure 1.15).[87,88] However, the Au clusters are required protonation for their cationization. The cationized Au clusters, which are stably cationic in every pH condition (persistently cationized), are desirable for leaving their widespread applicability in diverse fields.

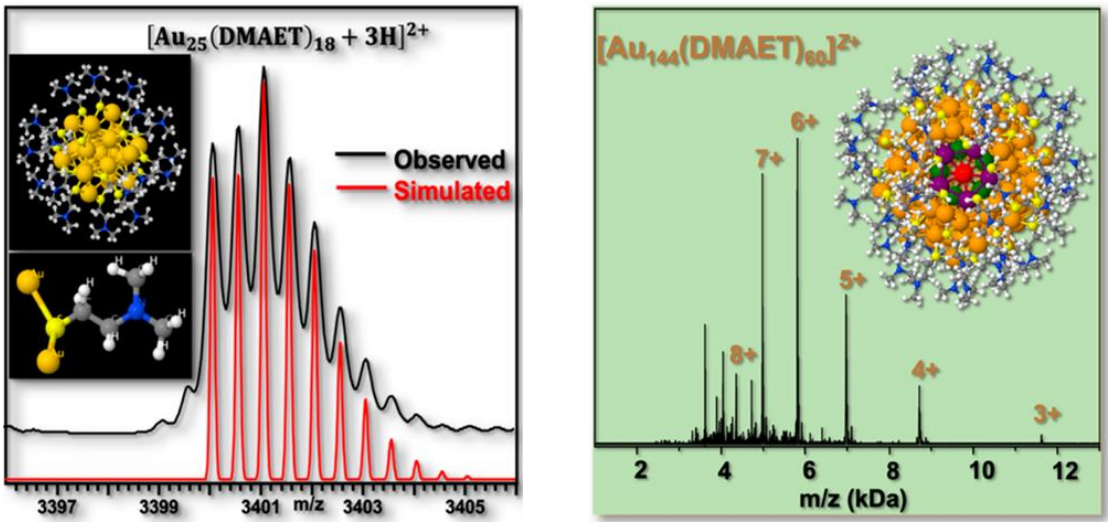

Figure 1.15 ESI-MS of the obtained captamino ($-S(CH_2)_2N(CH_3)_2$)-capped Au_{25} and Au_{144} clusters. Reproduced with permission from ref. (87,88). Copyright 2019 American Chemical Society.

In 2009, Murray group succeeded in the first synthesis of persistently cationized Au clusters using the ligand-exchange method.[89] They used a quaternary ammonium-terminated ligand, $HSC_{11}H_{22}(CH_2CH_3)_3N^+$ ($HSTEA^+$), as a cationic ligand. The starting

hexanethiolate (HSC_6H_{13}, HSC6)-protected Au_{140} clusters were ligand-exchanged with $HSTEA^+$. HSTEA+ was added to the starting Au_{140} clusters dissolved in methylene chloride in the mole ratio of 80:1 = ligands:nanoparticle, and stirred for 30 min. Positive-mode ESI-QQQ results showed two types of size-transformed Au clusters, $Au_{144}(SR)_{60}$ and $Au_{146}(SR)_{59}$ in the six different charge states (10+~15+), indicating the 10-15 ligands were successfully exchanged with cationic thiols (Figure 1.16). Although the resultant products include 2 sizes of clusters (Au_{144} and Au_{146}) and the ligand-exchange ratio was only ca. 20%, this was the first report of the synthesis of the persistently cationized Au clusters.

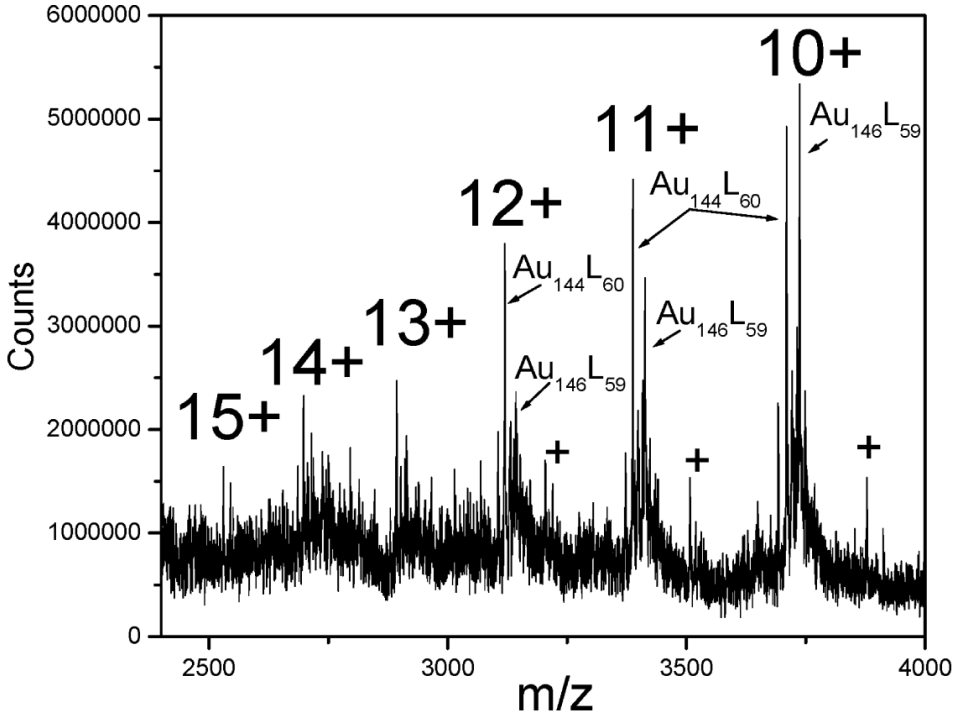

Figure 1.16 Positive-mode ESI-QQQ-MS of the hexanethiolate-protected Au_{140} clusters exchanged with $[HSC_{11}H_{22}(CH_2CH_3)_3N^+][Cl^-]$. Reproduced with permission from ref. (89). Copyright 2009 American Chemical Society.

1.4 Difficulties on synthesizing fully cationized Au clusters with atomic precision

From the aforementioned works, the persistently fully cationized Au clusters seems to be difficult to synthesize with atomic precision. Indeed, this was clearly mentioned in the following statement made in 2005. “Small positively charged ligands do not support the production of MPCs in the Brust synthesis”.[90] Basically, there are two approaches to synthesize cationized Au clusters, (i) size-focusing method and (ii) ligand-exchange method. The critical problems on each method are explained below.

1.4.1 Problems on synthesizing cationized Au clusters using size-focusing method

Size-focusing method involves the formation of the Au(I)-SR complex as an initial step, followed by the reduction to form Au clusters. Needless to say, the formation of the Au(I)-SR complex is one of the most important step, and the complex must be dissolved in the homogeneous solution to obtain atomically pure Au clusters. When using cationic thiols as ligands, $[Au(I)]^{-}$–SR^{+} ionic polymer complexes are formed in this step (Figure 1.17).[91-93] This polymerization makes them insoluble to the solution, leading to hinder the homogeneous reduction of the precursors and the formation of atomically pure clusters. Another problem is the coulombic repulsion between the cationic groups of the ligands when the cluster forms (Figure 1.17).[91-93] The repulsion leads the decrease of the stability of cluster structures, resulting in the decomposition of clusters. Note that the repulsion will be strong when the using cationic thiols with short chain (i.e., 2-mercaptoethyl-*N,N,N*-trimethylammonium: $HS(CH_2)_2N(CH_3)_3^{+}$, thiocholine), while it

will be weak when using the cationic thiols with long chain (i.e., 11-mercaptoundecyl-*N,N,N*-trimethylammonium: $HS(CH_2)_{11}N(CH_3)_3^+$).

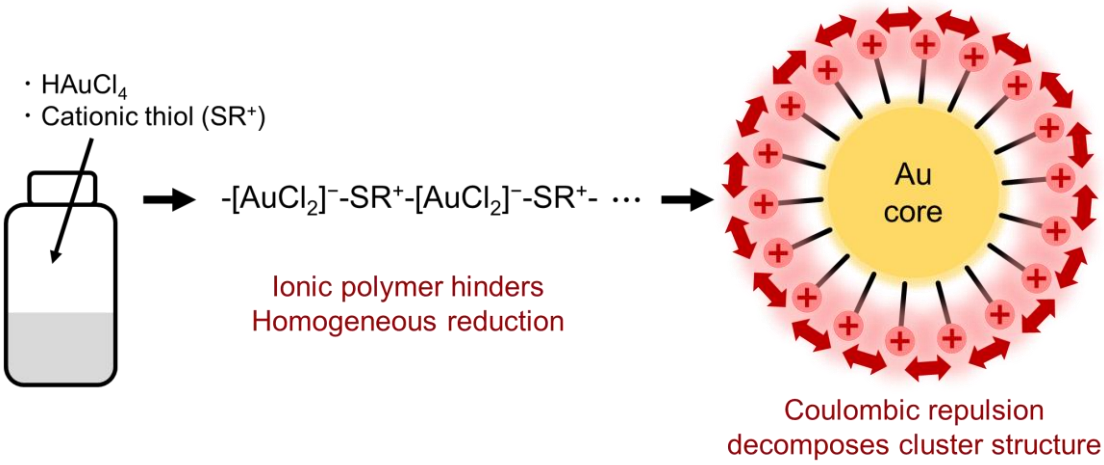

Figure 1.17 Problems on synthesizing cationized Au clusters using size-focusing method

1.4.2 Problems on synthesizing cationized Au clusters using ligand-exchange method

In the ligand-exchange method, the initial surface ligands of the cluster are collided and physically replaced by the desired ligands. As needed, the reaction efficiency is improved by increasing temperature, increasing the amount of the additional ligands, increasing stirring speed, and so on.[33] However, when using cationic thiols, two types of repulsion between cationic thiols hinder the reaction (Figure 1.18).[94] (i) the repulsion between the surface cationic ligand and the incoming cationic ligand in solution, and (ii) among the cationic ligands on the cluster surface. These repulsion will be the crucial impediment for the efficient ligand-exchange reaction.

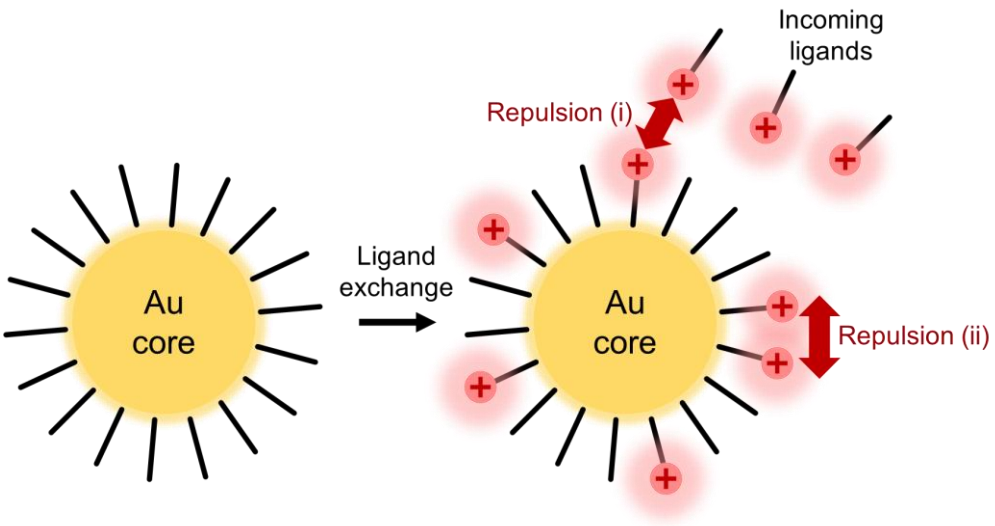

Figure 1.18 Problems on synthesizing cationized Au clusters using ligand-exchange method.

1.5 Recent development on cationized Au clusters

Although the synthesis of fully cationized Au clusters is a very challenging research topic as described above, new things have being revealed by our group on cationized Au clusters towards their successful synthesis after 2016.

In 2018, the unique kinetics of the cationic-ligand-exchange process, in which neutral surface ligands on Au_{25} clusters were exchanged by cationic ligands, has been revealed.[94] In this research, the synthesized $Au_{25}(PET)_{18}$ clusters and KPF_6 powders are dissolved in acetone, followed by the addition of incoming cationic thiols (11-mercaptoundecyl-*N*,*N*,*N*-trimethylammonium: $HS(CH_2)_{11}N(CH_3)_3^+$). The ligand-exchange process was monitored by electrospray ionization mass spectrometry (ESI-MS), and the reaction kinetics was discussed in combination with ^1H NMR results. The cationized Au clusters $Au_{25}(HS(CH_2)_{11}N(CH_3)_3^+)_x(PET)_{18-x}$ (x=1-6) were successfully synthesized, and the unique reaction kinetics that different from the typical neutral-thiol-to-neutral-thiol ligand exchange was observed. The reaction kinetics was determined by two types of coulombic repulsions (i) between the attached cationic ligands and incoming cationic ligands in solution, which hinder further ligand-exchange, and (ii) among the surface cationic ligands on the cluster surface, which promote the thermal decomposition of the clusters (Figure 1.19). The reaction kinetics was divided into two phases based on the coulombic repulsion. The exchange rate was relatively high in the beginning of the reaction hindered by only coulombic repulsion (i), and the rate became very low in the latter reaction hindered by both types of coulombic repulsion (i) and (ii) (Figure 1.20). Although the ligand-exchange ratio was ca. 20% similar with the earlier work of cationic-ligand-exchange,[89] this was the first report that cationic-ligand-exchange was conducted

preserving the size of Au core and its unique kinetics of the reaction was revealed.

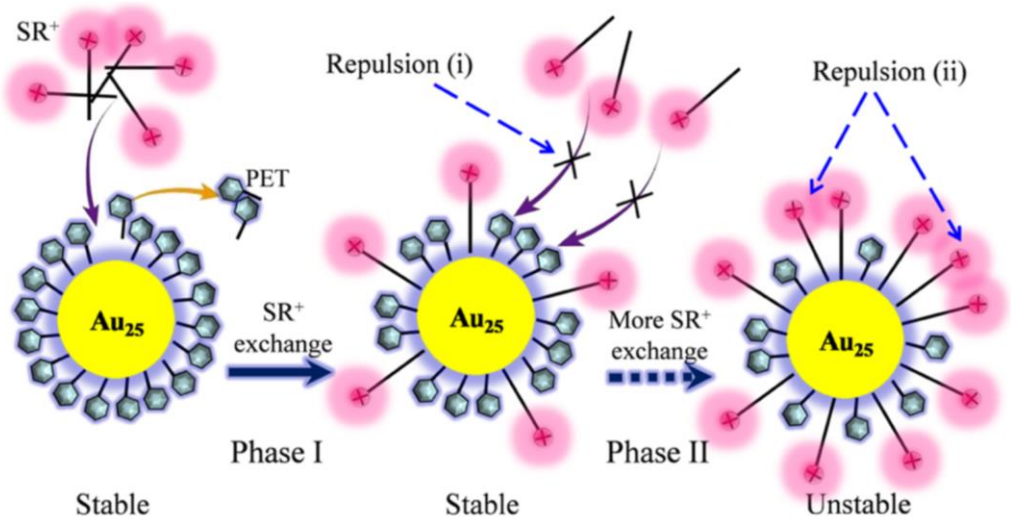

Figure 1.19 Schematic representation of various Coulombic repulsions during cationic-ligand exchange: (i) between the surface SR^+ and the incoming SR^+ in solution and (ii) between the SR^+ ligands on the cluster surface (SR^+: (11-mercaptoundecyl)-*N*,*N*,*N*-trimethylammonium). Reproduced with permission from ref. (94). Copyright 2018 American Chemical Society.

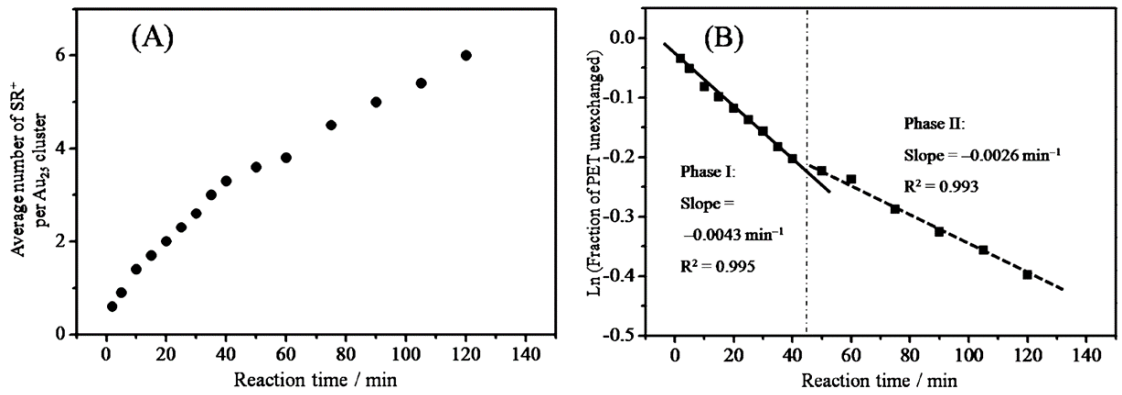

Figure 1.20 (A) Average number of SR^+ ligands per cluster (max: 18) on the cluster surface during the ligand-exchange reaction as determined by ^1H NMR spectroscopy. (B) Ln (fraction of unexchanged PET on the cluster surface) for the ligand-exchange reaction with SR^+ as a function of reaction time. The two lines in (B) are the lines of best fit at 0−40 min (phase I) and 50−120 min (phase II), respectively. Reproduced with permission from ref. (94). Copyright 2018 American Chemical Society.

In 2019, it was reported that cationized Au clusters might have unique structure different from the structures of neural and anionic Au clusters.[95] In this research, the synthesized neutral $Au_{25}(PyET)_{18}$ clusters (4-PyET = $–SCH_2CH_2Py$, where Py = pyridyl group) were dissolved in MeOH, and the different amount of HCl–MeOH solution were added separately. The $Au_{25}(PyET)_{18}$ clusters were protonated in the different degrees, and this process was monitored by UV-Vis absorption. As shown in Figure 1.21, when the $Au_{25}(PyET)_{18}$ clusters were given positive charges on the surface through the protonation reaction, the changes in absorption spectra were observed before and after the reaction, and the degree of the changes were proportional to the amount of the additional HCl–MeOH solution. This observation suggests that the geometric structure of Au_{25} core was

distorted due to the surface charge anisotropy[12,21] during the addition of positive charges on the cluster surface.

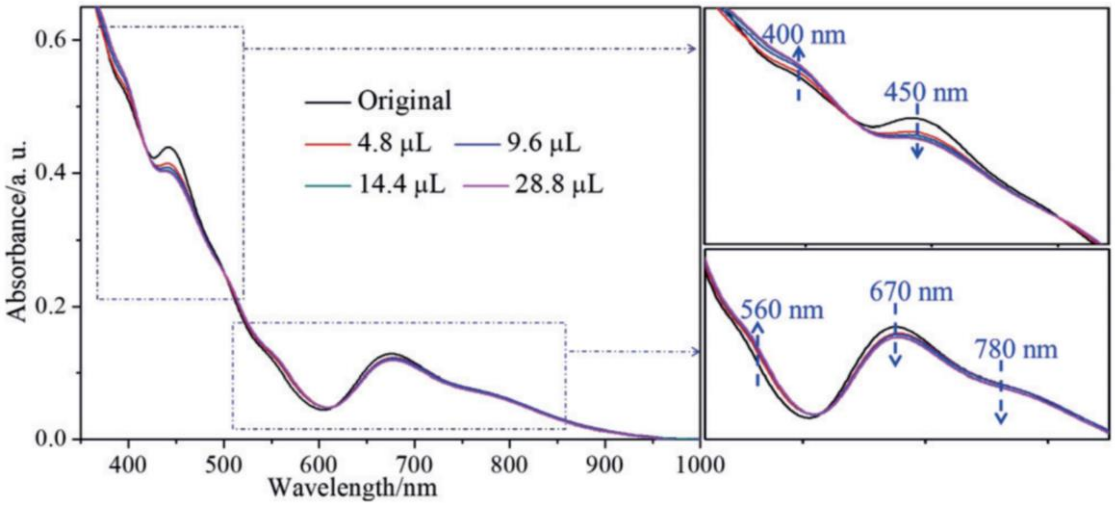

Figure 1.21 UV-Vis absorption spectrum of the obtained $Au_{25}(4\text{-PyET})_{18}$ in MeOH on addition of methanolic HCl (500 mm). The blue arrows denote changes during the protonation. Reproduced with permission from ref. (95). Copyright 2019 Wiley-VCH.

The synthesis of fluorescent Au clusters using the shortest cationic thiol, 2-mercaptoethyl-*N,N,N*-trimethylammonium (TC, $HS(CH_2)_2N(CH_3)_3^+$), has been reported in 2016 (but not atomically precise due to the very short TC ligands and their strong coulombic repulsion on the ultrasmall cluster surfaces).[96] The simple reduction of $HAuCl_4$ with excess $NaBH_4$ in the presence of TC produced nanoparticles with a size larger than 4 nm, which exhibited plasmon absorption at around 540 nm. By introducing the negatively charged surfactant, sodium dodecylsulfate (SDS, $CH_3(CH_2)_{11}OSO_3^-Na^+$), to neutralize the coulombic repulsion between cationic thiols, the fluorescent Au clusters, which exhibited no more plasmonic absorption, were successfully obtained (Figure

1.22(A)). Interestingly, the obtained Au clusters also showed blue emission at around 448 nm (Figure 1.22(B)). Judging from the results of TEM, UV-Vis absorption, and STEM-HAADF, the Au_8 clusters or Au clusters with similar size were obtained. The exact size of the obtained Au clusters was unknown; however this was the first report using size-focusing method to synthesize cationized Au clusters, and the strategy, using negatively-charged surfactant to neutralize the cationic thiols, is generally applicable for the synthesis of cationized metal clusters.

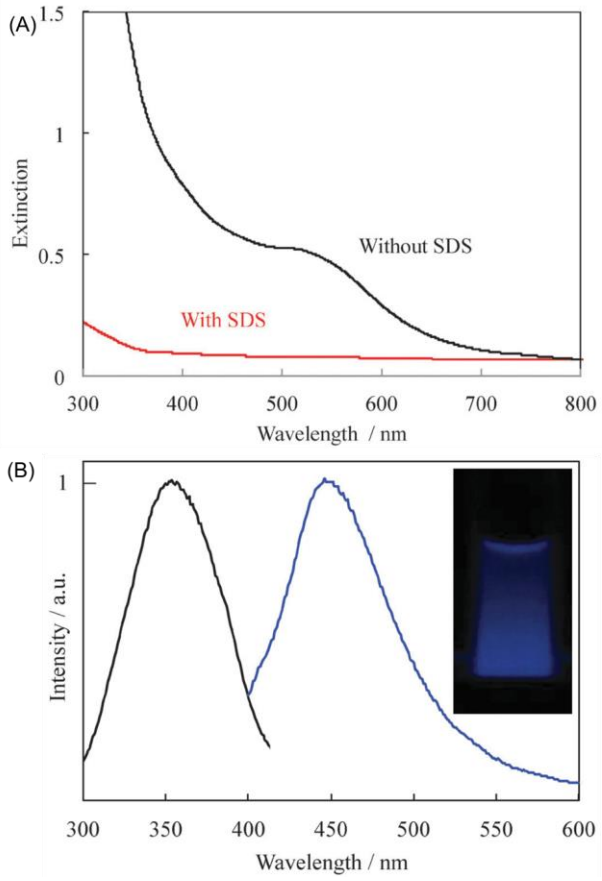

Figure 1.22 (A) UV-Vis extinction spectra of Au nanoparticles and nanoclusters synthesized in the absence or presence of SDS, and (B) fluorescence emission (blue) and excitation (black) spectra of synthesized gold nanoclusters. Reproduced with permission from ref. (96). Copyright 2016 The Owner Societies.

1.6 Applications of cationized Au nanoparticles/clusters

Owing to the unique characteristics such as tunable surface properties as well as interesting optical properties, noble metal nanoparticles/clusters have been widely applied in environmental monitoring, chemical sensing, drug delivery, cancer therapy, bioimaging, biolabeling, nanomedicine, and photodynamic therapy.[9,18-21,97-102] Especially in some special areas such as biological signaling, particle transportation, cellular toxicity, and environmental impact, the metal nanoparticles/clusters protected by positively charged ligands have great advantages with respect to their behaviors at the nano-bio interface.[103-107] Tuning the surface charge of metal nanoparticles/clusters is particularly important in rational design of their applications.

Quan *et al.*[108] investigated the role of ligand charge during Au nanoparticles penetration through the liquid bilayers by computational simulations. They used the three types of ligands with different charged states (neutral, negative, and positive), and checked how they interact with the different types of membrane (the symmetric lipid membrane (neutral), the symmetric lipid membrane (negatively charged), and the asymmetric lipid membrane (negatively charged)), as shown in Figure 1.23(A). Figure 1.23(B) shows the hydrophobic (or neutral) Au nanoparticles do not adsorb onto the all three types of membranes. Although the anionic Au nanoparticles attached to the all three types of membranes, further penetration was not observed. On the other hand, the cationic Au nanoparticles have the strong affinities to the all types of membranes, and the penetration of cationic Au nanoparticles through the membrane was observed for the negatively charged membranes, indicating the strong coulombic attractions between the surface ligands on the Au nanoparticles and the charged groups in membranes. In addition,

the equilibrated states of cationic Au nanoparticles with different surface charge densities (10-100%) interacting with the asymmetric lipid membrane (negatively charged) were shown in Figure 1.23(C). The results indicate that the coulombic interactions are important for the Au nanoparticles penetration mechanism.

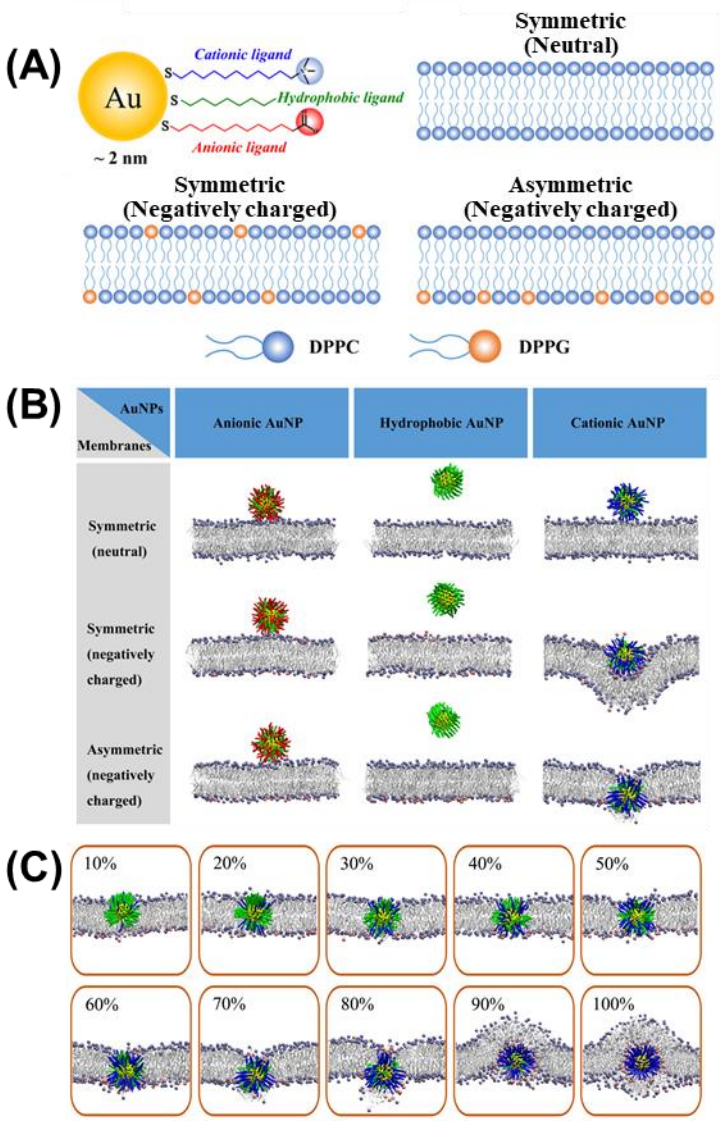

Figure 1.23 (A) Schematic illustration of the models of AuNPs decorated with different ligands, the symmetric lipid membrane (neutral), the symmetric lipid membrane (negatively charged), and the asymmetric lipid membrane (negatively charged). (B) Representative snapshots of equilibrated states for AuNPs with different signs of charge interacting with the three kinds of lipid membranes. (C) Equilibrated states of cationic AuNPs with different surface charge densities interacting with the asymmetric lipid membrane. Reproduced with permission from ref. (108). Copyright 2017 American Chemical Society.

Elci *et al.*[109] studied how surface-ligand charge affects the biodistribution of 2-nm Au NPs in vivo. They prepared the four types of Au nanoparticles using different ligands as shown in Figure 1.24(A) (cationic (AuNP1 and 2), neutral (AuNP3), and anionic (AuNP4)). The sub-organ distributions of Au nanoparticles were observed by laser ablation inductively coupled plasma mass spectrometry (LA-ICP-MS), and the distribution image of the Au nanoparticles in the spleen and liver are shown in Figure 1.24(B). Neutral Au nanoparticles (AuNP3) accumulated in the marginal zone and white pulp regions of the spleen and with the Kupffer cells of the liver, indicating that they are more likely to interact with the immune system. Positively charged Au nanoparticles (AuNP1 and 2) were found more extensively in the filtering regions of the spleen and the detoxifying hepatocytes of the liver. Negatively charged nanoparticles accumulated extensively in the red pulp of the spleen and broadly distributed in the liver. The positively charged Au nanoparticles were not observed in the liver blood vessels 24h after injection of them, whereas the negatively charged Au nanoparticles were observed. These results indicate that the Au nanoparticles show different behavior in the sub-organ, depending on the charge state of the surface ligand, and the positively charged Au nanoparticles are cleaned faster than the neutral and negatively charged Au nanoparticles.

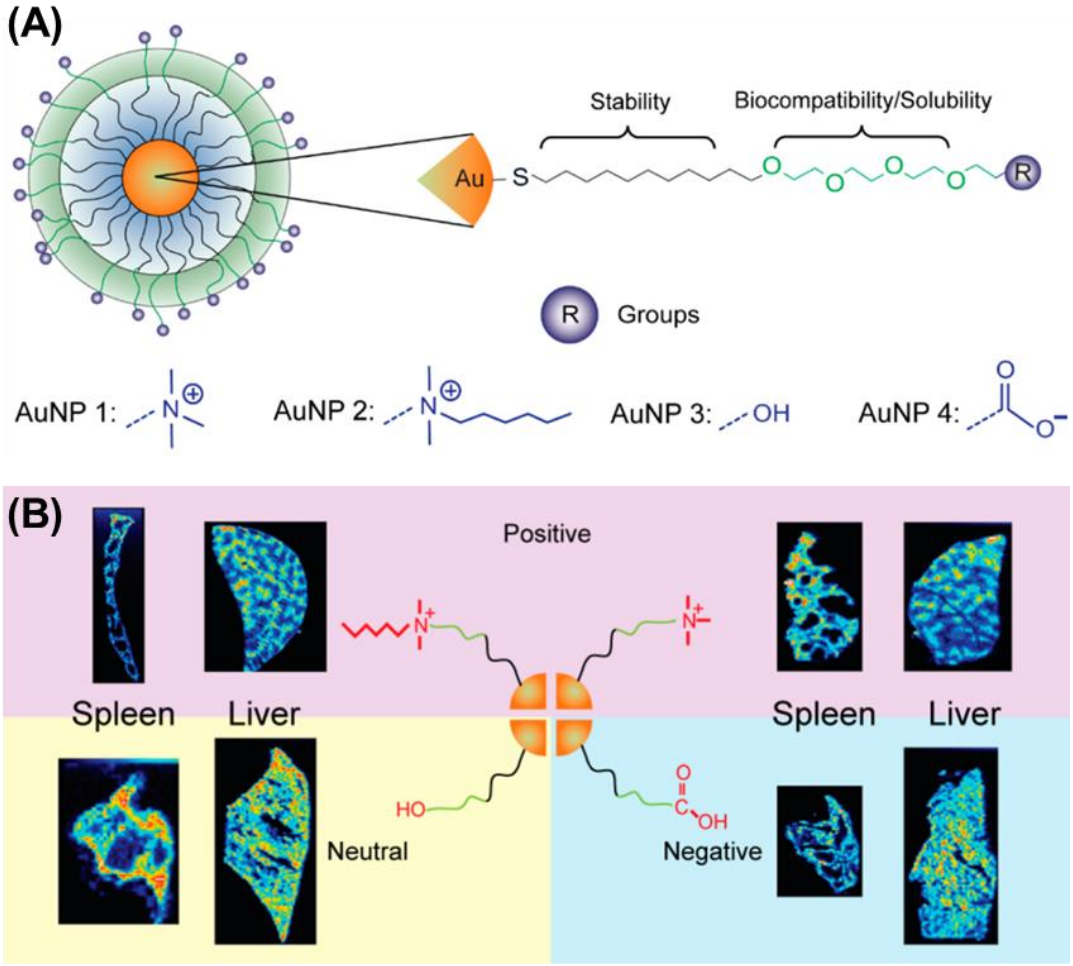

Figure 1.24 (A) Design and structure of the Au NPs. (B) Laser ablation ICP-MS results of the biodistribution of Au NPs in the spleen and liver tissues. Reproduced with permission from ref. (109). Copyright 2016 American Chemical Society.

It was also revealed that surface coating and surface charges of the nanoparticles influence their toxic behavior. [110-112] In 2004, Goodman et al. investigated how the electrostatic attraction between the Au nanoparticles and the cell membrane affects the toxicity of the Au nanoparticles.[110] They prepared the anionic and cationized Au nanoparticles (Figure 1.25(A), and investigated how they disrupt the negatively charged

vesicles, respectively. The cationized Au nanoparticles lysed the vesicles more efficiently than anionic Au nanoparticles, due to the electrostatic complementarity of the cationic substituents and the negatively charged vesicles (Figure 1.25(B)). The role of the surface charges of metal nanoparticles is still unclear and widely debated, as the potential toxicity of metal nanoparticles on biological targets is crucial for their clinical translation.

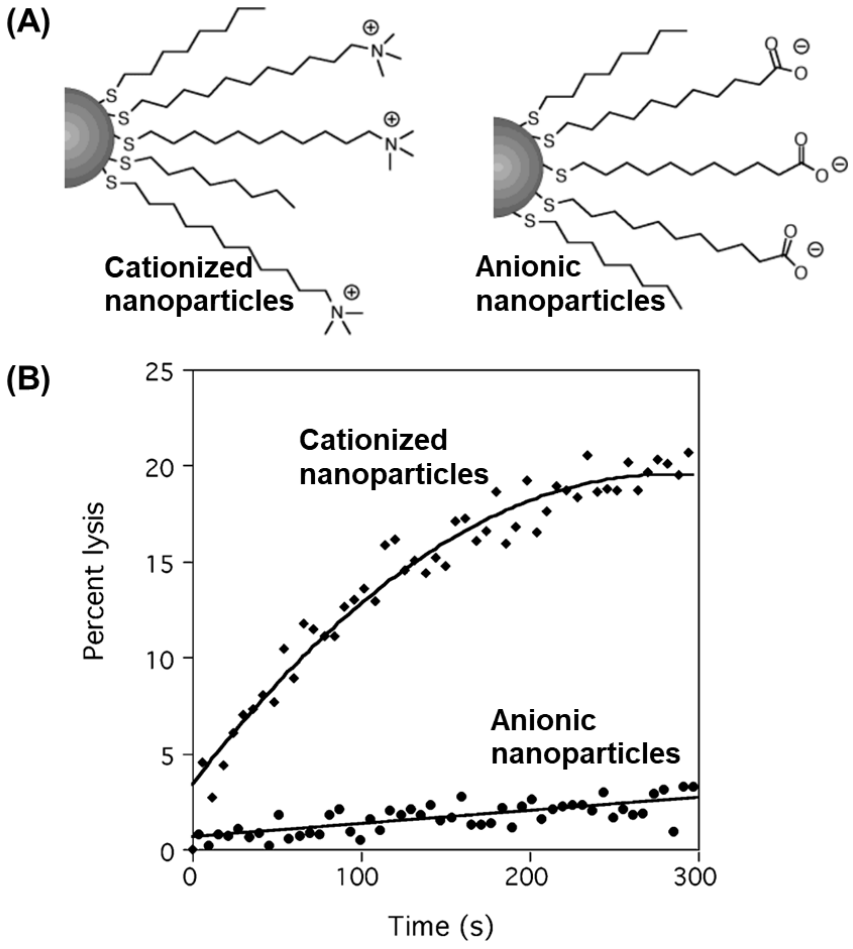

Figure 1.25 (A) Schematic illustrations of the structures of the cationized nanoparticles and anionic nanoparticles, (B) different ability on disrupting negatively charged vesicles between cationized and anionic nanoparticles. Reproduced with permission from ref. (110). Copyright 2004 American Chemical Society.

The aforementioned applications are of the cationized Au nanoparticles, not the Au clusters. Unfortunately, to the best of my knowledge, there are no report of cationized Au cluster applications due to their infrequent synthetic works. However, there are peculiar applications using Au clusters, but using Au nanoparticles.

Xie group[113] found the unique property of $Au_{25}(MHA)_{18}$ clusters (MHA = 6-mercaptohexanoic acid), which kills both Gram-positive and Gram-negative bacteria. As shown in Figure 1.26, compared with the Au NPs and Au(I)−MHA complexes, only the Au_{25} clysters hold the high killing efficiency. The antimicrobial mechanism of Au_{25} clusters is the internalization of clusters, inducing a metabolic imbalance in bacterial cells, which lead to an increase of intracellular reactive oxygen species (ROS) generation that kills bacteria consequently. Thus, the Au clusters and nanoparticles have different properties for their application.

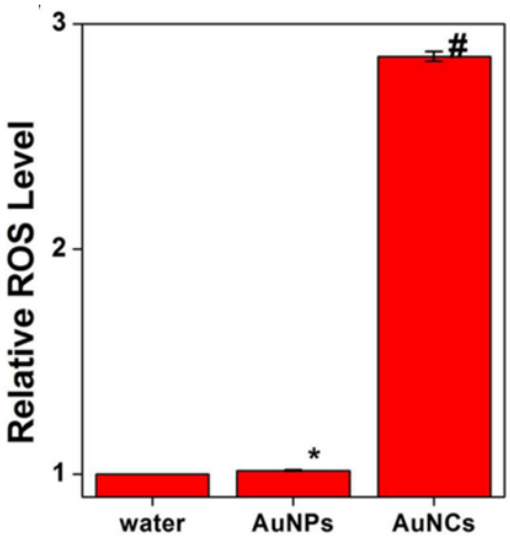

Figure 1.26 Unique property of $Au_{25}(MHA)_{18}$ clusters that kills the bacteria efficiently. Compared with the Au NPs and Au(I)−MHA complexes, only the Au_{25} clusters hold the high killing efficiency (high ROS level). Reproduced with permission from ref. (113). Copyright 2018 American Chemical Society.

1.7 Summary and perspective

Au clusters have been a subject of major interest in nanoscience and nanotechnology, because of their unique optical features, electrochemical behaviors, and catalytic properties. To date, more than 40 core sizes of atomically precise Au clusters such as Au_{18}, Au_{24}, Au_{25}, Au_{28}, Au_{34}, Au_{36}, Au_{38}, Au_{40}, Au_{42}, Au_{49}, Au_{60}, Au_{92}, Au_{130}, Au_{133}, Au_{144}, Au_{187}, Au_{246}, Au_{279}, Au_{329}, and so on, have been synthesized using various types of surface ligands, as shown in Table 1.1. However, the ligands used for Au cluster syntheses are neutral or anionic, and cationic-ligand-protected Au clusters have never been synthesized. In some special areas, such as biological signaling, particle transportation, cellular toxicity, and environmental impact, cationized Au clusters would be indispensable due to the good affinity of the cationic ligand for the biomaterial. Thus, there is an urgent need for the establishment of synthetic protocols of cationized Au clusters with high-yield and high-purity, especially with atomic precision.

1.8 Objective of this study

This study aims to establish the synthesis method of atomically pure cationized Au clusters.

(1) The cationized Au clusters are synthesized by size-focusing method which is the most famous synthesis method of clusters. $Au_{25}(SR^{+})_{18}$ and $Au_{144}(SR^{+})_{60}$, the smallest and largest size Au clusters in the most stable and studied Au clusters, are synthesized.

(2) In recent years, surface reaction method have been receiving significant attention, and there are few reports on such reactions, two of which are azido- and amide-bond formation reactions on the Au cluster surface.[114,115] Surface Menshutkin reaction is investigated on the Au_{25} clusters for their cationization and functionalization.

(3) The unique reaction kinetics is revealed by monitoring the cationic-ligand-exchange reaction on the cationized $Au_{25}(4\text{-PyET-}CH_3^{+})_x(4\text{-PyET})_{18-x}$ ($x\approx9$) clusters, which containing both neutral and cationic ligands at the nearly equivalent amount.

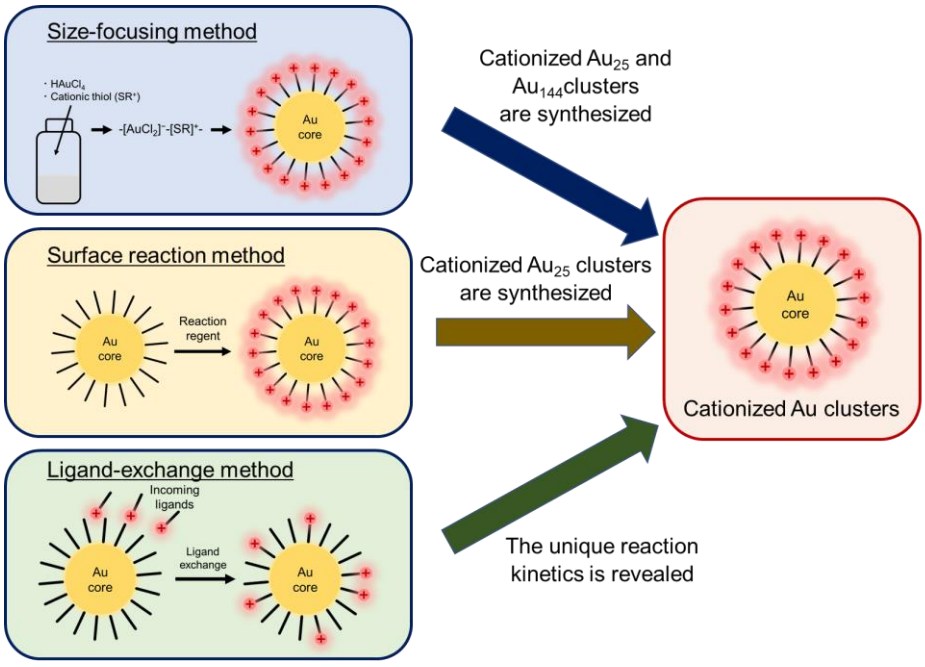

Figure 1.27 Strategy for synthesizing the atomically pure cationized Au clusters.

1.9 Outline of this thesis

This thesis consists of six chapters. The key contents of each chapter are outlined as follows.

Chapter 1 summarizes the general background including the history and synthesis method of Au clusters with atomic precision, previous and recent researches of the cationized Au clusters, and the problems on synthesizing atomically pure cationized Au clusters. The objective and outline of the thesis were provided.

Chapter 2 reports the first synthesis of fully cationized $Au_{25}(SR^{+})_{18}$ clusters with atomic precision by size-focusing method. 11-mercaptoundecyl-*N*,*N*,*N*-trimethylammonium ($HS(CH_2)_{11}N(CH_3)_3^{+}$) was used as the cationic ligand.

Chapter 3 reports the synthesis of fully cationized $Au_{144}(SR^{+})_{60}$ clusters with atomic precision by size-focusing method. Au_{144} is the largest size in the most stable and studied clusters. 11-mercaptoundecyl-*N*,*N*,*N*-trimethylammonium ($HS(CH_2)_{11}N(CH_3)_3^{+}$) was used as the cationic ligand.

Chapter 4 demonstrates the surface Menshutkin reaction on the neutral $Au_{25}(4\text{-PyET})_{18}$ clusters to transform them into the cationized $Au_{25}(4\text{-PyET-}CH_3^{+})_x(4\text{-PyET})_{18-x}$ clusters (4-PyET = $HS(CH_2)_2C_5H_4N$).

Chapter 5 presents the unique ligand-exchange kinetics by investigating the ligand-exchange to cationic ligands on the cationized $Au_{25}(4\text{-PyET-}CH_3^{+})_x(4\text{-PyET})_{18-x}$ ($x\approx9$) clusters, which containing both neutral and cationic ligands.

Chapter 6 presents the summary of this thesis.

1.10 References

(1) Yao, Q.; Chen, T.; Yuan, X.; Xie, J. Toward Total Synthesis of Thiolate-Protected Metal Nanoclusters. *Acc. Chem. Res.*, **2018**, *51*, 1338–1348.

(2) Hossain, S.; Niihori, Y.; Nair, L. V.; Kumar, B.; Kurashige, W.; Negishi, Y. Alloy Clusters: Precise Synthesis and Mixing Effects. *Acc. Chem. Res.*, **2018**, *51*, 3114–3124.

(3) Luo, G. G.; Guo, Q. L.; Wang, Z.; Sun, C. F.; Lin, J. Q.; Sun, D. New protective ligands for atomically precise silver nanoclusters. *Dalton Trans.*, **2020**, *49*, 5406–5415.

(4) Yang, J.; Jin, R. New Advances in Atomically Precise Silver Nanoclusters. *ACS Mater. Lett.*, **2019**, *1*, 482–489.

(5) Shan, J.; Tenhu, H. Recent advances in polymer protected gold nanoparticles: synthesis, properties and applications. *Chem. Commun.* **2007**, *44*, 4580–4598.

(6) Grzelczak, M.; Pérez-Juste, J.; Mulvaney, P.; Liz-Marzán, L. M. Shape control in gold nanoparticle synthesis. *Chem. Soc. Rev.* **2008**, *37*, 1783–1791.

(7) Sardar, R.; Funston, A. M.; Mulvaney, P.; Murray, R. W. Gold nanoparticles: past, present, and future. *Langmuir*, **2009**, *25*, 13840–13851.

(8) Li, Y.; Higaki, T.; Du, X.; Jin, R. Surface Chemistry of Atomically Precise Coinage−Metal Nanoclusters: From Structural Control to Surface Reactivity and Catalysis. *Adv. Mater.*, **2020**, *32*, e1905488.

(9) Jin, R. C.; Zeng, C. J.; Zhou, M.; Chen, Y. X. Atomically Precise Colloidal Metal Nanoclusters and Nanoparticles: Fundamentals and Opportunities. *Chem. Rev.*, **2016**, *116*, 10346–10413.

(10) Walter, M.; Akola, J.; Lopez-Acevedo, O.; Jadzinsky, P. D.; Calero, G.; Ackerson, C. J.; Whetten, R. L.; Gronbeck, H.; Hakkinen, H.; A unified view of ligand-protected gold clusters as superatom complexes, *PNAS*, **2008,** *105* 9157–9162.

(11) Bergmann, T.; Limberger, H.; Martin, T. P. Evidence of Electronic Shell Structure in Cs-0 Clusters. *Phys. Rev. Lett.*, **1988**, *60*, 1767-1770.

(12) Malola, S.; Hakkinen, H. Electronic Structure and Bonding of Icosahedral Core-Shell Gold-Silver Nanoalloy Clusters $Au_{144-x}Ag_x(SR)_{60}$. *J. Phys. Chem. Lett.* **2011**, *2*, 2316–2321.

(13) Lopez-Acevedo, O.; Akola, J.; Whetten, R. L.; Gronbeck, H.; Hakkinen, H. Structure and Bonding in the Ubiquitous Icosahedral Metallic Gold Cluster $Au_{144}(SR)_{60}$. *J. Phys. Chem. C* **2009**, *113*, 5035–5038.

(14) Chakraborty, P.; Nag, A.; Chakraborty, A.; Pradeep, T. Approaching Materials with Atomic Precision Using Supramolecular Cluster Assemblies. *Acc. Chem. Res.*, **2019**, *52*, 2–11.

(15) Yan, J.; Teo, B. K.; Zheng, N. Surface Chemistry of Atomically Precise Coinage−Metal Nanoclusters: From Structural Control to Surface Reactivity and Catalysis. *Acc. Chem. Res.*, **2018**, *51*, 3084–3093.

(16) Gan, Z.; Xia, N.; Wu, Z. Discovery, Mechanism, and Application of Antigalvanic Reaction. *Acc. Chem. Res.*, **2018**, *51*, 2774– 2783.

(17) Faraday, M. The bakerian lecture: experimental relations of gold (and other metals) to Light. *Philos. Trans. R. Soc. London* **1857**, *147*, 145−181.

(18) Crooks, R. M.; Zhao, M.; Sun, L.; Chechik, V.; Yeung, L. K. Dendrimer-encapsulated metal nanoparticles: synthesis, characterization, and applications to catalysis. *Acc. Chem. Res.* **2001**, *34*, 181–190.

(19) Liu, L.; Corma, A. Metal catalysts for heterogeneous catalysis: from single atoms to nanoclusters and nanoparticles. *Chem. Rev.* **2018**, *118*, 4981–5079.

(20) Chakraborty, I., Pradeep, T. Atomically precise clusters of noble metals: emerging link between atoms and nanoparticles. *Chem. Rev.* **2017**, *117*, 8208–8271.

(21) Kang, H.; Buchman, J. T.; Rodriguez, R. S.; Ring, H. L.; He, J.; Bantz, K. C.; Haynes, C. L. Stabilization of silver and gold nanoparticles: preservation and improvement of plasmonic functionalities. *Chem. Rev.* **2018**, *119*, 664–699.

(22) Jin, R.; Cao, Y. C.; Hao, E.; Metraux, G. S.; Schatz, G. C.; Mirkin, C. A. Controlling anisotropic nanoparticle growth through plasmon excitation. *Nature* **2003**, *425*, 487−490.

(23) Wang, Y.; Zheng, Y.; Huang, C. Z.; Xia, Y. Synthesis of Ag nanocubes 18−32 nm in edge length: the effects of polyol on reduction kinetics, size control, and reproducibility. *J. Am. Chem. Soc.* **2013**, *135*, 1941−1951.

(24) Jin, R. Atomically precise metal nanoclusters: stable sizes and optical properties. *Nanoscale* **2015**, *7*, 1549−1565.

(25) Brust, M.; Walker, M.; Bethell, D.; Schiffrin, D. J.; Whyman, R. Synthesis of thiol-derivatised gold nanoparticles in a two-phase liquid–liquid system. *J. Am. Chem. Soc. Chem. Commun.* **1994**, *7*, 801–802.

(26) Whetten, R. L.; Khoury, J. T.; Alvarez, M. M.; Murthy, S.; Vezmar, I.; Wang, Z. L.; Stephens, P. W.; Cleveland, C. L.; Luedtke, W. D.; Landman, U. Nanocrystal Gold Molecules. *Adv. Mater. Weinheim* **1996**, *8*, 428–433.

(27) Schaaff, T. G.; Shafigullin, M. N.; Khoury, J. T.; Vezmar, I.; Whetten, R. L.; Cullen, W. G.; First, P. N.; Gutiérrez-Wing, C.; Ascensio, J.; Jose-Yacamán, M. J. Isolation

of Smaller Nanocrystal Au Molecules: Robust Quantum Effects in Optical Spectra. *J. Phys. Chem. B* **1997**, *101*, 7885–7891.

(28) Templeton, A. C.; Hostetler, M. J.; Warmoth, E. K.; Chen, S.; Hartshorn, C. M.; Krishnamurthy, Vijay M. M.; Forbes, D. E.; Murray, R. W.; Gateway Reactions to Diverse, Polyfunctional Monolayer-Protected Gold Clusters. *J. Am. Chem. Soc.* **1998**, *120*, 4845–4849.

(29) Kiely, C. J.; Fink, J.; Brust, M.; Bethell, D.; Schiffrin, D. J. Spontaneous ordering of bimodal ensembles of nanoscopic gold clusters. *Nature* **1998**, *396*, 444–446.

(30) Schaaff, T. G.; Shafigullin, M. N.; Khoury, J. T.; Vezmar, I.; Whetten, R. L.; Cullen, W. G.; First, P. N.; Gutierrez-Wing, C.; Ascensio, J.; Jose-Yacaman, M. J. Isolation of smaller nanocrystal Au molecules: robust quantum effects in optical spectra. *J. Phys. Chem. B* **1997**, *101*, 7885−7891.

(31) Tracy, J. B.; Crowe, M. C.; Parker, J. F.; Hampe, O.; Fields- Zinna, C. A.; Dass, A.; Murray, R. W. Electrospray ionization mass spectrometry of uniform and mixed monolayer nanoparticles: $Au_{25}[S(CH_2)_2Ph]_{18}$ and $Au_{25}[S(CH_2)_2Ph]_{18-x}(SR)_x$. *J. Am. Chem. Soc.***2007**, *129*, 16209−16215.

(32) Negishi, Y.; Nobusada, K.; Tsukuda, T. Glutathione-protected gold clusters revisited: bridging the gap between gold(I)−thiolate complexes and thiolate-protected gold nanocrystals. *J. Am. Chem. Soc.* **2005**, *127*, 5261−5270.

(33) Zhu, M.; Lanni, E.; Garg, N.; Bier, M. E.; Jin, R. Kinetically controlled, high-yield synthesis of Au_{25} clusters. *J. Am. Chem. Soc.* **2008**, *130*, 1138−1139.

(34) Zeng, C.; Chen, Y.; Das, A.; Jin, R. Transformation chemistry of gold nanoclusters: From one stable size to another. *J. Phys. Chem. Lett.* **2015**, *6*, 2976–2986.

(35) Jadzinsky, P. D.; Calero, G.; Ackerson, C. J.; Bushnell, D. A.; Kornberg, R. D.

Structure of a thiol monolayer-protected gold nanoparticle at 1.1 Å resolution. *Science* **2007**, *318*, 430–433.

(36) Zhu, M.; Aikens, C. M.; Hollander, F. J.; Schatz, G. C.; Jin, R. Correlating the Crystal Structure of A Thiol-Protected Au_{25} Cluster and Optical Properties. *J. Am. Chem. Soc.* **2008**, *130*, 5883–5885.

(37) Kang, X.; Chong, H.; Zhu, M. $Au_{25}(SR)_{18}$: the captain of the great nanocluster ship. *Nanoscale* **2018**, *10*, 10758–10834.

(38) Kang, X.; Zhu, M. Tailoring the photoluminescence of atomically precise nanoclusters. *Chem. Soc. Rev.* **2019**, *48*, 2422–2457.

(39) Xu, W. W. Zeng, X. C.; Gao, Y. Application of electronic counting rules for ligand-protected gold nanoclusters. *Acc. Chem. Res.* **2018**, *51*, 2739–2747.

(40) Sakthivel, N. A.; Dass, A. Aromatic thiolate-protected series of gold nanomolecules and a contrary structural trend in size evolution. *Acc. Chem. Res.* **2018**, *51*, 1774–1783.

(41) Chen, Y.; Zeng, C.; Liu, C.; Kirschbaum, K.; Gayathri, C.; Gil, R. R.; Rosi, N. L; Jin, R. Crystal structure of barrel-shaped chiral Au_{130}(*p*-MBT)$_{50}$ nanocluster. *J. Am. Chem. Soc.* **2015**, *137*32, 10076–10079.

(42) Zeng, C.; Li, T.; Das, A.; Rosi, N. L.; Jin, R. Chiral structure of thiolate-protected 28-gold-atom nanocluster determined by X-ray crystallography. *J. Am. Chem. Soc.* **2013**, *135*, 10011–10013.

(43) Qian, H.; Eckenhoff, W. T.; Zhu, Y.; Pintauer, T.; Jin, R. Total structure determination of thiolate-protected Au_{38} nanoparticles. *J. Am. Chem. Soc.* **2010**, *132*, 8280–8281.

(44) Chen, S.; Wang, S.; Zhong, J.; Song, Y.; Zhang, J.; Sheng, H.; Pei, Y.; Zhu, M. The structure and optical properties of the ($Au_{18}(SR)_{14}$) nanocluster. *Angew. Chem., Int. Ed.* **2015**, *54*, 3145−3149.

(45) Zeng, C.; Qian, H.; Li, T.; Li, G.; Rosi, N. L.; Yoon, B.; Barnett, R. N.; Whetten, R. L.; Landman, U.; Jin, R. Total structure and electronic properties of the gold nanocrystal $Au_{36}(SR)_{24}$. *Angew. Chem., Int. Ed.* **2012**, *51*, 13114−13118.

(46) Das, A.; Li, T.; Nobusada, K.; Zeng, C.; Rosi, N. L.; Jin, R. Nonsuperatomic $[Au_{23}(SC_6H_{11})_{16}]^-$nanocluster featuring bipyramidal Au_{15} kernel and trimeric $Au_3(SR)_4$ motif. *J. Am. Chem. Soc.* **2013**, *135*, 18264−18267.

(47) Crasto, D.; Barcaro, G.; Stener, M.; Sementa, L.; Fortunelli, A.; Dass, A. $Au_{24}(SAdm)_{16}$nanomolecules: x-ray crystal structure, theoretical analysis, adaptability of adamantane ligands to form $Au_{23}(SAdm)_{16}$ and $Au_{25}(SAdm)_{16}$, and its relation to $Au_{25}(SR)_{18}$. *J. Am. Chem. Soc.* **2014**, *136*, 14933−14940.

(48) Heaven, M. W.; Dass, A.; White, P. S.; Holt, K. M.; Murray, R. W. Crystal structure of the gold nanoparticle $[N(C_8H_{17})_4][Au_{25}(SCH_2CH_2Ph)_{18}]$. *J. Am. Chem. Soc.* **2008**, *130*, 3754−3755.

(49) Zhu, M.; Aikens, C. M.; Hollander, F. J.; Schatz, G. C.; Jin, R. Correlating the crystal structure of a thiol-protected Au_{25} cluster and optical properties. *J. Am. Chem. Soc.* **2008**, *130*, 5883−5885.

(50) Crasto, D.; Malola, S.; Brosofsky, G.; Dass, A.; Häkkinen, H. Single crystal XRD structure and theoretical analysis of the chiral $Au_{30}S(S\text{-}t\text{-}Bu)_{18}$ cluster. *J. Am. Chem. Soc.* **2014**, *136*, 5000−5005.

(51) Zeng, C.; Chen, Y.; Liu, C.; Nobusada, K.; Rosi, N. L.; Jin, R. Gold tetrahedra coil up: Kekulé-like and double helical superstructures. *Sci. Adv.* **2015**, *1*, e1500425.

(52) Zeng, C.; Chen, Y.; Iida, K.; Nobusada, K.; Kirschbaum, K.; Lambright, K. J.; Jin, R. Gold quantum boxes: on the periodicities and the quantum confinement in the Au_{28}, Au_{36}, Au_{44}, and Au_{52} magic series. *J. Am. Chem. Soc.* **2016**, *138*, 3950–3953.

(53) Dass, A.; Theivendran, S.; Nimmala, P. R.; Kumara, C.; Jupally, V. R.; Fortunelli, A.; Sementa, L.; Barcaro, G.; Zuo, X.; Noll, B. C. $Au_{133}(SPh\text{-}tBu)_{52}$nanomolecules: X-ray crystallography, optical, electrochemical, and theoretical analysis. *J. Am. Chem. Soc.* **2015**, *137*, 4610−4613.

(54) Higaki, T.; Zhou, M.; Lambright, K. J.; Kirschbaum, K.; Sfeir, M. Y.; Jin, R. Sharp transition from nonmetallic Au_{246} to metallic Au_{279} with nascent surface Plasmon resonance. *J. Am. Chem. Soc.* **2018**, *140*, 5691–5695.

(55) Zhou, M.; Higaki, T.; Hu, G.; Sfeir, M. Y.; Chen, Y.; Jiang, D. E.; Jin, R. Three-orders-of-magnitude variation of carrier lifetimes with crystal phase of gold nanoclusters. *Science*, **2019**, *364*, 279–282.

(56) Negishi, Y.; Nakazaki, T.; Malola, S.; Takano, S.; Niihori, Y.; Kurashige, W.; Yamazoe, S.; Tsukuda, T.; Häkkinen, H. A Critical Size for Emergence of Nonbulk Electronic and Geometric Structures in Dodecanethiolate-Protected Au Clusters. *J. Am. Chem. Soc.* **2015**, *137*, 1206–1212.

(57) Wan, X. K.; Wang, J. Q.; Nan, Z. A.; Wang, Q. M. Ligand effects in catalysis by atomically precise gold nanoclusters. *Sci. Adv.* **2017**, *3*, e1701823.

(58) Zheng, K.; Setyawati, M. I.; Leong, D. T.; Xie, J. Surface Ligand Chemistry of Gold Nanoclusters Determines Their Antimicrobial Ability. *Chem. Mater.* **2018**, *30*, 2800–2808.

(59) Zheng, K.; Setyawati, M. I.; Leong, D. T.; Xie, J. Antimicrobial Gold Nanoclusters. *ACS Nano*, **2017**, *11*, 6904–6910.

(60) Chen, Y.; Zeng, C.; Kauffman, D. R.; Jin, R. Tuning the Magic Size of Atomically Precise Gold Nanoclusters via Isomeric Methylbenzenethiols. *Nano Lett.* **2015**, *15*, 3603–3609.

(61) Ackerson, C. J.; Jadzinsky, P. D.; Kornberg, R. D. Thiolate Ligands for Synthesis of Water-Soluble Gold Clusters. *J. Am. Chem. Soc.* **2005**, *127*, 6550–6551.

(62) Knoppe, S.; Bürgi, T. Chirality in Thiolate-protected Gold Clusters. *Acc. Chem. Res.* **2014**, *47*, 1318–1326.

(63) Yang, H.; Wang, Y.; Lei, J.; Shi, L.; Wu, X.; Makinen, V.; Lin, S.; Tang, Z.; He, J.; Hakkinen, H.; Zheng, L.; Zheng, N. Ligand-Stabilized $Au_{13}Cu_x$ (x = 2, 4, 8) Bimetallic Nanoclusters: Ligand Engineering to Control the Exposure of Metal Sites. *J. Am. Chem. Soc.* **2013**, *135*, 9568–9571.

(64) Yuan, X.; Goswami, N.; Chen, W.; Yao, Q.; Xie, J. Insights into the Effect of Surface Ligands on the Optical Properties of Thiolated Au_{25} Nanoclusters. *Chem. Commun.* **2016**, *52*, 5234–5237.

(65) Parker, J. F.; Weaver, J. E.; McCallum, F.; Fields-Zinna, C. A.; Murray, R. W. Synthesis of monodisperse $[Oct_4N^+][Au_{25}(SR)_{18}^-]$ nanoparticles, with some mechanistic observations. *Langmuir* **2010**, *26*, 13650–13654.

(66) Yuan, X.; Zhang, B.; Luo, Z.; Yao, Q.; Leong, D. T.; Yan, N.; Xie, J. Balancing the rate of cluster growth and etching for gram-scale synthesis of thiolate-protected Au_{25} nanoclusters with atomic precision. *Angew. Chem., Int. Ed.* **2014**, *53*, 4623–4627.

(67) Qian, H.; Zhu, Y.; Jin, R. Size-focusing synthesis, optical and electrochemical properties of monodisperse $Au_{38}(SC_2H_4Ph)_{24}$ nanoclusters. *ACS Nano* **2009**, *3*, 3795–3803.

(68) Zeng, C.; Chen, Y.; Li, G.; Jin, R. Magic size Au64 $(S\text{-}c\text{-}C_6H_{11})_{32}$ nanocluster

protected by cyclohexanethiolate. *Chem. Mater.* **2014**,*26*, 2635–2641.

(69) Li, G.; Zeng, C.; Jin, R. Thermally robust $Au_{99}(SPh)_{42}$ nanoclusters for chemoselective hydrogenation of nitrobenzaldehyde derivatives in water. *J. Am. Chem. Soc.* **2014**, *136*, 3673–3679.

(70) Qian, H.; Jin, R. Ambient synthesis of $Au_{144}(SR)_{60}$ nanoclusters in methanol. *Chem. Mater.* **2011**, *23*, 2209–2217.

(71) Tracy, J. B.; Crowe, M. C.; Parker, J. F.; Hampe, O.; Fields-Zinna, C. A.; Dass, A.; Murray, R. W. Electrospray ionization mass spectrometry of uniform and mixed monolayer nanoparticles: $Au_{25}[S(CH_2)_2Ph]_{18}$ and $Au_{25}[S(CH_2)_2Ph]_{18-x}(SR)_x$. *J. Am. Chem. Soc.* **2007**, *129*, 16209–16215.

(72) Dass, A.; Stevenson, A.; Dubay, G. R.; Tracy, J. B.; Murray, R. W. Nanoparticle MALDI-TOF mass spectrometry without fragmentation: $Au_{25}(SCH_2CH_2Ph)_{18}$ and mixed monolayer $Au_{25}(SCH_2CH_2Ph)_{18-x}(L)_x$. *J. Am. Chem. Soc.* **2008**, *130*, 5940–5946.

(73) Fields-Zinna, C. A.; Parker, J. F.; Murray, R. W. Mass spectrometry of ligand exchange chelation of the nanoparticle $[Au_{25}(SCH_2CH_2C_6H_5)_{18}]^{1-}$ by $CH_3C_6H_3(SH)_2$. *J. Am. Chem. Soc.* **2010**, *132*, 17193–17198.

(74) Ni, T. W.; Tofanelli, M. A.; Phillips, B. D.; Ackerson, C. J. Structural basis for ligand exchange on $Au_{25}(SR)_{18}$. *Inorg. Chem.* **2014**, *53*, 6500–6502.

(75) Zeng, C.; Liu, C.; Chen, Y.; Rosi, N. L.; Jin, R. Gold−thiolate ring as a protecting motif in the $Au_{20}(SR)_{16}$ nanocluster and implications. *J. Am. Chem. Soc.***2014**, *136*, 11922−11925.

(76) Zeng, C.; Liu, C.; Pei, Y.; Jin, R. Thiol ligand-induced transformation of $Au_{38}(SC_2H_4Ph)_{24}$ to $Au_{36}(SPh\text{-}t\text{-}Bu)_{24}$. *ACS Nano* **2013**, *7*, 6138–6145.

(77) Zeng, C.; Chen, Y.; Kirschbaum, K.; Appavoo, K.; Sfeir, M. Y.; Jin, R. Structural patterns at all scales in a nonmetallic chiral $Au_{133}(SR)_{52}$ nanoparticle. *Sci. Adv.* **2015**, *1*, e1500045.

(78) Schaaff, T. G.; Knight, G.; Shafigullin, M. N.; Borkman, R. F.; Whetten, R. L. *J. Phys. Chem. B* **1998**, *102*, 10643−10646.

(79) Schaaff, T. G.; Whetten, R. L. Giant Gold−Glutathione Cluster Compounds: Intense Optical Activity in Metal-Based Transitions. *J. Phys. Chem. B* **2000**, *104*, 2630−2641.

(80) Negishi, Y.; Takasugi, Y.; Sato, S.; Yao, H.; Kimura, K.; Tsukuda, T. Magic-Numbered Au_n Clusters Protected by Glutathione Monolayers (n = 18, 21, 25, 28, 32, 39): Isolation and Spectroscopic Characterization. *J. Am. Chem. Soc.* **2004**, *126*, 6518–6519.

(81) Ghosh, A.; Hassinen, J.; Pulkkinen, P.; Tenhu, H.; Ras, R. H. A.; Pradeep, T. Simple and Efficient Separation of Atomically Precise Noble Metal Clusters. *Anal. Chem.* **2014**, *86*, 12185–12190.

(82) Cliffel, D. E.; Zamborini, F. P.; Gross, S. M.; Murray, R. W. Mercaptoammonium-Monolayer-Protected, Water-Soluble Gold, Silver, and Palladium Clusters. *Langmuir* **2000**, *16*, 9699–9702.

(83) Tetsu, Y.; Shin-ya, O.; Nobuo, K.; Metal Coating of DNA Molecules by Cationic, Metastable Gold Nanoparticles. *Chem. Lett.* **2002**, *31*, 1172-1173.

(84) McIntosh, C. M.; Esposito, E. A.; Boal, A. K.; Simard, J. M.; Martin, C. T.; Rotello, V. M. Inhibition of DNA Transcription Using Cationic Mixed Monolayer Protected Gold Clusters. *J. Am. Chem. Soc.* **2001**, *123*, 7626–7629.

(85) Cho, T. J.; MacCuspie, R. I.; Gigault, J.; Gorham, J. M.; Elliott, J. T.; Hackley, V. A. Highly Stable Positively Charged Dendron-Encapsulated Gold Nanoparticles. *Langmuir* **2014**, *30*, 3883–3893.

(86) Yonezawa, T.; Genda, H.; Koumoto, K. Cationic Silver Nanoparticles Dispersed in Water Prepared From Insoluble Salts. *Chem. Lett.* **2003**, 194–195.

(87) Hoque, M. M.; Black, D. M.; Mayer, K. M.; Dass, A.; Whetten, R. L. The Base Side of Noble Metal Clusters: Efficient Route to Captamino-Gold, $Au_n(-S(CH_2)_2N(CH_3)_2)_p$, n= 25–144. *J. Phys. Chem. Lett.* **2019**, *10*, 3307−3311.

(88) Hoque, M. M.; Dass, A.; Mayer, K. M.; Whetten, R. L. Protein-like Large Gold Clusters Based on the ω-Amino-Thiolate DMAET: Precision Thermal and Reaction Control Leads to Selective Formation of Cationic Gold Clusters in the Critical Size Range, n= 130–144 Au Atoms. *J. Phys. Chem. C* **2019**, *123*, 14871−14879.

(89) Fields-Zinna, C. A.; Sardar, R.; Beasley, C. A.; Murray, R. W. Electrospray Ionization Mass Spectrometry of Intrinsically Cationized Nanoparticles, $[Au_{144/146}(SC_{11}H_{22}N(CH_2CH_3)_3{}^{3+})_X\text{-}(S(CH_2)_5CH_3)_Y]^{X+}$. *J. Am. Chem. Soc.* **2009**, *131*, 16266−16271.

(90) Ackerson, C. J.; Jadzinsky, P. D.; Kornberg, R. D., Thiolate Ligands for Synthesis of Water-Soluble Gold Clusters. *Journal of the American Chemical Society* **2005**, *127*, 6550−6551.

(91) Ishida, Y.; Narita, K.; Yonezawa, T.; Whetten, R. L. Fully Cationized Gold Clusters: Synthesis of $Au_{25}(SR^+)_{18}$. *J. Phys. Chem. Lett.* **2016**, *7*, 3718−3722.

(92) Ishida, Y.; Huang, Y.-L.; Yonezawa, T.; Narita, K. Charge Neutralization Strategy: A Novel Synthetic Approach to Fully Cationized Thiolate-Protected $Au_{25}(SR^+)_{18}$ Clusters with Atomic Precision. *ChemNanoMat* **2017**, *3*, 298−302.

(93) Narita, K.; Ishida, Y.; Yonezawa, T; Huang, Z. Super Polycationic Molecular Compounds: $Au_{144}(SR^{+})_{60}$ Clusters. *J. Phys. Chem. C* **2019**, *123*, 21768−21773.

(94) Huang, Z.; Ishida, Y.; Narita, K.; Yonezawa, T. Kinetics of Cationic-Ligand-Exchange Reactions in Au_{25} Nanoclusters. *J. Phys. Chem. C* **2018**, *122*, 18142−18150.

(95) Huang, Z.; Ishida, Y.; Yonezawa, T. Basic $[Au_{25}(SCH_2CH_2Py)_{18}]^{-} \cdot Na^{+}$ Clusters: Synthesis, Layered Crystallographic Arrangement, and Unique Surface Protonation. *Angew. Chem., Int. Ed.* **2019**, *58*, 13411–13415.

(96) Corpuz, R. D.; Ishida, Y.; Yonezawa, T. Controlling an Electrostatic Repulsion by Oppositely Charged Surfactants Towards Positively Charged Fluorescent Gold Nanoclusters. *Phys. Chem. Chem. Phys.* **2016**, *18*, 8773–8776.

(97) Daniel, M. C.; Astruc, D. Gold nanoparticles: assembly, supramolecular chemistry, quantum-size-related properties, and applications toward biology, catalysis, and nanotechnology. *Chem. Rev.* **2004,** *104*, 293–346.

(98) Jain, P. K.; El-Sayed, I. H.; El-Sayed, M. A. Au nanoparticles target cancer. *Nano Today*, **2007**, *2*, 18–29.

(99) Saha, K.; Agasti, S. S.; Kim, C.; Li, X.; Rotello, V. M. Gold nanoparticles in chemical and biological sensing. *Chem. Rev.* **2012**, *112*, 2739–2779.

(100) Sperling, R. A.; Gil, P. R.; Zhang, F.; Zanella, M.; Parak, W. J. Biological applications of gold nanoparticles. *Chem. Soc. Rev.* **2008**, *37*, 1896–1908.

(101) Fedlheim, D. L.; Foss, C. A. *Metal nanoparticles: synthesis, characterization, and applications*. **2001**, CRC press.

(102) Rosi, N. L.; Mirkin, C. A. Nanostructures in biodiagnostics. *Chem. Rev.* **2005**, *105*, 1547–1562.

(103) Allen, C.; Qiu, T. A.; Pramanik, S.; Buchman, J. T.; Krause, M. O.; Murphy, C. J. Research highlights: investigating the role of nanoparticle surface charge in nano–bio interactions. *Environ. Sci.: Nano* **2017**, *4*, 741−746.

(104) Albanese, A.; Tang, P. S.; Chan, W. C. The effect of nanoparticle size, shape, and surface chemistry on biological systems. *Annu. Rev. Biomed. Eng.* **2012**, *14*, 1−16.

(105) Fröhlich, E. The role of surface charge in cellular uptake and cytotoxicity of medical nanoparticles. *Int. J. Nanomed.* **2012**, *7*, 5577−5591.

(106) Verma, A.; Stellacci, F. Effect of surface properties on nanoparticle-cell interactions. *Small* **2010**, *6*, 12−21.

(107) Jo, D. H.; Kim, J. H.; Lee, T. G.; Kim, J. H. Size, surface charge, and shape determine therapeutic effects of nanoparticles on brain and retinal diseases. *Nanomed- Nanotechnol.* **2015**, *11*, 1603−1611.

(108) Quan, X.; Peng, C.; Zhao, D.; Li, L.; Fan, J.; Zhou, J. Molecular understanding of the penetration of functionalized gold nanoparticles into asymmetric membranes. *Langmuir* **2016**, *33*, 361−371.

(109) Elci, S. G.; Jiang, Y.; Yan, B.; Kim, S. T.; Saha, K.; Moyano, D. F.; Tonga, G. Y.; Jackson, L. F.; Rotello, V. M.; Vachet, R. W. Surface charge controls the suborgan biodistributions of gold nanoparticles. *ACS Nano*, **2016**, *10*, 5536−5542.

(110) Goodman, C. M.; Mccusker, C. D.; Yilmaz, T.; Rotello, V. M. Toxicity of Gold Nanoparticles Functionalized with Cationic and Anionic Side Chains. *Bioconjugate Chem.* **2004**, *15*, 897−900.

(111) Canepa, E.; Salassi, S.; Simonelli, F.; Ferrando, R.; Rolandi, R.; Lambruschini, C.; Canepa, F.; Dante, S.; Relini, A.; Rossi, G. Non-disruptive uptake of anionic and

cationic gold nanoparticles in neutral zwitterionic membranes. *Sci. Rep.* **2021**, *11*, 1256.

(112) Charbgoo, F.; Nejabat, M.; Abnous, K.; Soltani, F.; Taghdisi, S. M.; Alibolandi, M.; Shier, W. T.; Steele, T. W. J.; Ramezani, M. Gold nanoparticle should understand protein corona for being a clinical nanomaterial. *J. Control. Release* **2018**, *272*, 39-53.

(113) Zheng, K.; Setyawati, M. I.; Leong, D. T.; Xie, J. Antimicrobial gold nanoclusters. *ACS Nano* **2017**, *11*, 6904−6910.

(114) Gunawardene, P. N.; Corrigan, J. F.; Workentin, M. S. Golden Opportunity: A Clickable Azide-Functionalized $[Au_{25}(SR)_{18}]^-$ Nanocluster Platform for Interfacial Surface Modifications, *J. Am. Chem. Soc.* **2019**, *141*, 11781−11785.

(115) Cui, X.; Wang, J.; Liu, B.; Ling, S.; Long, R.; Xiong, Y. Turning Au Nanoclusters Catalytically Active for Visible-Light-Driven CO_2 Reduction through Bridging Ligands, *J. Am. Chem. Soc.* **2018**, *140*, 16514−16520.

Chapter 2

Fully Cationized Gold Clusters: Synthesis of $Au_{25}(SR^{+})_{18}$

2.1 Introduction

Thiolate-protected gold (Au) clusters are ultra-small Au particles stabilized by a number of thiolate ligands with core diameters of < 2 nm.[1-5] Owing to the strong quantum confinement effects operative such core size ranges, Au clusters exhibit interesting molecular-like HOMO-LUMO transitions and other functional properties, which make them promising as new nanomaterials applicable in diverse fields, including energy conversion[6], catalysis[7], and bioimaging.[8-10] Recent advances in their synthesis, as well as isolation and characterization techniques, have revealed a series of magic clusters that exhibit extraordinary stability, such as $Au_{25}(SR)_{18}$, $Au_{38}(SR)_{24}$, $Au_{44}(SR)_{28}$, $Au_{68}(SR)_{34}$, $Au_{102}(SR)_{44}$, and $Au_{144}(SR)_{60}$ (where SR represents thiolate ligand).[4,5,10,11] Among them, the smallest magic cluster, $Au_{25}(SR)_{18}$, has been intensively studied due to its ease of synthesis and characterization by mass spectrometry.

There are two commonly exploited systems for $Au_{25}(SR)_{18}$ clusters that involve the use of neutral and anionic thiolate ligands, such as alkanethiols, 2-phenylethanethiol, glutathione, and several mercaptocarboxylic acids.[3-5,11-16] However, there is no established method for the synthesis of $Au_{25}(SR)_{18}$ clusters using cationic thiols. Indeed, the formation of cationic thiolate-protected Au clusters may be limited on the basis of two possible mechanisms: (i) coulombic attraction between cationic thiol (SR^{+}) and anionic Au ion ($AuCl_4^{-}$) and (ii) strong coulombic repulsion between the

cationic ligands on the surface of Au clusters. In the case of the former, the common synthetic method for $Au_{25}(SR)_{18}$ involves the formation of a Au(I)−SR complex as an initial step. When a cationic thiol is adopted, the anionic Au(I) group and cationic SR^+ easily form an ionic complex via coulombic interaction. Because the formation of ionic complexes drastically changes the solubility of the Au(I)−SR species in a reaction solvent, the homogeneous reduction and growth of the Au clusters are highly restricted. Atomically pure cationic Au clusters are thus difficult to produce. With respect to issue (ii), cationic groups such as trimethylammonium or methylpyridinium groups have positive charges under any pH conditions. Because the cationic groups would be densely populated on the surface of a very small Au cluster (depending on the ligand's chain length and cluster size), the coulombic repulsion between the cationic ligands on the cluster surface would be strong and able to decompose the Au_{25} structure, as reported for anionic charged Au_{25}(mercaptocarboxylic acid)$_{18}$ clusters with different chain lengths.[17] This rapid decomposition of the cluster structures due to the surface charge makes the synthesis difficult. Au clusters capped with thiolate ligands bearing amino groups ($-NH_2$) such as cysteamine, which can be cationized via protonation under acidic conditions, have, on the contrary, been stably obtained.[16,18,19]

Predictably, because of the aforementioned mechanistic considerations, cationic thiolate-protected molecular Au clusters have not yet been synthesized. Several reports have described the use of cationic thiols for the synthesis of gold or other metal nanoparticles with diameters exceeding ca. 2 nm.[20−23] A cationized Au cluster has only been reported for a mixture of $Au_{144/146}$ clusters through the partial ligand exchange of the initial hexanethiolate with a cationic thiolate ligand with an uncontrollable exchange ratio.[24] A very small, fluorescent, cationic Au cluster has also been reported; however, its

composition could not be ascertained and remains unknown.[25] Cationic thiolate-protected Au clusters are expected to play a significant role in bioimaging and sensing, as cellular proteins show higher affinity for positively charged nanocomposites than for neutral and anionic nanocomposites. We hereby report the first synthesis of fully cationized thiolate-protected $Au_{25}(SR^{+})_{18}$ clusters. The key strategy was the control of the coulombic interactions between the cationic thiolates and precursor Au ions.

2.2 Experimental section

2.2.1 Chemicals

Hydrogen tetrachloroaurate (III) ($HAuCl_4 \cdot 4H_2O$, >99.99%, Wako), (11-mercaptoundecyl)-*N*,*N*,*N*-trimethylammonium bromide ($SR^+ \cdot Br^-$, 99%, Aldrich), sodium hydroxide (NaOH, 97%, Junsei), potassium hexafluorophosphate (KPF_6, 99%, Wako), sodium borohydride ($NaBH_4$, 99%, Wako), were used as received without further purification. The counter ions of thiol ligand was exchanged to Cl^- by using ion-exchange column (Organo Amberlite IRA400JCL) before the use. Deionized pure water (>18.2 MΩ) was prepared by an Organo/ELGA PURELAB system.

2.2.2 Synthesis of $Au_{25}(SR^+)_{18}$ clusters

The fully cationized thiolate-protected $Au_{25}(SR^+)_{18}$ clusters were synthesized after modification of the NaOH-mediated $NaBH_4$ reduction method reported by Xie's group.[16] In brief, aqueous solutions of $HAuCl_4$ (20 mM) and the thiolate ligand, (11-mercaptoundecyl)-*N*,*N*,*N*-trimethylammonium chloride ($-S(CH_2)_{11}N(CH_3)_3^+ \cdot Cl^-$: SR^+) (80 mM), were prepared. In a water (2.5 mL)−ethanol (4 mL) solution, the $HAuCl_4$ (1.0 mL) and SR^+ aq. solutions (0.5 mL) (Au:SR^+ mol ratio 1:2) were mixed to form the Au(I)−SR complex. After stirring for 5 min, the solution became colorless; then, 1 M NaOH aq. (0.2 mL) was added, followed by the addition of $NaBH_4$ solution (0.2 mL, 21.5 mg in 5 mL 0.2 M NaOH aq.). Note that it is necessary to replace the Br^- counterion of the purchased cationic thiolate ligand SR^+ with Cl^- using an ion-exchange resin because the Br^- decomposes the Au cluster via oxidation as previously reported.[26] The described synthesis fails when Br^- is used as the counterion.

An optimized concentration of NaOH in the reaction solution in this protocol has

a significant impact. NaOH not only decreases the reduction ability of $NaBH_4$ due to its self-hydrolysis but also increases the etching ability of the free thiolate ligands due to the deprotonation of the sulfhydryl (RS−H) groups in alkaline solution. The well-balanced reversible reaction for Au_{25} cluster formation, thanks to the weakened reduction capability and improved etching rates, results in the rapid formation (3h) of the thermodynamically stable Au_{25} clusters. It is also important to note that this NaOH-mediated synthesis has crucial advantages toward fully cationized Au clusters. First, the addition of NaOH suppresses the formation of the ionic complex between the $AuCl_4^-$ anion and SR^+, which is thought to hinder the homogeneous reduction and growth of Au clusters (mechanism (i) described above). Second, the short reaction time (3h) compared with other common syntheses (typically 1-4 days[3−5,11−16]) enables the formation of Au_{25} clusters before the cluster structures decompose as a result of the densely populated cationic groups on the cluster surfaces (mechanism (ii)).

After reacting for 3h, ethanolic KPF_6 solution (50 mM, 3 mL) was added to the reaction solution in order to displace the Cl^- and OH^- counterions with PF_6^-. This treatment is crucial for the observation of the electrospray ionization mass spectra (ESI-MS), as described later. The resultant brown precipitate was dissolved in acetonitrile and purified by repeated reprecipitation with dichloromethane, ethanol, and water, to afford a mixture of $Au_{25}^{\pm0}(S(CH_2)_{11}N(CH_3)_3^+)_{18}\cdot(PF_6^-)_{18}$ and $Au_{25}^{-1}(S(CH_2)_{11}N(CH_3)_3^+)_{18}\cdot(PF_6^-)_{17}$ (ca. 1.5 mg, 16% yield based on Au, see below).

2.2.3 Characterization

UV-Vis absorption spectra of the obtained samples in acetonitrile were recorded using a JASCO V-630 spectrophotometer using a glass cuvette with a 10 mm optical path. Electrospray Ionization Mass Spectrometry (ESI-MS) was performed using a Bruker

Daltonics micrOTOF-HS mass spectrometer. The sample in acetonitrile solution was directly infused at 400 μL/min. The concentration of the infused solution was 1 μM. For the data shown here, a 0-3000 *m/z* mass spectrometer acquisition range was used. The nebulizer pressure was set to 0.4 bar, and the sheath gas was set to 4.0 L/min. The dry temperature was kept at 180 °C. The electrospray emitter potential was held at 4000 V (positive mode). The capillary exit, skimmer 1, hexapole 1, and skimmer 2 voltage settings were 70, 30, 23, and 24 V, respectively.

2.3 Results and discussion

2.3.1 Optical absorption spectroscopy

The as-synthesized Au clusters were characterized by optical absorption spectroscopy. As shown in Figure 2.1, the obtained Au clusters exhibit two distinct absorption peaks at 441 and 677 nm and two weak peaks at 546 and 783 nm, which correspond well to the reported characteristic absorptions of thiolate-protected Au_{25} clusters.[4,27,28] The energy band at 677 nm corresponds to the HOMO-LUMO transition of the Au_{25} structure, as previously reported.[27] The absorption spectrum suggests that highly pure Au_{25} clusters were produced. In addition, the relatively broad absorption peaks suggest that a mixture of two types of core charge states (Au_{25}^{-1} and $Au_{25}^{\pm0}$) was obtained, as reported in the literature.[29]

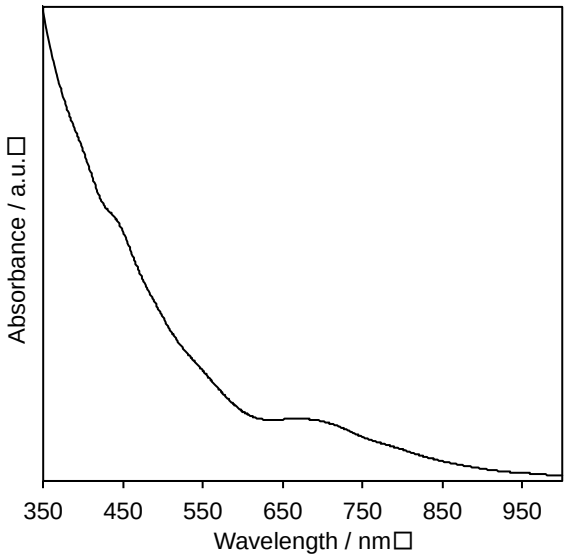

Figure 2.1 Absorption spectrum of the obtained Au cluster dissolved in acetonitrile.

2.3.2 ESI-MS

Figure 2.2 shows the mass spectrometric evidence of the fully cationized Au_{25} clusters in acetonitrile solution, obtained by positive-mode high-resolution ESI-MS. The wide spectrum in Figure 2.2(i) shows prominent groups of peaks for the 4+ to 14+ charge states, labeled *a*-*v*, which are assigned to $Au_{25}^{-1/\pm0}(SR^{+})_{18}\cdot(PF_6^{-})_{3\text{-}14}$, wherein two types of core charge states (Au_{25}^{-1} and $Au_{25}^{\pm0}$) and a varying number of counterions $(PF_6^{-})_{3\text{-}14}$ can be identified. The relatively broad absorption peak observed in Figure 2.1 supports the observation of both Au_{25}^{-1} and $Au_{25}^{\pm0}$ core charges in the spectrum. It is important to note that these multiple charge states from 4+ to 14+ charges with varied "ion-pairing" with PF_6^{-} counteranions are first observed in molecular Au clusters. Moreover, the well-known fragmentation product, $Au_4(SR^{+})_4$, with different numbers of counterions $(PF_6^{-})_{0\text{–}2}$ (labeled as *Fa*-*Fc*) is also observed. The compositions and charge assignments of each peak (*a*-*v*, *Fa*-*Fc*) are summarized in Table 2.1. Expanded ESI-MS spectra for several observed peaks are shown in Figures 2.2(ii)-(v), with simulated isotope patterns as red lines (see other expanded spectra in the Supporting Information). The isotope distributions closely match the simulated spectra.

It is important to note that the PF_6^{-} counterions play dominant roles in both the acetonitrile solubility and the ESI-MS observations. The synthesized products lacking the KPF_6 treatment (i.e., having Cl^{-} or OH^{-} counteranions), when dissolved in water or methanol, did not produce any peaks attributable to $Au_{25}(SR^{+})_{18}$ by ESI-MS. As shown in Figure 2.2, all the observed $Au_{25}(SR^{+})_{18}$ peaks have varying numbers of PF_6^{-} groups as counterions, and no $Au_{25}(SR^{+})_{18}^{18+}$ without PF_6^{-} was observed. These results strongly suggest that an appropriate number of cationic charges must be neutralized, or "ion-paired", in the $Au_{25}(SR^{+})_{18}$ by the appropriate number of PF_6^{-} counteranions. The

strongest peak observed for the Au_{25} cluster is $[Au_{25}^{\pm0}(SR^{+})_{18}\cdot(PF_6^{-})_9]^{9+}$ (peak *l* in Figure 2.2). Under the electrospray conditions, the peak intensity of the Au_{25} cluster decreases when it is neutralized to a greater (9+) extent.

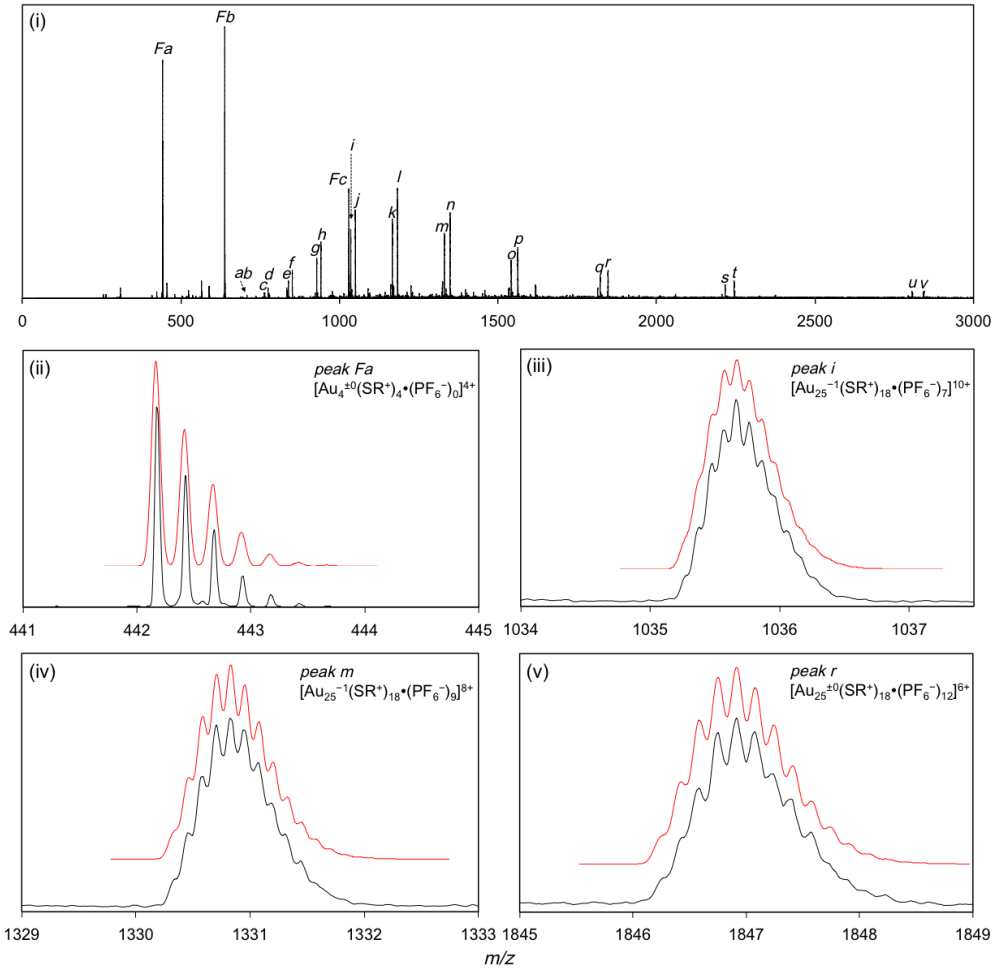

Figure 2.2 Wide range (i) and magnified (ii-v) positive mode high-resolution electrospray ionization mass spectra (ESI-MS) of the obtained fully cationized $Au_{25}(SR^{+})_{18}$ clusters. Black lines indicate the observed data, and red lines in (ii-v) indicate the simulated isotope patterns. Other magnified spectra are shown in Supporting Information. Structural and charge assignments of each peak (*a-v*, *Fa-Fc*) are summarized in Table 2.1.

Table 2.1 Structural and charge assignments of ESI-MS in Figure 2.2

peak	Structure	Charge state	*m/z* (obs.)	*m/z* (calc.)
a	$Au_{25}^{-1}(SR^{+})_{18}\bullet(PF_6^{-})_3$	14+	698.37	698.36
b	$Au_{25}^{\pm0}(SR^{+})_{18}\bullet(PF_6^{-})_4$	14+	708.71	708.71
c	$Au_{25}^{-1}(SR^{+})_{18}\bullet(PF_6^{-})_4$	13+	763.20	763.23
d	$Au_{25}^{\pm0}(SR^{+})_{18}\bullet(PF_6^{-})_5$	13+	774.37	774.38
e	$Au_{25}^{-1}(SR^{+})_{18}\bullet(PF_6^{-})_5$	12+	838.90	838.91
f	$Au_{25}^{\pm0}(SR^{+})_{18}\bullet(PF_6^{-})_6$	12+	850.98	850.99
g	$Au_{25}^{-1}(SR^{+})_{18}\bullet(PF_6^{-})_6$	11+	928.34	928.35
h	$Au_{25}^{\pm0}(SR^{+})_{18}\bullet(PF_6^{-})_7$	11+	941.51	941.53
i	$Au_{25}^{-1}(SR^{+})_{18}\bullet(PF_6^{-})_7$	10+	1035.66	1035.68
j	$Au_{25}^{\pm0}(SR^{+})_{18}\bullet(PF_6^{-})_8$	10+	1050.16	1050.18
k	$Au_{25}^{-1}(SR^{+})_{18}\bullet(PF_6^{-})_8$	9+	1166.85	1166.87
l	$Au_{25}^{\pm0}(SR^{+})_{18}\bullet(PF_6^{-})_9$	9+	1182.96	1182.97
m	$Au_{25}^{-1}(SR^{+})_{18}\bullet(PF_6^{-})_9$	8+	1330.83	1330.85
n	$Au_{25}^{\pm0}(SR^{+})_{18}\bullet(PF_6^{-})_{10}$	8+	1348.95	1348.97
o	$Au_{25}^{-1}(SR^{+})_{18}\bullet(PF_6^{-})_{10}$	7+	1541.65	1541.67
p	$Au_{25}^{\pm0}(SR^{+})_{18}\bullet(PF_6^{-})_{11}$	7+	1562.36	1562.38
q	$Au_{25}^{-1}(SR^{+})_{18}\bullet(PF_6^{-})_{11}$	6+	1822.76	1822.78
r	$Au_{25}^{\pm0}(SR^{+})_{18}\bullet(PF_6^{-})_{12}$	6+	1846.91	1846.94
s	$Au_{25}^{-1}(SR^{+})_{18}\bullet(PF_6^{-})_{12}$	5+	2216.30	2216.33
t	$Au_{25}^{\pm0}(SR^{+})_{18}\bullet(PF_6^{-})_{13}$	5+	2245.27	2245.32
u	$Au_{25}^{-1}(SR^{+})_{18}\bullet(PF_6^{-})_{13}$	4+	2806.62	2806.65
v	$Au_{25}^{\pm0}(SR^{+})_{18}\bullet(PF_6^{-})_{14}$	4+	2842.82	2842.90
		Fragments		
Fa	$Au_4(SR^{+})_4\bullet(PF_6^{-})_0$	4+	442.17	442.18
Fb	$Au_4(SR^{+})_4\bullet(PF_6^{-})_1$	3+	637.89	637.90
Fc	$Au_4(SR^{+})_4\bullet(PF_6^{-})_2$	2+	1029.32	1029.33

2.4 Conclusion

Many kinds of neutral and anionic Au clusters have been reported, so far. This chapter has demonstrated here the final piece of the series of thiolate-protected Au cluster molecules: fully cationized $Au_{25}(SR^{+})_{18}$ clusters. This study would widen the spectrum of Au cluster chemistry. The fully cationized clusters should show advantages, provided by their affinity toward negative substrates, in materials and biomedical applications. The synthesis methods of this study may prove applicable to larger noble-metal clusters and to other cation ligands, where different chain length could vary the effect of cationic charge on the electric state of Au cluster core.

2.5 Supporting information

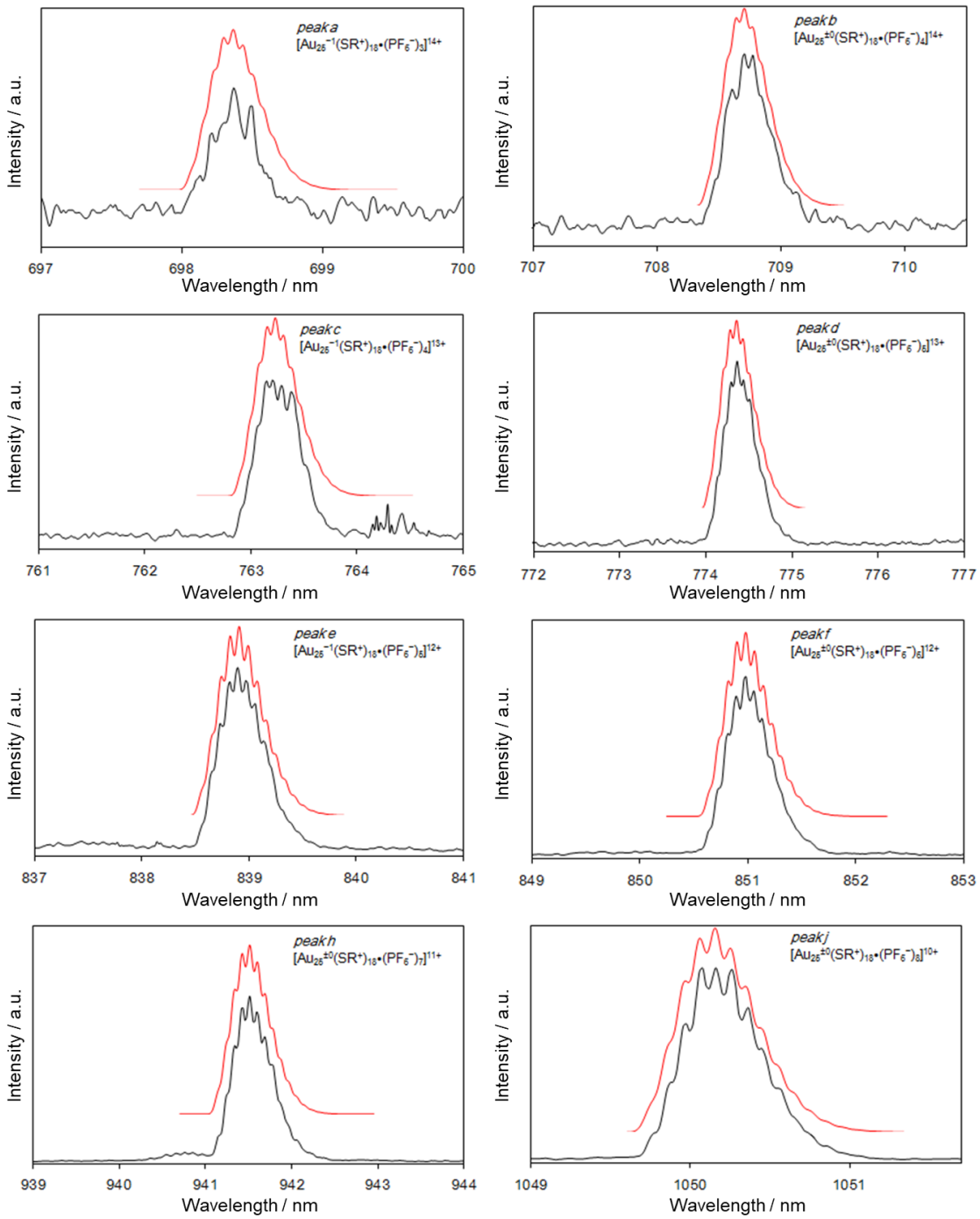

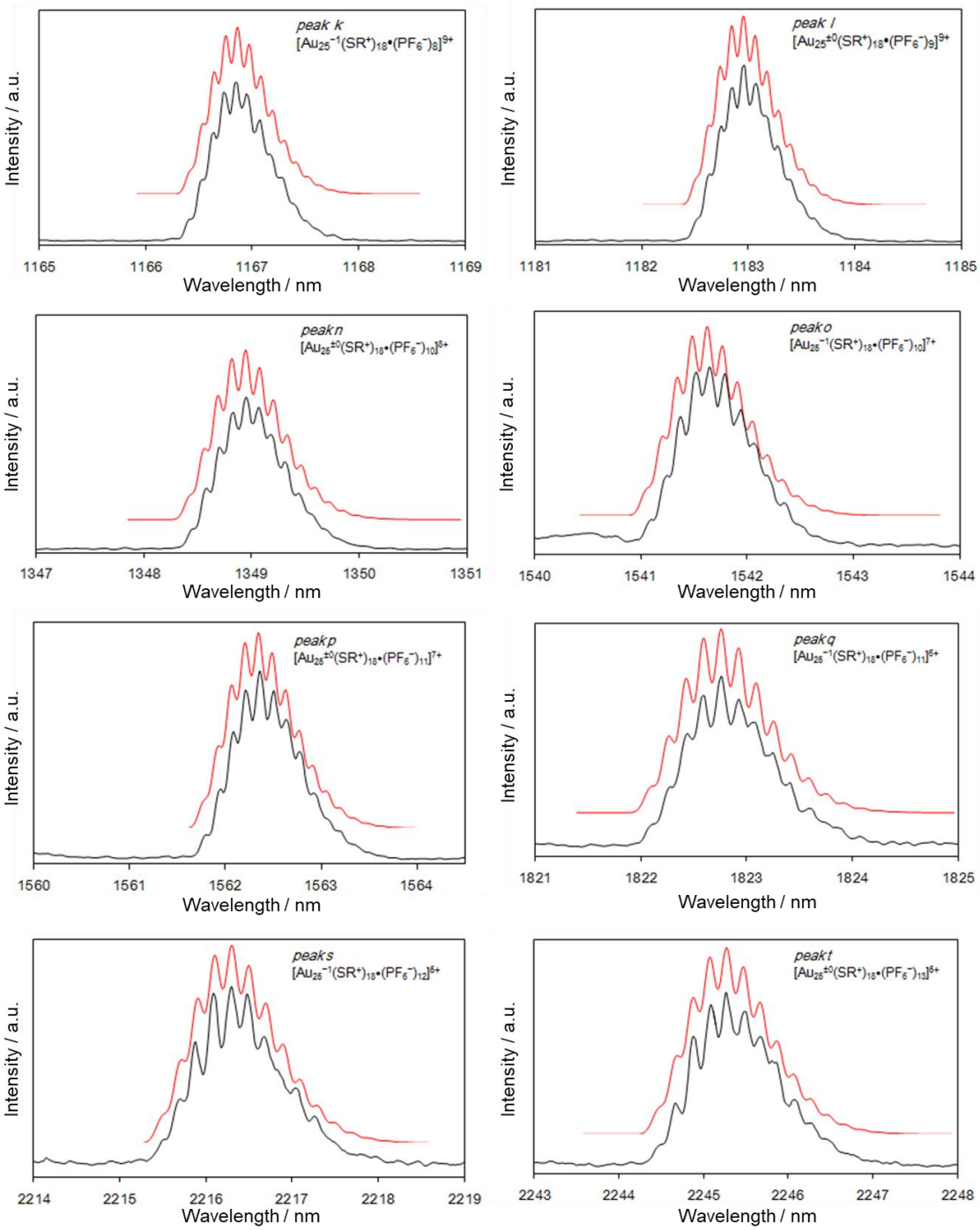
peak k
$[Au_{25}^{-1}(SR^{+})_{18}\bullet(PF_6^{-})_8]^{9+}$
peak l
$[Au_{25}^{\pm0}(SR^{+})_{18}\bullet(PF_6^{-})_9]^{9+}$
peak n
$[Au_{25}^{\pm0}(SR^{+})_{18}\bullet(PF_6^{-})_{10}]^{8+}$
peak o
$[Au_{25}^{-1}(SR^{+})_{18}\bullet(PF_6^{-})_{10}]^{7+}$
peak p
$[Au_{25}^{\pm0}(SR^{+})_{18}\bullet(PF_6^{-})_{11}]^{7+}$
peak q
$[Au_{25}^{-1}(SR^{+})_{18}\bullet(PF_6^{-})_{11}]^{6+}$
peak s
$[Au_{25}^{-1}(SR^{+})_{18}\bullet(PF_6^{-})_{12}]^{6+}$
peak t
$[Au_{25}^{\pm0}(SR^{+})_{18}\bullet(PF_6^{-})_{13}]^{6+}$
Intensity / a.u.
Wavelength / nm
1165 1166 1167 1168 1169
1181 1182 1183 1184 1185
1347 1348 1349 1350 1351
1540 1541 1542 1543 1544
1560 1561 1562 1563 1564
1821 1822 1823 1824 1825
2214 2215 2216 2217 2218 2219
2243 2244 2245 2246 2247 2248

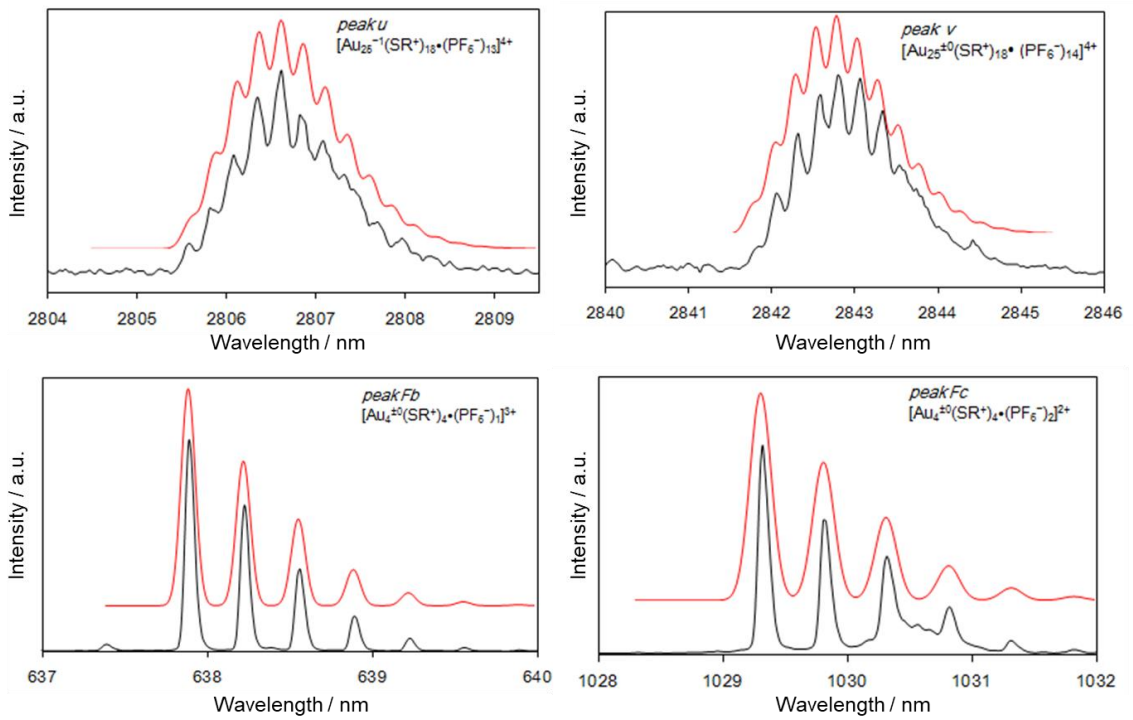

Figure S2.1 Magnified ESI-MS (black lines) and simulations (red lines) for peaks summarized in Table 2.1 in the main text.

2.6 References

(1) Whetten, R. L.; Khoury, J. T.; Alvarez, M. M.; Murthy, S.; Vezmar, I.; Wang, Z. L.; Stephens, P. W.; Cleveland, C. L.; Luedtke, W. D.; Landman, U. Nanocrystal Gold Molecules. *Adv. Mater.* **1996**, *8*, 428−433.

(2) Schaaff, T. G.; Whetten, R. L. Giant Gold−Glutathione Cluster Compounds: Intense Optical Activity in Metal-Based Transitions. *J. Phys. Chem. B* **2000**, *104*, 2630−2641.

(3) Price, R. C.; Whetten, R. L. All-Aromatic, Nanometer-Scale, Gold-Cluster Thiolate Complexes. *J. Am. Chem. Soc.* **2005**, *127*, 13750−13751.

(4) Negishi, Y.; Chaki, N. K.; Shichibu, Y.; Whetten, R. L.; Tsukuda, T. Origin of Magic Stability of Thiolated Gold Clusters: a Case Study on $Au_{25}(SC_6H_{13})_{18}$. *J. Am. Chem. Soc.* **2007**, *129*, 11322−11323.

(5) Tsukuda, T. Toward an Atomic-Level Understanding of Size-Specific Properties of Protected and Stabilized Gold Clusters. *Bull. Chem. Soc. Jpn.* **2012**, *85*, 151−168.

(6) Chen, Y.-S.; Choi, H.; Kamat, P. V. Metal-Cluster-Sensitized Solar Cells, a New Class of Thiolated Gold Sensitizers Delivering Efficiency Greater Than 2%. *J. Am. Chem. Soc.* **2013**, *135*, 8822−8825.

(7) Gao, Y.; Shao, N.; Pei, Y.; Chen, Z.; Zeng, X. C. Catalytic Activities of Subnanometer Gold Clusters (Au_{16}−Au_{18}, Au_{20}, and Au_{27}−Au_{35}) for CO Oxidation. *ACS Nano* **2011**, *5*, 7818−7829.

(8) Zhou, C.; Long, M.; Qin, Y.; Sun, X.; Zheng, J. Luminescent Gold Nanoparticles with Efficient Renal Clearance. *Angew. Chem., Int. Ed.* **2011**, *50*, 3168−3172.

(9) Zhang, L.; Wang, E. Metal Nanoclusters: New Fluorescent Probes for Sensors and Bioimaging. *Nano Today* **2014**, *9*, 132−157.

(10) Alvarez, M. M.; Chen, J.; Plascencia-Villa, G.; Black, D. M.; Griffith, W. P.; Garzon, I. L.; Jose-Yacaman, M.; Demeler, B.; Whetten,´ R. L. Hidden Components in Aqueous "Gold-144" Fractionated by PAGE: High-Resolution Orbitrap ESI−MS Identifies the Gold-102 and Higher All-Aromatic Au-pMBA Cluster Compounds. *J. Phys. Chem. B* **2016**, *120*, 6430−6438.

(11) Kumar, S.; Jin, R. Water-Soluble $Au_{25}(Capt)_{18}$ Nanoclusters: Synthesis, Thermal Stability, and Optical Properties. *Nanoscale* **2012**, *4*, 4222−4227.

(12) Dainese, T.; Antonello, S.; Gascon, J. A.; Pan, F.; Perera, N. V.;´ Ruzzi, M.; Venzo, A.; Zoleo, A.; Rissanen, K.; Maran, F. $Au_{25}(SEt)_{18}$, a Nearly Naked Thiolate-Protected Au_{25} Cluster: Structural Analysis by Single Crystal X-Ray Crystallography and Electron Nuclear Double Resonance. *ACS Nano* **2014**, *8*, 3904−3912.

(13) Heaven, M. W.; Dass, A.; White, P. S.; Holt, K. M.; Murray, R. W. Crystal Structure of the Gold Nanoparticle $[N(C_8H_{17})_4]$-$[Au_{25}(SCH_2CH_2Ph)_{18}]$. *J. Am. Chem. Soc.* **2008**, *130*, 3754−3755.

(14) Dharmaratne, A. C.; Krick, T.; Dass, A. Nanocluster Size Evolution Studied by Mass Spectrometry in Room Temperature $Au_{25}(SR)_{18}$ Synthesis. *J. Am. Chem. Soc.* **2009**, *131*, 13604−13605.

(15) Negishi, Y.; Nobusada, K.; Tsukuda, T. Glutathione-Protected Gold Clusters Revisited: Bridging the Gap Between Gold(I)−Thiolate Complexes and Thiolate-Protected Gold Nanocrystals. *J. Am. Chem. Soc.* **2005**, *127*, 5261−5270.

(16) Yuan, X.; Zhang, B.; Luo, Z.; Yao, Q.; Leong, D. T.; Yan, N.; Xie, J. Balancing the Rate of Cluster Growth and Etching for Gram-Scale Synthesis of Thiolate-Protected Au_{25} Nanoclusters with Atomic Precision. *Angew. Chem., Int. Ed.* **2014**, *53*, 4623−4627.

(17) Yuan, X.; Goswami, N.; Mathews, I.; Yu, Y.; Xie, J. Enhancing Stability Through Ligand-Shell Engineering: a Case Study with $Au_{25}(SR)_{18}$ Nanoclusters. *Nano Res.* **2015**, *8*, 3488−3495.

(18) Liu, J.-M.; Chen, J.-T.; Yan, X.-P. Near Infrared Fluorescent Trypsin Stabilized Gold Nanoclusters as Surface Plasmon Enhanced Energy Transfer Biosensor and in Vivo Cancer Imaging Bioprobe. *Anal. Chem.* **2013**, *85*, 3238−3245.

(19) Shang, L.; Dörlich, R. M.; Trouillet, V.; Bruns, M.; Ulrich Nienhaus, G. Ultrasmall Fluorescent Silver Nanoclusters: Protein Adsorption and Its Effects on Cellular Responses. *Nano Res.* **2012**, *5*, 531−542.

(20) Cho, T. J.; MacCuspie, R. I.; Gigault, J.; Gorham, J. M.; Elliott, J. T.; Hackley, V. A. Highly Stable Positively Charged Dendron-Encapsulated Gold Nanoparticles. *Langmuir* **2014**, *30*, 3883−3893.

(21) Cliffel, D. E.; Zamborini, F. P.; Gross, S. M.; Murray, R. W. Mercaptoammonium-Monolayer-Protected, Water-Soluble Gold, Silver, and Palladium Clusters. Langmuir **2000**, *16*, 9699−9702.

(22) Yonezawa, T.; Onoue, S.-Y.; Kimizuka, N. Metal Coating of DNA Molecules by Cationic, Metastable Gold Nanoparticles. *Chem. Lett.* **2002**, *31*, 1172−1173.

(23) McIntosh, C. M.; Esposito, E. A.; Boal, A. K.; Simard, J. M.; Martin, C. T.; Rotello, V. M. Inhibition of DNA Transcription Using Cationic Mixed Monolayer Protected Gold Clusters. *J. Am. Chem. Soc.* **2001**, *123*, 7626−7629.

(24) Fields-Zinna, C. A.; Sardar, R.; Beasley, C. A.; Murray, R. W. Electrospray Ionization Mass Spectrometry of Intrinsically Cationized Nanoparticles, $[Au_{144/146}(SC_{11}H_{22}N(CH_2CH_3)_3{}^{3+})_X\text{-}(S\text{-}(CH_2)_5CH_{¥})_Y]^{X+}$. *J. Am. Chem. Soc.* **2009**, *131*, 16266−16271.

(25) Corpuz, R. D.; Ishida, Y.; Yonezawa, T. Controlling an Electrostatic Repulsion by Oppositely Charged Surfactants Towards Positively Charged Fluorescent Gold Nanoclusters. *Phys. Chem. Chem. Phys.* **2016**, *18*, 8773−8776.

(26) Zhu, M.; Chan, G.; Qian, H.; Jin, R. Unexpected Reactivity of $Au_{25}(SCH_2CH_2Ph)_{18}$ Nanoclusters with Salts. *Nanoscale* **2011**, *3*, 1703−1707.

(27) Zhu, M.; Aikens, C. M.; Hollander, F. J.; Schatz, G. C.; Jin, R. Correlating the Crystal Structure of a Thiol-Protected Au_{25} Cluster and Optical Properties. *J. Am. Chem. Soc.* **2008**, *130*, 5883−5885.

(28) Parker, J. F.; Fields-Zinna, C. A.; Murray, R. W. The Story of a Monodisperse Gold Nanoparticle: $Au_{25}L_{18}$. *Acc. Chem. Res.* **2010**, *43*, 1289−1296.

(29) Parker, J. F.; Weaver, J. E. F.; McCallum, F.; Fields-Zinna, C. A.; Murray, R. W. Synthesis of Monodisperse $[Oct_4N^+][Au_{25}(SR)_{18}^-]$ Nanoparticles, with Some Mechanistic Observations. *Langmuir* **2010**, *26*, 13650−13654.

Chapter 3

Super Polycationic Molecular Compounds: $Au_{144}(SR^+)_{60}$ Clusters

3.1 Introduction

Investigation of Au cluster synthesis over the past two decades has revealed a series of magic clusters with extraordinary stabilities, including $Au_{25}(SR)_{18}$, $Au_{38}(SR)_{24}$, $Au_{44}(SR)_{28}$, $Au_{68}(SR)_{34}$, $Au_{102}(SR)_{44}$, and $Au_{144}(SR)_{60}$, where SR represents thiolate ligands.[1-6] Precisely size-controlled nanoclusters have been widely pursued because size is a key factor in determining their basic physical and chemical properties.[7-9] Although many Au cluster species with different core sizes and diverse thiolate ligands have been synthesized, only neutral and anionic thiolate ligands, such as 2-phenylethanethiol, alkanethiols, glutathione, and mercaptocarboxylic acid, have been used as protecting groups.[3,5,10-13] When cationic ligands are used for Au cluster synthesis, two limitations are observed during the cluster formation process: (i) Coulombic attraction between the anionic $AuCl_4^-$ and the cationic thiol (SR^+), lowers the solubility of the Au(I)-SR^+ complexes in solution, restricting homogeneous reduction and Au cluster growth, and (ii) coulombic repulsion between the densely populated cationic ligands on the small cluster surface, decreases the thermal stability of the clusters.[14-16] These two limitations have hindered the chemistry of fully cationized molecular Au cluster compounds.

The latest reports by Whetten et al.[17,18] revealed the earlier evidence of polydisperse captamino ($–S(CH_2)_2N(CH_3)_2$)-capped Au clusters with atom numbers ranging from 25-144. A partial ligand exchange reaction of neutral $Au_{144}(SR)_{60}$ with

cationic thiols was investigated by Fields-Zinna et al.,[6] however, only 10-15(+) cationic Au_{144} was detected with an uncontrollable exchange ratio. Recently, Hoque et al.[18] reported an Au_{144} capped with tertiary amine terminated ligands, but it requires protonation in acidic conditions for cationization. These few works seemed to be an exception to the statement made in 2005: "Small positively charged ligands do not support the production of MPCs in the Brust synthesis".[19]

In chapter 2, atomically pure fully cationized $Au_{25}(SR^+)_{18}$ clusters were successfully synthesized using a modified Brust method.[14,15] This chapter reports a new series of cationized Au cluster compounds, among which $Au_{144}(SR^+)_{60}$, is the largest compound reported with the most stable and studied molecular Au cluster (Au_{144}). In this study, Au_{144} clusters capped with all cationic ligands are obtained by direct synthesis using quaternary ammonium terminated ligands (SR^+). The icosahedral Au_{144} structure is of interest due to its extraordinarily high symmetry and compactness, and its 60-fold equivalence of the ligands.[20-24] This challenge will be the key focus for future research on cationized Au clusters because various Au cluster compounds with structures intermediate between our previous ($Au_{25}(SR^+)_{18}$) and current ($Au_{144}(SR^+)_{60}$), such as $Au_{38}(SR^+)_{24}$, $Au_{44}(SR^+)_{28}$, $Au_{68}(SR^+)_{34}$, $Au_{102}(SR^+)_{44}$, are expected to be synthesized using the same strategy (there is a need to optimize the condition of the ratio of $HAuCl_4$, ligands, and $NaBH_4$, reaction time, reaction temperature, solvent, and so on, though). Furthermore, the $Au_{144}(SR^+)_{60}$ cluster compound with +60 charge is, to the best of my knowledge, the most polycationic molecular compound reported this far, while other candidates include polycationic dendrimers (with charges ranging from +4 to +16).[25] Notably, highly charged (+12-+96) supramolecular compounds, such as coordinated frameworks, were reported,[26] however, they are not molecular compounds. Fully

cationized Au_{144} clusters not only have an advantage in the interaction with nano-bio interfaces,[27,28] but may also provide a novel chemical reaction field due to the uniformly and densely located cationic groups on the Au_{144} *pseudo*-sphere.

3.2 Experimental section

3.2.1 Chemicals

Hydrogen tetrachloroaurate (III) ($HAuCl_4 \cdot 4H_2O$, >99.99%, Wako), (11-mercaptoundecyl)-*N*,*N*,*N*-trimethylammonium bromide ($SR^+ \cdot Br^-$, 99%, Aldrich), sodium hydroxide (NaOH, 97%, Junsei), potassium hexafluorophosphate (KPF_6, 99%, Wako), sodium borohydride ($NaBH_4$, 99%, Wako), were used as received without further purification. High-performance liquid chromatography-grade acetonitrile and methanol were purchased from RCI labscan and Wako. Guaranteed reagent grade dichloromethane was purchased from Junsei. Deionized pure water (>18.2 MΩ) was prepared by an Organo/ELGA PURELAB system.

3.2.2 Synthesis of $Au_{144}(SR^+)_{60}$ clusters

The cationized $Au_{144}(SR^+)_{60}$ cluster was synthesized using the following method (Scheme 3.1). $HAuCl_4 \cdot 4H_2O$ (7.4 mg, 18 μmol) and (11-mercaptoundecyl)-*N,N,N*-trimethylammonium bromide ($SR^+ \cdot Br^-$, 18 mg, 55 μmol) were dissolved in a 50:50 methanol-water solution (6 mL) while stirring. After 5 min, the solution turned colorless, indicating the formation of Au(I)-SR^+ complex. This change was followed by the addition of 1 M NaOH aq (0.6 mL). The reaction mixture was stirred for 24 h, then 0.6 mL of an aqueous $NaBH_4$ (3.4 mg, 90 μmol) was added, under vigorous stirring. After 3 h, a KPF_6 aqueous solution (0.1 M, 5 mL) was added to the reaction mixture to precipitate clusters and displace the Cl^- and OH^- counter anions with PF_6^-. The resultant precipitate was

dissolved in acetonitrile and thermal etching was performed (60 °C) for 3 days with excess $SR^{+}\cdot PF_6^{-}$ (55 μmol). Note that thermal etching for 1 day produced impure Au_{144} clusters. After 3 days, the clusters were precipitated by adding a KPF_6 aqueous solution, and washed with water and methanol. At this stage, analysis indicates the sample included two stable clusters, $Au_{25}(SR^{+})_{18}$ and $Au_{144}(SR^{+})_{60}$. To remove the Au_{25} clusters, the resultant brown precipitate was dissolved in acetonitrile (1 mL) and the Au_{144} clusters were selectively reprecipitated by dichloromethane (2 mL), due to their larger size. The synthetic yield was ~30% (in Au basis).

Scheme 3.1 Synthetic scheme of $Au_{144}(SR^{+})_{60}$ clusters.

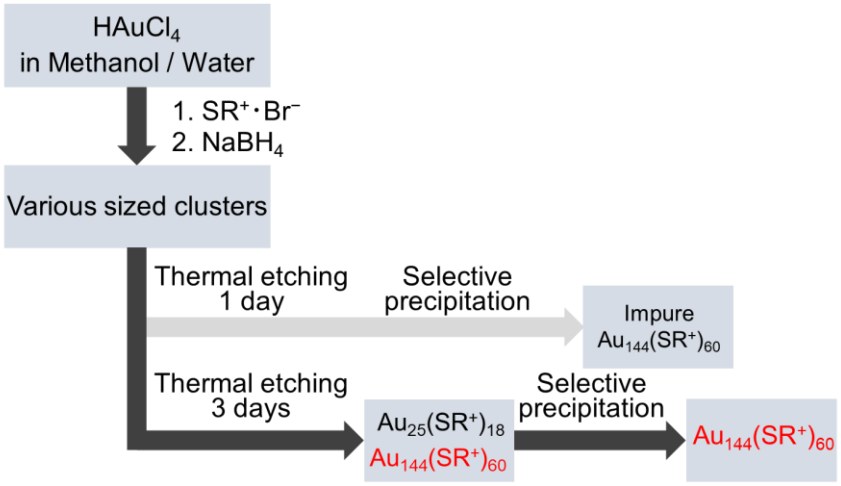

3.2.3 Characterization

UV-Vis absorption spectra of the obtained samples in acetonitrile were recorded using a JASCO V-630 spectrophotometer using a glass cuvette with a 1 mm optical path. Electrospray Ionization Mass Spectrometry (ESI-MS) was performed using a Bruker Daltonics micrOTOF-HS mass spectrometer. The sample in acetonitrile solution was directly infused at 400 μL/min. The concentration of the infused solution was 1 μM. For the data shown here, a 50-10000 *m/z* mass spectrometer acquisition range was used. The nebulizer pressure was set to 0.4 bar, and the sheath gas was set to 4.0 L/min. The dry temperature was kept at 180 °C. The electrospray emitter potential was held at 4000 V (positive mode). The capillary exit, skimmer 1, hexapole 1, and skimmer 2 voltage settings were 120, 70, 23, and 24 V, respectively. TG-DTA was carried out using a thermogravimetry analyzer (TGA, Shimadzu DTG60H). Measurement was operated using air at a flow rate of 100 mL/min; and temperature was increased from room temperature to approximately 500 °C at a heating rate of 0.5 °C/min. Scanning Transmission Electron Microscopy (STEM) images in high-angle annular dark field (HAADF) mode and bright field (BF) mode were acquired using a JEM-ARM200F at 80 kV.

3.3 Results and discussion

3.3.1 Optical absorption spectroscopy

Figure 3.1 shows the UV-Vis absorption spectra for the Au clusters obtained at different synthesis steps: (a) after reduction (3 h), (b) after thermal etching for 1 day, (c) after thermal etching for 3 days, and (d) after selective precipitation. The samples were dissolved in acetonitrile. After thermal etching (1 or 3 days), the samples began to show two absorption peaks around 500 and 700 nm, which corresponds to the reported characteristic absorptions of neutral thiolate-protected Au_{144} clusters.[29] The two peaks became stronger after selective precipitation. Electrospray ionization mass spectrometry (ESI-MS) results of the Au_{25} cluster during the size focusing process (Figure S3.1), support the beneficial effect of thermal etching and selective precipitation. After 1 day of thermal etching, the samples included Au_{25} clusters as an impurity, but the amount of Au_{25} clusters decreased with additional thermal etching up to 3 days. The Au_{25} clusters were completely removed by selective precipitation. The sample obtained after thermal etching for 1 day and selective precipitation (Figure S3.2) and after thermal etching for 3 days and selective precipitation (Figure 3.1(d)) showed similar absorption spectra. However, a large difference was observed in the ESI-MS results between these two samples and is described below.

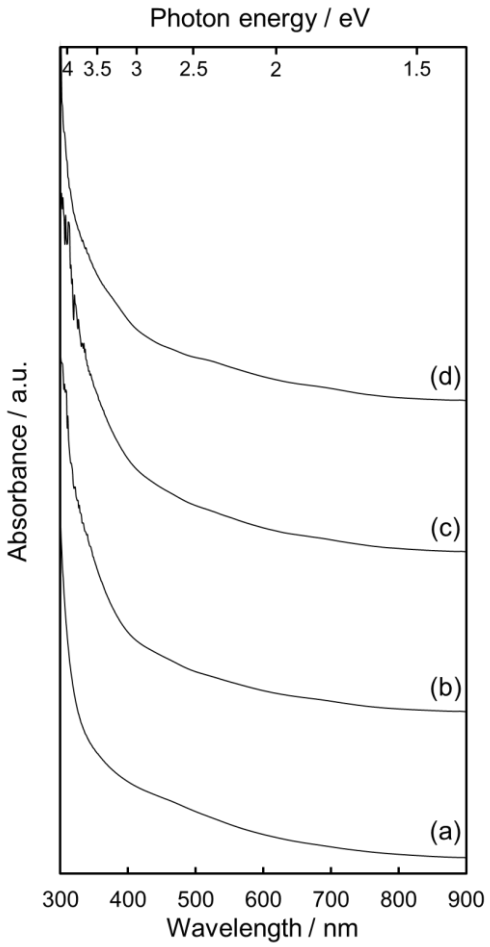

Figure 3.1 UV-Vis absorption spectra of the Au clusters obtained at different synthesis steps (a) after reduction (3h), (b) after thermal etching for 1 day, (c) after thermal etching for 3 days and (d) after selective precipitation.

3.3.2 TGA

The TGA profile of the obtained the Au cluster demonstrates its high purity (Figure 3.2). The total weight loss of 45.0% matched the theoretical weight ratio of organic components in $Au_{144}(SR^{+})_{60}\cdot(PF_6^{-})_{60}$ (45.2%). The decreases of weight started at 180 °C and 320 °C correspond to the evaporation of thiolate ligands and PF_6^{-} anions, respectively. Compared to the TGA profile of neutral Au_{144} clusters capped with different

carbon chain length where longer carbon chain show higher thermal stability ($Au_{144}(SC_4H_9)_{60}$, $Au_{144}(SC_5H_{11})_{60}$, $Au_{144}(SC_6H_{13})_{60}$ and $Au_{144}(SCH_2Ph)_{60}$ start to lose ligands at 178 °C, 195 °C, 205 °C and 200 °C, respectively),[30,31] the $Au_{144}(SR^+)_{60}$ capped with even longer thiolate (SC_{11}-NMe_3) showed lesser thermal stability. These data strongly suggest that the coulombic repulsion between cationic ligands affects the thermal stability of fully cationized Au clusters and decreases their stability.

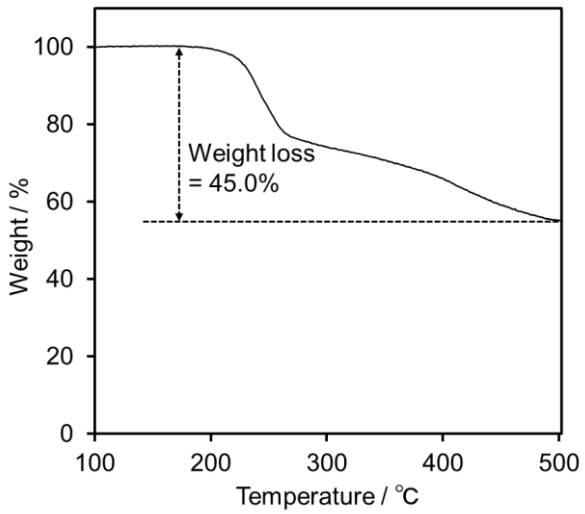

Figure 3.2 TGA profile of obtained Au clusters at a heating rate 0.5 °C/min until approximately 500 °C. Theoretical weight loss of $Au_{144}(SR^+)_{60}\cdot(PF_6^-)_{60}$ is 45.2%.

3.3.3 ESI-MS

Figure 3.3 shows the positive-mode high-resolution ESI-MS of the Au clusters obtained after thermal etching for 1 day and selective precipitation. It is important to note that the synthesized $Au_{144}(SR^{+})_{60}\cdot(PF_6^{-})_{60}$ loses several number of PF_6^{-} anions during the ESI process. As shown in the top spectrum in Figure 3.3(i), prominent groups of peaks for the +12 to +21-charged states, which could be assigned to the mixture of clusters with $Au_{144}(SR^{+})_{60}$ as the main product, were observed. The peak *Fa* is a fragment peak. Expanded ESI-MS spectra for the two observed peaks are shown in Figures 3.3(ii)-(iii), with the simulated isotopic patterns shown as red lines. A large difference was observed between the observed and simulated patterns in the peak maxima (m/z) and peak widths. The reason should be the similar sized quasi-stable compounds of Au_{144}, such as Au_{142}, Au_{143}, and Au_{146}, etc., which make the size-focusing into a single Au_{144} structure difficult. Note that the average value of the peak maxima difference in cationized Au_{144} compounds (this study) was 187.95 Da, which is smaller than 197 Da (molecular weight of Au) and 390 Da (molecular weight of thiolate ligand). These values strongly suggest that the synthetic condition of 1 day thermal etching produced $Au_{144}(SR^{+})_{60}$ clusters as the main product, though not with high atomic precision.

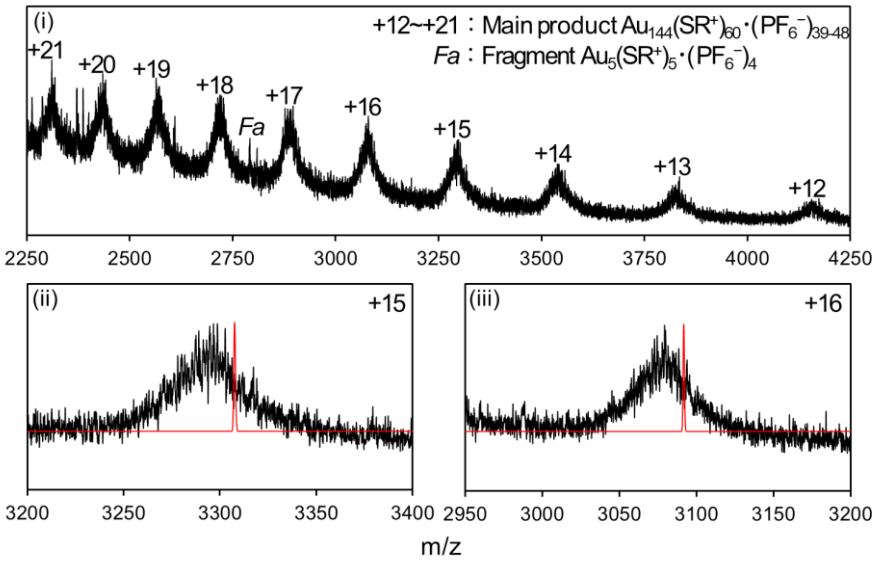

Figure 3.3 Wide range (+12-+21) and expanded (+15, +16) positive-mode electrospray ionization mass spectra (ESI-MS) of the obtained Au clusters after thermal etching (60 °C) for 1 day and selective precipitation. Black lines indicate the observed spectra, and red lines in (ii, iii) indicate the simulated isotopic patterns.

In the optimized condition of thermal etching, single Au_{144} component was successfully obtained with high atomic precision. Figure 3.4 shows the positive-mode high-resolution ESI-MS spectra of the Au clusters obtained after thermal etching for 3 days and selective precipitation. The top spectrum in Figure 3.4(i) shows prominent groups of peaks for the +12 to +21-charged states labeled a-y, which are assigned to $Au_{144}^{+1/0}(SR^+)_{60}\cdot(PF_6^-)_{39\text{-}48}$ and $Au_{144}^{+2}(SR^+)_{59}\cdot(PF_6^-)_{40\text{-}48}$, respectively. In the peak band of each charge state (Figures 3.4(ii)-3.4(v)), two clusters were observed, $Au_{144}(SR^+)_{60}$ and $Au_{144}(SR^+)_{59}$. $Au_{144}(SR^+)_{59}$ is a potential oxidation product in the ESI process of the dominant compound $Au_{144}(SR^+)_{60}$, where $Au_{144}(SR^+)_{59}$ always appear with a core-charge +2, whereas $Au_{144}(SR^+)_{60}$ is +1 or neutral. The well-known fragmentation products

$Au_4(SR^+)_4$ (not seen in *m/z*=2250-4450), $Au_5(SR^+)_5$ (*Fa*) and $Au_6(SR^+)_6$ (*Fb*) with different numbers of PF_6^- were also observed. The composition and charge assignment for each peak (*a-y, Fa, Fb*) are summarized in Table 1. The expanded ESI-MS spectra for several observed peaks are shown in Figures 3.4(ii)-3.4(v) with simulated isotopic patterns presented as three different colored lines (see additional expanded spectra in Figure S3.3). Note that the simulated isotopic patterns of ~ 50 kDa compounds in this case become continuous curves, not discrete. The observed spectra closely match the simulated patterns. The strongest peak observed for the Au_{144} cluster is $[Au_{144}^0(SR^+)_{60}\cdot(PF_6^-)_{44}]^{16+}$ (Figure 3.4). Under the electrospray conditions, the peak intensity of the Au_{144} cluster decreased when it was neutralized to a greater (<+16) or lesser (>+16) extent. Fields-Zinna et al.[6] reported ESI-MS results interpreted as charge states of +10 to +15 on cationic-ligand exchanged Au_{144}, where the same number of cationic ligands are introduced as the charge state detected. Detected charging was expected to increase toward the limit of +60 by increasing the number of exchanged ligands. However, the maximum detected charging of the $Au_{144}(SR^+)_{60}$ with PF_6^- anions obtained by direct synthesis in this study was +21, and the $Au_{144}(SR^+)_{60}$ without any PF_6^- anions was not observed. Besides, the $Au_{144}(SR^+)_{60}$ with Cl^- or OH^- counter anions (not PF_6^-) in water or methanol solvent, was not detected by ESI−MS. These results strongly suggest certain number of appropriate counter anions are required to detect Au_{144} with all cationic ligands. Furthermore, similar sized nanoclusters (~2.0 nm) were observed in high-angle annular dark field (HAADF) and bright field (BF) scanning/transmission electron microscopy (STEM) images (Figure S3.4). The Au clusters were not stable under 80 kV electron beam irradiation, which led to some decomposition or coalescence to occur. Although it is difficult to make quantitative observations from these STEM images,

the observation of ~2.0 nm clusters supports the successful synthesis of Au_{144} structures, similar to neutral 2-phenylethanethiol protected Au_{144} cluster compounds.[32]

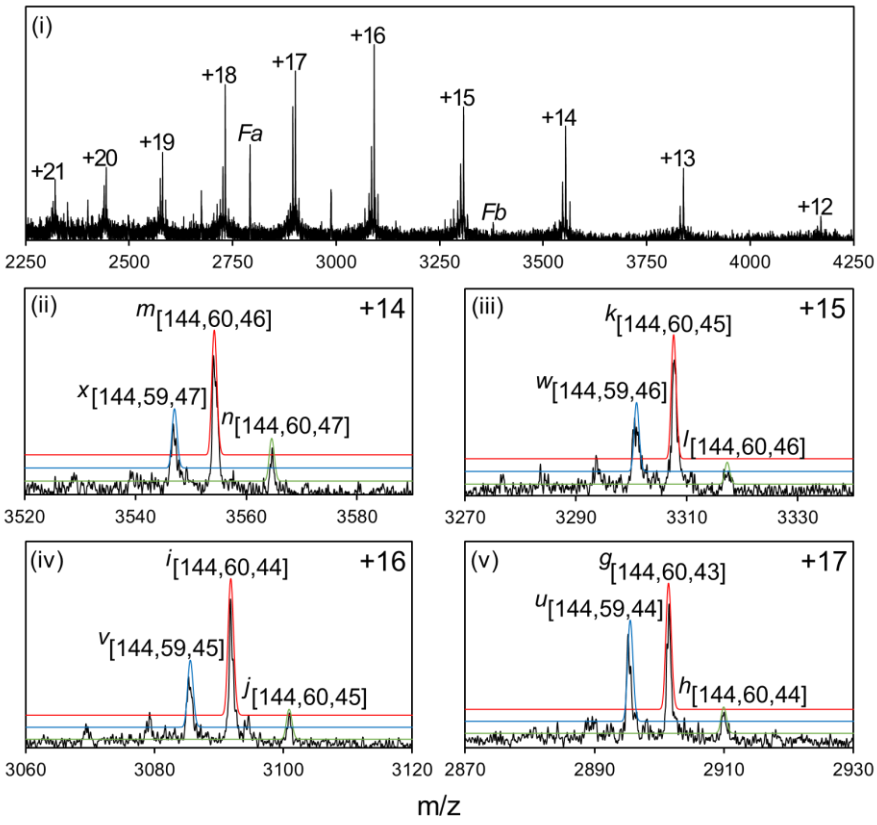

Figure 3.4 Wide-range (+12-+21) and expanded (+14, +15, +16, and +17) positive-mode electrospray ionization mass spectra (ESI-MS) of the obtained fully cationized $Au_{144}(SR^+)_{60}$ clusters with different numbers of PF_6^- counter anions after thermal etching (60 °C) for 3 days and selective precipitation. Black lines indicate the observed spectra, and red, green, blue lines in (+14, +15, +16, and +17) indicate the simulated isotopic patterns. The values in the brackets denote [number of Au, number of SR^+, number of PF_6^- anions].

Table 3.1. Structural and charge assignments of ESI-MS in Figure 3.4.

Peak	Core charge	Number of Au atoms	Number of SR^+	Number of PF_6^-	Total charge (z)*	m/z (obs.)	m/z (calc.)
			$Au_{144}(SR^+)_{60}$ clusters				
a	0	144	60	39	+ 21	2321.05	2321.17
b	0	144	60	40	+ 20	2444.56	2444.48
c	0	144	60	41	+ 19	2580.82	2580.76
d	+ 1	144	60	42	+ 19	2588.32	2588.38
e	0	144	60	42	+ 18	2732.03	2732.18
f	+ 1	144	60	43	+ 18	2740.19	2740.25
g	0	144	60	43	+ 17	2901.52	2901.43
h	+ 1	144	60	44	+ 17	2910.00	2909.96
i	0	144	60	44	+ 16	3091.78	3091.83
j	+ 1	144	60	45	+ 16	3100.90	3100.89
k	0	144	60	45	+ 15	3307.63	3307.61
l	+ 1	144	60	46	+ 15	3317.18	3317.29
m	0	144	60	46	+ 14	3554.18	3554.22
n	+ 1	144	60	47	+ 14	3564.66	3564.59
o	0	144	60	47	+ 13	3838.88	3838.79
p	0	144	60	48	+ 12	4170.63	4170.76
			$Au_{144}(SR^+)_{59}$ clusters				
q	+ 2	144	59	40	+ 21	2316.33	2316.39
r	+ 2	144	59	41	+ 20	2439.58	2439.45
s	+ 2	144	59	42	+ 19	2575.10	2575.47
t	+ 2	144	59	43	+ 18	2726.55	2726.61
u	+ 2	144	59	44	+ 17	2895.24	2895.52
v	+ 2	144	59	45	+ 16	3085.43	3085.55
w	+ 2	144	59	46	+ 15	3300.79	3300.92
x	+ 2	144	59	47	+ 14	3546.94	3547.05
y	+ 2	144	59	48	+ 13	3849.73	3849.94
			Fragmentation products: $Au_5(SR^+)_5$ (*Fa*), $Au_6(SR^+)_6$ (*Fb*)				
Fa	0	5	5	4	+ 1	2792.08	2792.00
Fb	0	6	6	5	+ 1	3379.25	3379.01

SR^+ represents $S(CH_2)_{11}N(CH_3)_3^+$ ligand.

* (Total charge) = (Number of SR^+) - (Number of PF_6^-) + (Core charge)

3.4 Conclusion

Fully cationized $Au_{144}(SR^{+})_{60}$ clusters were successfully synthesized. Through a strict size focusing process, optimized thermal etching and selective precipitation, fully cationized single Au_{144} components were obtained with high atomic precision. The $Au_{144}(SR^{+})_{60}$ cluster compound with +60 charge is, to the best of my knowledge, the most polycationic molecular compound reported thus far. This larger series of fully cationized Au clusters compounds should be beneficial in diverse fields, such as catalysis, optics, or interaction with nano-bio interfaces, and may also provide a novel chemical reaction field due to the uniformly and densely located cationic groups with high atomic purity.

3.5 Supporting information

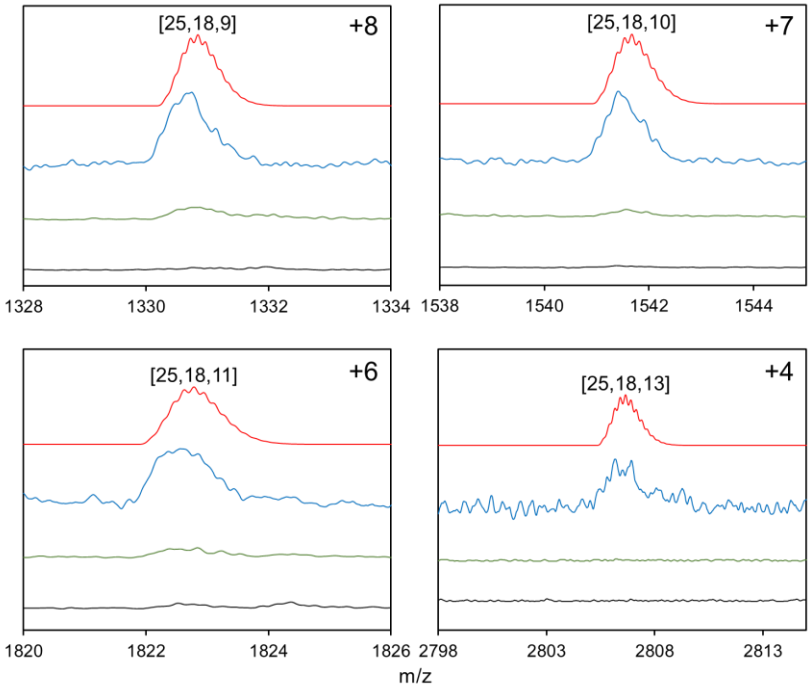

Figure S3.1 The effect of thermal etching and selective-reprecipitation. ESI-MS of after thermal etching for 1 day (blue) and after thermal etching for 3 days (green) and after selective precipitation (black), with the simulated isotopic patterns (red). The values in the brackets denote [number of Au, number of SR^+, number of PF_6^- anions]. The theoretical m/z values of each cluster are, m/z=1330.84 (+8), 1541.67 (+7), 1822.78 (+6), 2806.65 (+4).

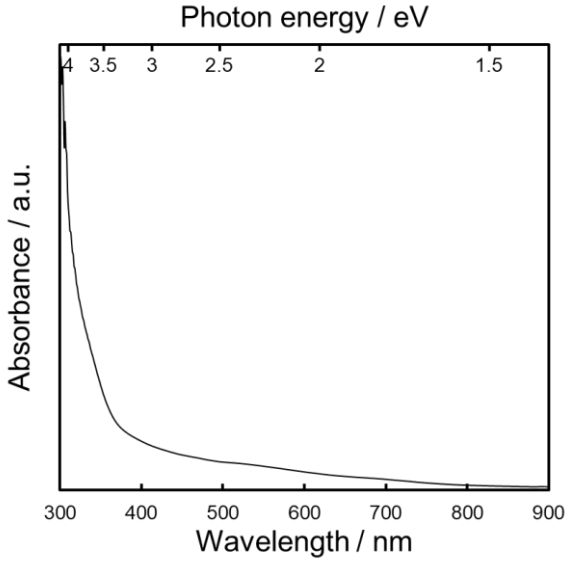

Figure S3.2 UV-Vis absorption spectra of the obtained Au clusters after thermal etching for 1 day and selective precipitation.

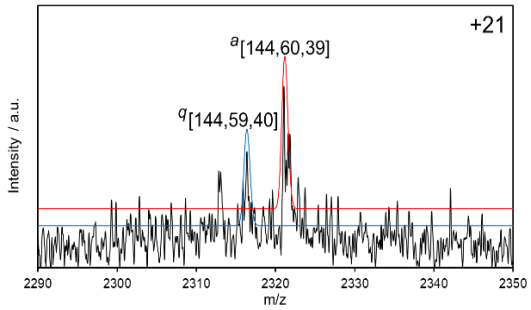
+21
a[144,60,39]
q[144,59,40]
Intensity / a.u.
2290 2300 2310 2320 2330 2340 2350
m/z

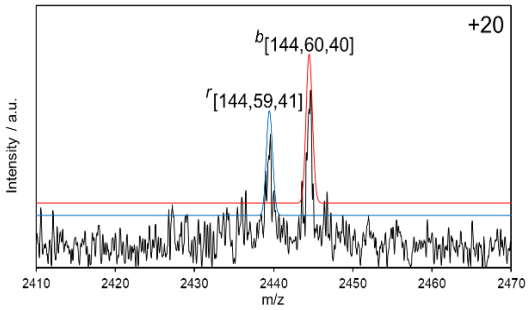
+20
b[144,60,40]
r[144,59,41]
Intensity / a.u.
2410 2420 2430 2440 2450 2460 2470
m/z

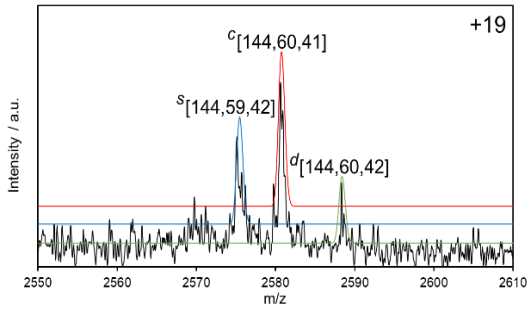
+19
c[144,60,41]
s[144,59,42]
d[144,60,42]
Intensity / a.u.
2550 2560 2570 2580 2590 2600 2610
m/z

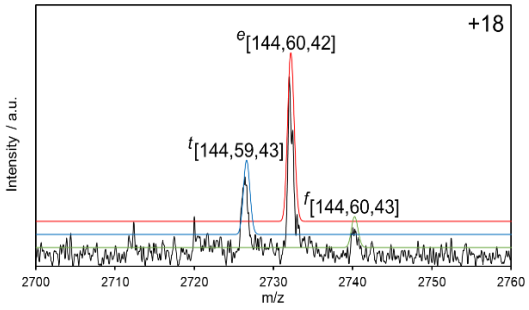
+18
e[144,60,42]
t[144,59,43]
f[144,60,43]
Intensity / a.u.
2700 2710 2720 2730 2740 2750 2760
m/z

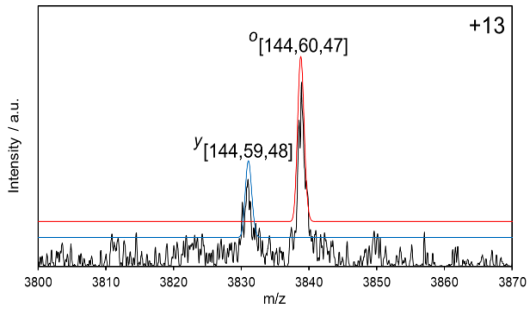
+13
o[144,60,47]
y[144,59,48]
Intensity / a.u.
3800 3810 3820 3830 3840 3850 3860 3870
m/z

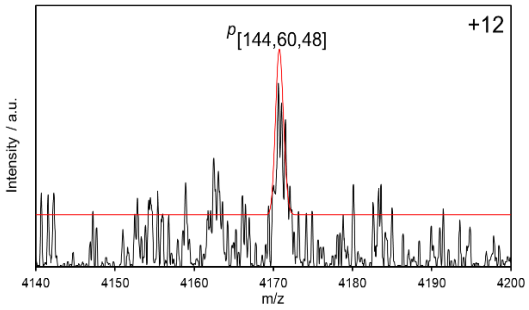
+12
p[144,60,48]
Intensity / a.u.
4140 4150 4160 4170 4180 4190 4200
m/z

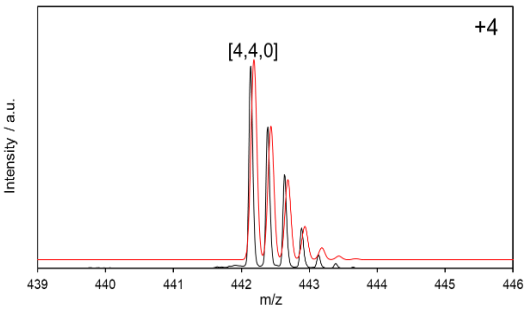
+4
[4,4,0]
Intensity / a.u.
439 440 441 442 443 444 445 446
m/z

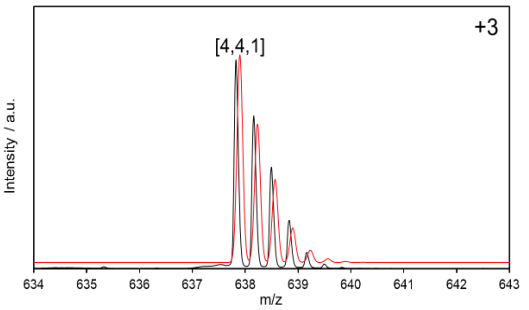
+3
[4,4,1]
Intensity / a.u.
634 635 636 637 638 639 640 641 642 643
m/z

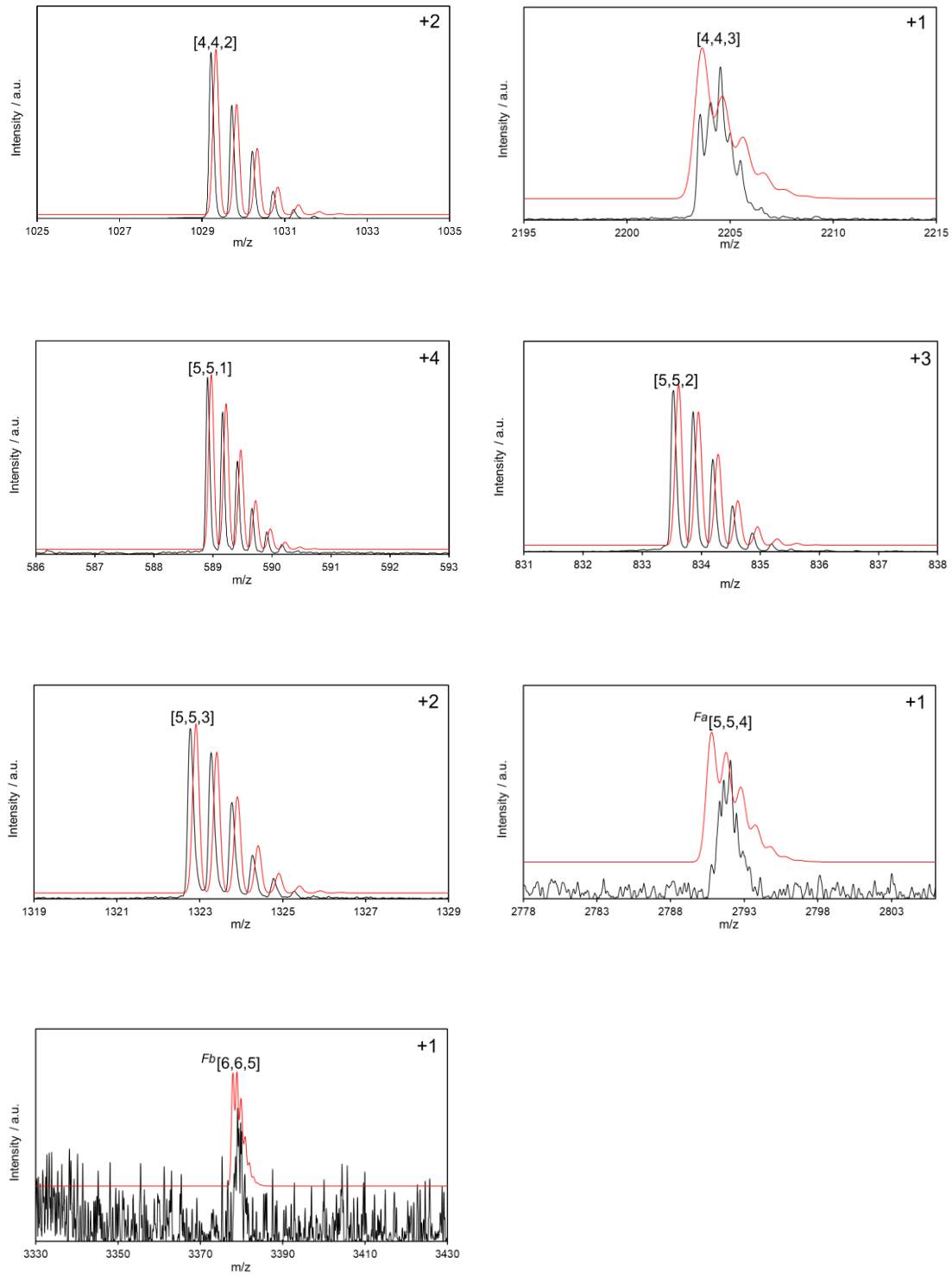

Figure S3.3 Magnified ESI-MS (black lines) and simulations (red, green and blue lines) for the other observed peaks. The values in the brackets denote [number of Au, number of SR^+, number of PF_6^- anions].

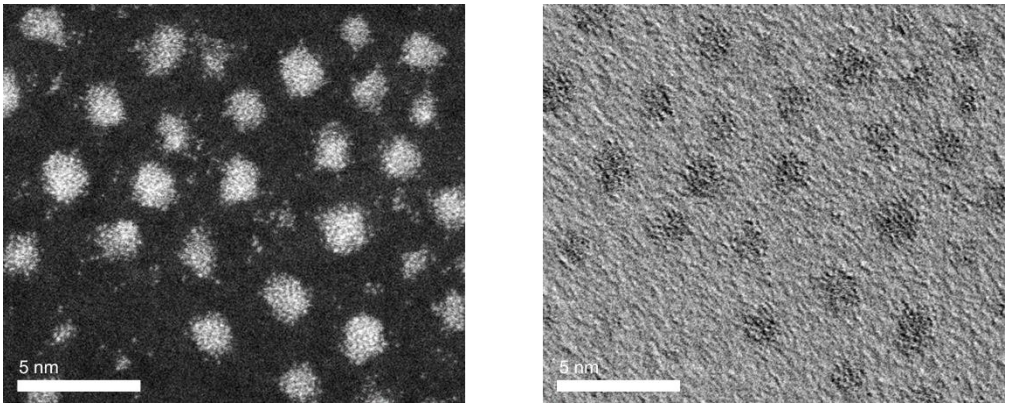

Figure S3.4 HAADF (left) and BF (right) STEM image of the obtained Au_{144} clusters.

3.6 References

(1) Whetten, R. L.; Khoury, J. T.; Alvarez, M. M.; Murthy, S.; Vezmar, I.; Wang, Z. L.; Stephens, P. W.; Cleveland, C. L.; Luedtke, W. D.; Landman, U. Nanocrystal Gold Molecules. *Adv. Mater.* **1996**, *8*, 428−433.

(2) Negishi, Y.; Chaki, N. K.; Shichibu, Y.; Whetten, R. L.; Tsukuda, T. Origin of Magic Stability of Thiolated Gold Clusters: a Case Study on $Au_{25}(SC_6H_{13})_{18}$. *J. Am. Chem. Soc.* **2007**, *129*, 11322−11323.

(3) Tsukuda, T. Toward an Atomic-Level Understanding of SizeSpecific Properties of Protected and Stabilized Gold Clusters. *Bull. Chem. Soc. Jpn.* **2012**, *85*, 151−168.

(4) Alvarez, M. M.; Chen, J.; Plascencia-Villa, G.; Black, D. M.; Griffith, W. P.; Garzón, I. L.; Jose-Yacaman, M.; Demeler, B.; Whetten, R. L. Hidden Components in Aqueous "Gold-144" Fractionated by PAGE: High-Resolution Orbitrap ESI−MS Identifies the Gold-102 and Higher All-Aromatic Au-pMBA Cluster Compounds. *J. Phys. Chem. B* **2016**, *120*, 6430−6438.

(5) Kumar, S.; Jin, R. Water-Soluble $Au_{25}(Capt)_{18}$ Nanoclusters: Synthesis, Thermal Stability, and Optical Properties. *Nanoscale* **2012**, *4*, 4222−4227.

(6) Fields-Zinna, C. A.; Sardar, R.; Beasley, C. A.; Murray, R. W. Electrospray Ionization Mass Spectrometry of Intrinsically Cationized Nanoparticles, $[Au_{144/146}(SC_{11}H_{22}N(CH_2CH_3)_3^{3+})_X\text{-}(S(CH_2)_5CH_3)_Y]^{X+}$. *J. Am. Chem. Soc.* **2009**, *131*, 16266−16271.

(7) Häkkinen, H. The Gold−Sulfur Interface at the Nanoscale. *Nat. Chem.* **2012**, *4*, 443−455.

(8) Bürgi, T. Properties of the Gold−Sulphur Interface: From Self−Assembled Monolayers to Clusters. *Nanoscale* **2015**, *7*, 15553−15567.

(9) Dass, A. Nano-scaling law: geometric foundation of thiolated gold nanomolecules. *Nanoscale* **2012**, *4*, 2260−2263.

(10) Price, R. C.; Whetten, R. L. All-Aromatic, Nanometer-Scale, Gold-Cluster Thiolate Complexes. *J. Am. Chem. Soc.* **2005**, *127*, 13750−13751.

(11) Dharmaratne, A. C.; Krick, T.; Dass, A. Nanocluster Size Evolution Studied by Mass Spectrometry in Room Temperature $Au_{25}(SR)_{18}$ Synthesis. *J. Am. Chem. Soc.* **2009**, *131*, 13604−13605.

(12) Jin, R.; Zeng, C.; Zhou, M.; Chen, Y. Atomically Precise Colloidal Metal Nanoclusters and Nanoparticles: Fundamentals and Opportunities. *Chem. Rev.* **2016**, *116*, 10346−10413.

(13) Qian, H.; Zhu, M.; Wu, Z.; Jin, R. Quantum Sized Gold Nanoclusters with Atomic Precision. *Acc. Chem. Res.* **2012**, *45*, 1470−1479.

(14) Ishida, Y.; Narita, K.; Yonezawa, T.; Whetten, R. L. Fully Cationized Gold Clusters: Synthesis of $Au_{25}(SR^{+})_{18}$. *J. Phys. Chem. Lett.* **2016**, *7*, 3718−3722.

(15) Ishida, Y.; Huang, Y.-L.; Yonezawa, T.; Narita, K. Charge Neutralization Strategy: A Novel Synthetic Approach to Fully Cationized Thiolate-Protected $Au_{25}(SR^{+})_{18}$ Clusters with Atomic Precision. *ChemNanoMat* **2017**, *3*, 298−302.

(16) Huang, Z.; Ishida, Y.; Narita, K.; Yonezawa, T. Kinetics of Cationic-Ligand-Exchange Reactions in Au_{25} Nanoclusters. *J. Phys. Chem. C* **2018**, *122*, 18142−18150.

(17) Hoque, M. M.; Black, D. M.; Mayer, K. M.; Dass, A.; Whetten, R. L. The Base Side of Noble Metal Clusters: Efficient Route to Captamino-Gold, $Au_n(-S(CH_2)_2N(CH_3)_2)_p$, n= 25–144. *J. Phys. Chem. Lett.* **2019**, *10*, 3307−3311.

(18) Hoque, M. M.; Dass, A.; Mayer, K. M.; Whetten, R. L. Protein-like Large Gold Clusters Based on the ω-Amino-Thiolate DMAET: Precision Thermal and Reaction Control Leads to Selective Formation of Cationic Gold Clusters in the Critical Size Range, n= 130–144 Au Atoms. *J. Phys. Chem. C* **2019**, *123*, 14871−14879.

(19) Ackerson, C. J.; Jadzinsky, P. D.; Kornberg, R. D., Thiolate Ligands for Synthesis of Water-Soluble Gold Clusters. *Journal of the American Chemical Society* **2005**, *127*, 6550−6551.

(20) Tlahuice-Flores, A.; Black, D. M.; Bach, S. B. H.; Jose-Yacaman, M.; Whetten, R. L. Structure & bonding of the gold-subhalide cluster *I*-$Au_{144}Cl_{60}^{[z]}$. *Phys. Chem. Chem. Phys.* **2013**, *15*, 19191−19195.

(21) Yan, N.; Xia, N.; Liao, L.; Zhu, M.; Jin, F.; Jin, R.; Wu, Z. Unraveling the long-pursued Au_{144} structure by x-ray crystallography. *Sci. Adv.* **2018**, *4*, 7259.

(22) Lei, Z.; Li, J.-J.; Wan, X.-K.; Zhang, W.-H.; Wang, Q.-M. Isolation and Total Structure Determination of an All-Alkynyl-Protected Gold Nanocluster Au_{144}. *Angew. Chem. Int. Ed.* **2018**, *57*, 8639−8643.

(23) Tran, N. T.; Powell, D. R.; Dahl, L. F. Nanosized $Pd_{145}(CO)_x(PEt_3)_{30}$ Containing a Capped Three-Shell 145-Atom Metal-Core Geometry of Pseudo Icosahedral Symmetry. *Angew. Chem. Int. Ed.* **2000**, *39*, 4121−4125.

(24) Wong, O. A.; Heinecke, C. L.; Simone, A. R.; Whetten, R. L.; Ackerson, C. J. Ligand symmetry-equivalence on thiolate protected gold nanoclusters determined by NMR spectroscopy. *Nanoscale* **2012**, *4*, 4099−4102.

(25) Tamesue, S.; Ohtani, M.; Yamada, K.; Ishida, Y.; Spruell, J. M.; Lynd, N. A.; Hawker, C. J.; Aida, T. Linear versus Dendritic Molecular Binders for Hydrogel Network Formation with Clay Nanosheets: Studies with ABA Triblock Copolyethers Carrying Guanidinium Ion Pendants. *J. Am. Chem. Soc.* **2013**, *135*, 15650−15655.

(26) Fujita, D.; Ueda, Y.; Sato, S.; Mizuno, N.; Kumasaka, T.; Fujita, M. Self-assembly of tetravalent Goldberg polyhedra from 144 small components. *Nature* **2016,** *540*, 563−566.

(27) Allen, C.; Qiu, T. A.; Pramanik, S.; Buchman, J. T.; Krause, M. O. P.; Murphy, C. J. Research highlights: investigating the role of nanoparticle surface charge in nano-bio interactions. *Environ. Sci.: Nano* **2017**, *4*, 741−746.

(28) Ishida, Y.; Corpuz, R. D.; Yonezawa, T. Matrix Sputtering Method: A Novel Physical Approach for Photoluminescent Noble Metal Nanoclusters. *Acc. Chem. Res.* **2017**, *50*, 2986−2995.

(29) Weissker, H.-Ch.; Escobar, H. B.; Thanthirige, V. D.; Kwak, K.; Ramakrishna, G.; Whetten, R. L.; Lopez-Lozano, X. Information on quantum states pervades the visible spectrum of the ubiquitous $Au_{144}(SR)_{60}$ gold nanocluster. *Nature Commun.* **2014**, *5*, 3785.

(30) Qian, H.; Jin, R. Ambient Synthesis of $Au_{144}(SR)_{60}$ Nanoclusters in Methanol. *Chem. Mater.* **2011**, *23*, 2209−2217.

(31) Liu, C.; Yan, C.; Lin, J.; Yu, C.; Huang, J.; Li, G. One-pot synthesis of $Au_{144}(SCH_2Ph)_{60}$ nanoclusters and their catalytic application. *J. Mater. Chem. A*, **2015**, *3*, 20167−20173.

(32) Bahena, D.; Bhattarai, N.; Santiago, U.; Tlahuice, A.; Ponce, A.; Bach, S. B. H.; Yoon, B.; Whetten, R. L.; Landman, U.; Jose-Yacaman, M. STEM Electron Diffraction and

High-Resolution Images Used in the Determination of the Crystal Structure of the $Au_{144}(SR)_{60}$ Cluster. *J. Phys. Chem. Lett.* **2013**, *4*, 975−981.

Chapter 4

Surface Menshutkin S_N2 Reaction on Basic Gold Clusters Provides Novel Opportunities for the Cationization and Functionalization of Molecular Metal Clusters

4.1 Introduction

Atomically precise, thiolate-protected gold clusters ($Au_m(SR)_n$) have potential applications in diverse fields, such as catalysis,[1,2] sensing,[3,4] and bio-applications,[5,6] owing to their interesting physicochemical properties. Surface SR ligands are of particular interest as they affect the magic size (stable number of metal atoms) and structures of the clusters.[6,7] Furthermore, the R-groups on the cluster surface are exposed to solutions and other phases; hence, they determine the molecular-like characteristics of clusters,[8] such as their hydrophobicities/hydrophilicities,[9] chiralities,[10] catalytic activities,[2,11] optical properties,[12] and interactions with host materials.[5,6] These R-groups are therefore crucial to the rational design of the functional properties and applications of clusters. In peculiar, clusters capped by cationic R-groups are desirable as they widen the applications of bioimaging and sensing;[13] however, the synthesis of cationized clusters is rarely reported owing to the difficulty in handling the positive charges of R-groups.[14-16] Recently, by preventing the formation of $[Au(I)]^-$–SR^+ ionic polymer complexes that hinder the homogeneous reduction of Au precursors and the formation of atomically pure clusters, the cationized Au clusters ($Au_{25}(S(CH_2)_{11}N(CH_3)_3^+)_{18}$,[14] $Au_{144}(S(CH_2)_{11}N(CH_3)_3^+)_{60}$,[15]

and $Au_{25}(S(CH_2)_{11}N(CH_3)_3^+)_x(S(CH_2)_2Ph)_{18-x}$ (x=1-6)[16]) were successfully synthesized.

To date, major protocols for the preparation of atomically precise clusters with various thiolate ligands have been categorized into size-focusing[14,15] and ligand-exchange method.[16,17] In the former case, the Au(I)–SR complex is prepared by mixing Au ion and thiols (HSR), followed by reduction into objected Au clusters. The latter involves the synthesis of Au clusters, followed by the replacement of their initial ligands with the desired ligands. Besides these methods, surface reactions have also received significant attention in recent years; however, there are few reports on such reactions, two of which are azido- and amide-bond formation reactions.[18,19]

The Menshutkin S_N2 reaction is a common method to obtain quaternary ammonium salt ($[–N(CH_3)_3]^+$) by reacting a tertiary amine with an alkylating agent.[20] This chapter demonstrate the Menshutkin (methylation) reaction of the surface pyridyl (Py) moieties on basic $Au_{25}(4\text{-PyET})_{18}$ clusters (4-PyET = $–SCH_2CH_2Py$) for their successful transformation into cationized $Au_{25}(4\text{-PyET-}CH_3^+)_x(4\text{-PyET})_{18-x}$ ($x \approx 18$) clusters (Scheme 4.1). This work proposes a novel strategy for not only the cationization of Au clusters by surface chemical reactions, but their functionalization as well.

Scheme 4.1 Menshutkin (methylation) reaction on $Au_{25}(4\text{-PyET})_{18}$ clusters. 4-PyET = $–SCH_2CH_2Py$, where Py = pyridyl group.

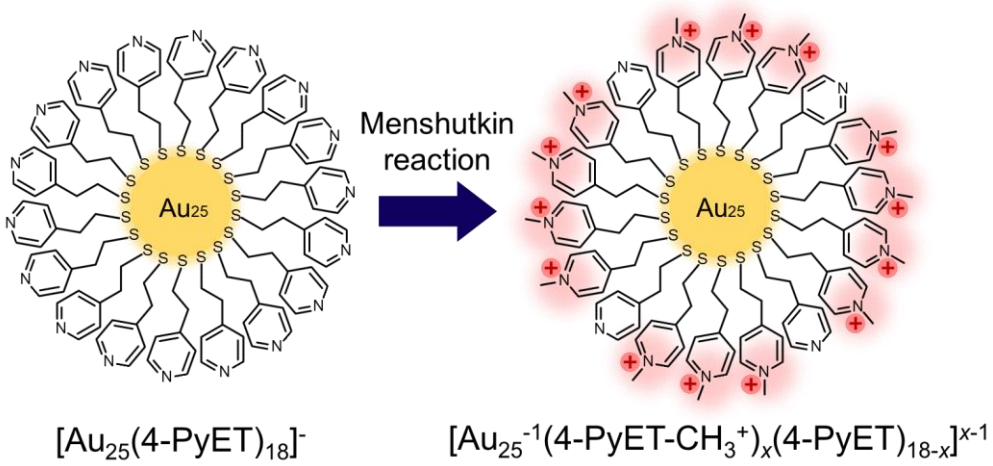

4.2 Experimental section

4.2.1 Chemicals

Hydrogen tetrachloroaurate (III) Tetrahydrate ($HAuCl_4 \cdot 4H_2O$, > 99%, Wako), 4-pyridineethanethiol hydrochloride (4-PyET·HCl, $C_7H_9NS \cdot HCl$, > 97%, TCI), sodium borohydride ($NaBH_4$, > 92%, Kanto), hydrochloric acid (HCl, 35~37%, Kanto), sodium hydroxide (NaOH, > 97%, Kanto), iodomethane (CH_3I, > 99.5%, TCI), dimethyl sulfate ($C_2H_6O_4S$, > 98%, TCI), methyl trifluoromethanesulfonate ($C_2H_3F_3O_3S$, > 95%, Wako), trimethyl oxonium tetrafluoroborate ($C_3H_9BF_4O$, > 95%, Ardrich), potassium hexafluorophosphate (KPF_6, > 95%, TCI). Tetrahydrofuran (THF, > 99.5%, Junsei), methanol (MeOH, > 99.6%, Junsei), dichloromethane (DCM, > 99%, Wako), *N,N*-dimethylformamide, super dehydrated (dehydrated DMF, > 99.5%, Kanto), diethyl ether, super dehydrated (> 99.5%, Wako), Acetonitrile (> 99.9%, RCI labscan). Deioized pure water (> 18.2 MΩ) was prepared by an Organo/ELGA purelab system.

4.2.2 Synthesis of $Au_{25}(4\text{-PyET})_{18}$ clusters

The $Au_{25}(4\text{-PyET})_{18}$ clusters were synthesized by following the recently reported works.[21] In brief, 8 mL of 4-PyET solution (MeOH, 100 mM) was added dropwise into 24 mL of $HAuCl_4$ solution (THF, 6.7 mM; 4-PyET:Au = 5:1 in molar ratio). The mixture changed into light reddish cloudy suspension, and then into white cloudy suspension during 4-PyET dropping. After overnight stirring, 1.6 mL of the fresh-made $NaBH_4$ solution (1.6 mmol, $NaBH_4$:Au = 5:1 in molar ratio; prepared by dissolving 189.2 mg of $NaBH_4$ in 5 mL of cold pure water) was rapidly added to the suspension under vigorous stirring. The color of the solution immediately turned black after addition of $NaBH_4$. Finally, the etching process was allowed to continue for at least 48h. Over the long time of etching process, the solution color would become dark brown slowly, suggesting the formation of monodisperse $Au_{25}(4\text{-PyET})_{18}$. The crude samples were purified based on the protonated states of the pendant Py moiety on Au_{25} cluster.

4.2.3 Menshutkin reaction on $Au_{25}(4\text{-PyET})_{18}$ clusters

The Menshutkin reaction was investigated in $Au_{25}(4\text{-PyET})_{18}$ clusters. 1st reaction cycle: $Au_{25}(4\text{-PyET})_{18}$ clusters (1 mg, ~0.13 μmol) were dissolved in dehydrated DMF (1 mL). In this solution, liquid methyl trifluoromethanesulfonate (27 μL, ~240 μmol) and KPF_6 (4.5 mg, ~24 μmol) were added in the mole ratio of methyl trifluoromethanesulfonate:KPF_6:4-PyET = 100:10:1. The solution was stirred at 200 rpm for 1 h. The obtained $Au_{25}(4\text{-PyET-}CH_3^+)_x(4\text{-PyET})_{18-x}$ clusters were precipitated by adding KPF_6 aqueous solution (0.1 M, 5 mL) and washed by water and DCM. 2nd reaction cycle: the obtained clusters were redissolved in dehydrated DMF (1 mL), and then were reacted and purified in the same method as 1st reaction. 3rd reaction cycle: the same operations as 2nd reaction were repeated.

4.2.4 Characterization

UV-Vis absorption spectra of samples were recorded using a JASCO V-630 spectrophotometer using a quartz cuvette with a 1 nm optical path. Electrospray Ionization Mass Spectrometry (ESI-MS) was performed using a Bruker Daltonics micrOTOF-HS mass spectrometer. The purified sample, dissolved in acetonitrile (~100 μg/mL), was directly infused at 4 mL/min. The nebulizer pressure was set to 1.5 bar, and the sheath gas was set to 4.0 L/min. The dry temperature was kept at 180 °C. The electrospray emitter potential was held at 4500 V (positive mode). The capillary exit, skimmer 1, hexapole 1, skimmer 2 voltage settings were 200, 50, 25, and 28 V, respectively. The lens 1 transfer and lens 1 pre puls storage were set at 160, and 30 μs, respectively. ^{1}H NMR analysis was performed on a JMTC-400/54/SS (JEOL) spectrometer operated at 400 MHz. Dimethyl sulfoxide-d_6 (DMSO-d_6, 750 μL) was used as the solvent to dissolve 3 mg of the cluster.

4.3 Results and discussion

4.3.1 Selection of methylating reagents

The following 4 chemicals were evaluated as methylating reagents: iodomethane (MeI), dimethyl sulfate (Me_2SO_4), methyl trifluoromethanesulfonate (TfOMe), and trimethyl oxonium tetrafluoroborate (Me_3OBF_4) (reactivity with Py group: MeI < Me_2SO_4 < TfOMe < Me_3OBF_4). The surface-reactive basic Au cluster Au_{25}(4-PyET)$_{18}$ was synthesized according to the previously reported method and characterized by electrospray ionization mass spectrometry (ESI-MS) and UV-Vis absorption (Figure S4.1).[21] Figures 4.1(a)-(d) show the UV-Vis absorption spectra of the samples before (0 min) and after the methylation reaction (30 min or 60 min) using each of the 4 methylating reagents. When MeI and Me_3OBF_4 were used (Figures 4.1(a) and (d), respectively), the characteristic absorption peaks of Au_{25} clusters[22,23] at 400, 450, 560, 670 and 780 nm disappeared after the reaction, indicating that these reagents decomposed the Au_{25} clusters. On the other hand, no obvious decreases in the absorption spectra were observed when using Me_2SO_4 and TfOMe (Figures 4.1(b) and (c)). The decomposition of the clusters by MeI is due to the nucleophilicity of the I^- ion generated by the reaction, as reported elsewhere.[24] Besides, methylating agents not only react with the Py group of the ligands, but with the –S moiety of the Au–S bonds as well. Their reaction with the –S group causes the Au–S bond to break, leading to the decomposition of the clusters. Me_3OBF_4 likely decomposed the clusters owing to its strong reactivity. On the other hand, Me_2SO_4 and TfOMe selectively react with the outer Py groups over the inner –S groups because of their moderate reactivity, allowing the methylation reaction to proceed without any decomposition of the clusters.

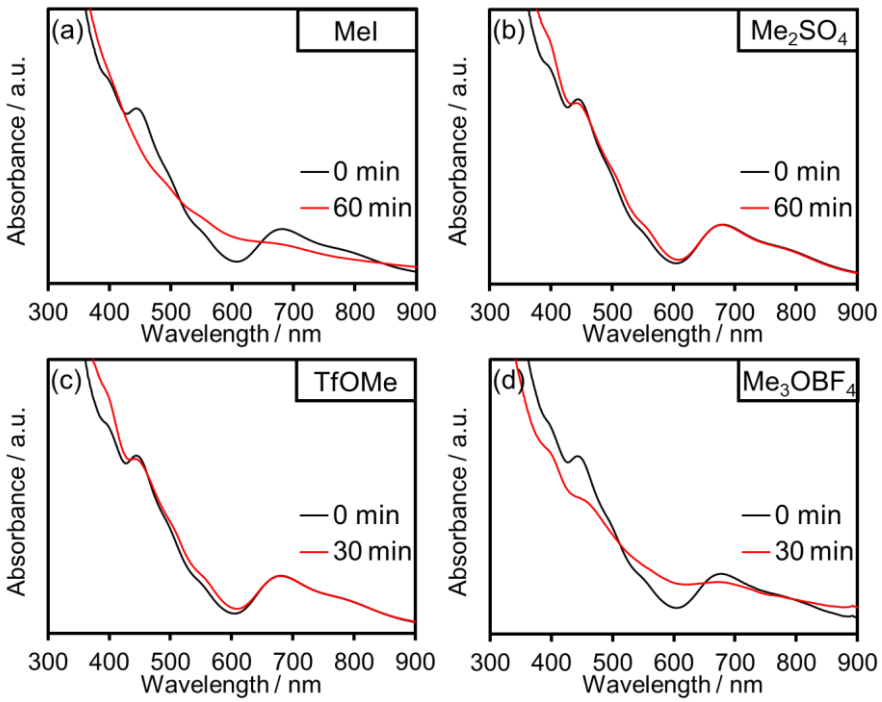

Figure 4.1 Selection of methylating reagents. UV-Vis absorption spectra of the samples before (0 min) and after reaction (30 min or 60 min) with (a) MeI, (b) Me_2SO_4, (c) TfOMe, and (d) Me_3OBF_4.

4.3.2 Optical absorption spectroscopy

TfOMe, which proceeded the most efficiently (see ESI-MS results in Figures S4.2-S4.4), was selected as the methylating reagent. The Menshutkin reaction on the Au_{25}(4-PyET)$_{18}$ cluster was conducted to obtain methylated, cationized Au_{25} clusters (see the detailed procedure in the Supporting Information). Trifluoromethanesulfonic acid (CF_3SO_3H) was noted as a decomposition product of TfOMe, which could hinder the Menshutkin reaction by protonating the unreacted Py groups. By performing the 1h reaction 3 times (i.e., 3 cycles), CF_3SO_3H was effectively removed and the reaction was proceeded efficiently. Notably, running 1 cycle for up to 2 days did not produce fully

methylated Au clusters as the main product and was less efficient than the 3-cycle reaction (Figure S4.5). UV-Vis absorption spectra of the sample before and after 1 cycle showed slight increases in the characteristic Au_{25} cluster bands[22,23] at 400 and 560 nm, whereas those at 450, 670, and 780 nm slightly decreased (Figure 4.2). Such absorption changes were also observed when Au_{25}(4-PyET)$_{18}$ clusters were treated with HCl, in which the reversible protonation of the Py group gave its positive form, $–C_5H_4NH^+$.[21] These results strongly suggest that the geometric structure of Au_{25} core was distorted due to the surface charge anisotropy[12,21] during the addition of positive charges. The absorption spectra showed negligible changes after the 2nd and 3rd reaction cycles (Figure S4.6), demonstrating the good stability of the methylated, cationized Au_{25} clusters and lack of geometrical changes in the Au_{25} core (discussed in detail in Figure 4.4).

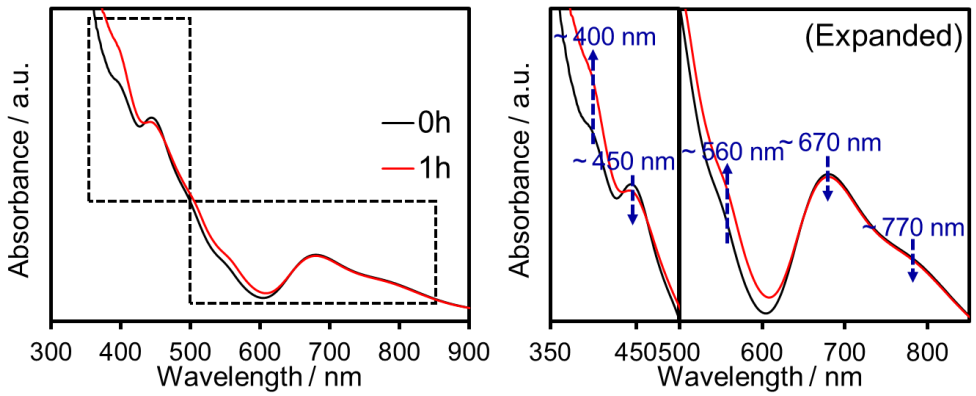

Figure 4.2 UV-Vis absorption spectra of the sample before (0h) and after 1-cycle reaction (1h).

4.3.3 ESI-MS

The positive-mode ESI-MS of the methylated Au_{25} clusters (Figure 4.3, left) showed 3 different charged states +2, +3, and +4 (depending on the number of attached PF_6^- anions). Specifically, $[Au_{25}^{-1}(4\text{-PyET-}CH_3^+)_x(4\text{-PyET})_{18-x}\cdot(PF_6^-)_{x-3}]^{2+}$ ($11 \leq x \leq 18$), $[Au_{25}^{-1}(4\text{-PyET-}CH_3^+)_x(4\text{-PyET})_{18-x}\cdot(PF_6^-)_{x-4}]^{3+}$ ($12 \leq x \leq 18$), and $[Au_{25}^{-1}(4\text{-PyET-}CH_3^+)_x(4\text{-PyET})_{18-x}\cdot(PF_6^-)_{x-5}]^{4+}$ ($14 \leq x \leq 18$) (groups Au_{25}(+2), Au_{25}(+3), and Au_{25}(+4), respectively) were observed. Figure 4.3 (right) shows the expanded ESI-MS of the methylated Au_{25} clusters with +3 charged state (group Au_{25}(+3)) observed with relatively high intensity (expanded ESI-MS of group Au_{25}(+2) and Au_{25}(+4) in Figure S4.7). After 1st reaction cycle (1h in total), the *x* values (the number of methylated ligands) ranged between 12 and 18. Note that after 2 min of reaction, *x* had already reached 10-18, indicating the reaction rate became very inefficient due to the decrease in the number of reaction sites and bulkiness of the counter anions $CF_3SO_3^-$ and PF_6^-, which geometrically impede further reaction of the unreacted ligands (Figure S4.2). After the 2nd and 3rd reaction cycles (2h and 3h in total, respectively), the *x* values increased to *x*=14-18 and 15-18 respectively. The average number of methylated ligands was calculated from the peak intensity ratio, assuming the mass spectral signal intensities are equal to the solution concentrations of the corresponding cluster species; the numbers for cycles 1-3 were 15.0 (83.1%), 16.7 (92.7%), and 17.3 (95.9%), respectively (refer to detailed calculation procedures in Table S4.1). The ^1H NMR spectrum of the sample after the 3rd reaction cycle (Figure S4.8) also showed a similar *x* value of 17.3 (96.0%), confirming that the *x* values calculated from the mass spectral signal intensities are reliable in the selected mass region (*m/z* = 2220-4950). The average *x* value gradually increased by the number of reaction cycles, and nearly per-methylated Au_{25} clusters were successfully obtained after

3 cycles. By further increasing the number of reaction cycles to 4 (4h in total), more clusters, with x=18, could be produced; however they exhibited more impurity peaks due to their decomposition (Figure S4.9). The compositions and charge assignments of the observed Au_{25} cluster peaks are summarized in Table 4.1. The isotope distributions matched well with the simulated isotope patterns (Figure S4.10). The well-known fragmentation product $[Au_4^0(4\text{-PyET-}CH_3^+)_x(4\text{-PyET})_{4-x}\cdot(PF_6^-)_{x-1}]^{1+}$ ($1 \leq x \leq 4$) was also observed (Figure S4.11). Moreover, the fragmentation products during the ESI process $[Au_{24}^0(4\text{-PyET-}CH_3^+)_x(4\text{-PyET})_{16-x}\cdot(PF_6^-)_{x-3}]^{3+}$ ($8 \leq x \leq 16$) and $[Au_{23}^0(4\text{-PyET-}CH_3^+)_x(4\text{-PyET})_{15-x}\cdot(PF_6^-)_{x-3}]^{3+}$ ($8 \leq x \leq 15$) were observed for $Au_{25}(SR)_{18}$; these corresponded to losses of $Au_1–SR_2$ and $Au_2–SR_3$ (Figure S4.11). Interestingly, like those of the whole Au_{25} clusters, the x values of these fragmentation products also increased with the number of reaction cycles (see the summary of compositions and charge assignments in Table S4.2).

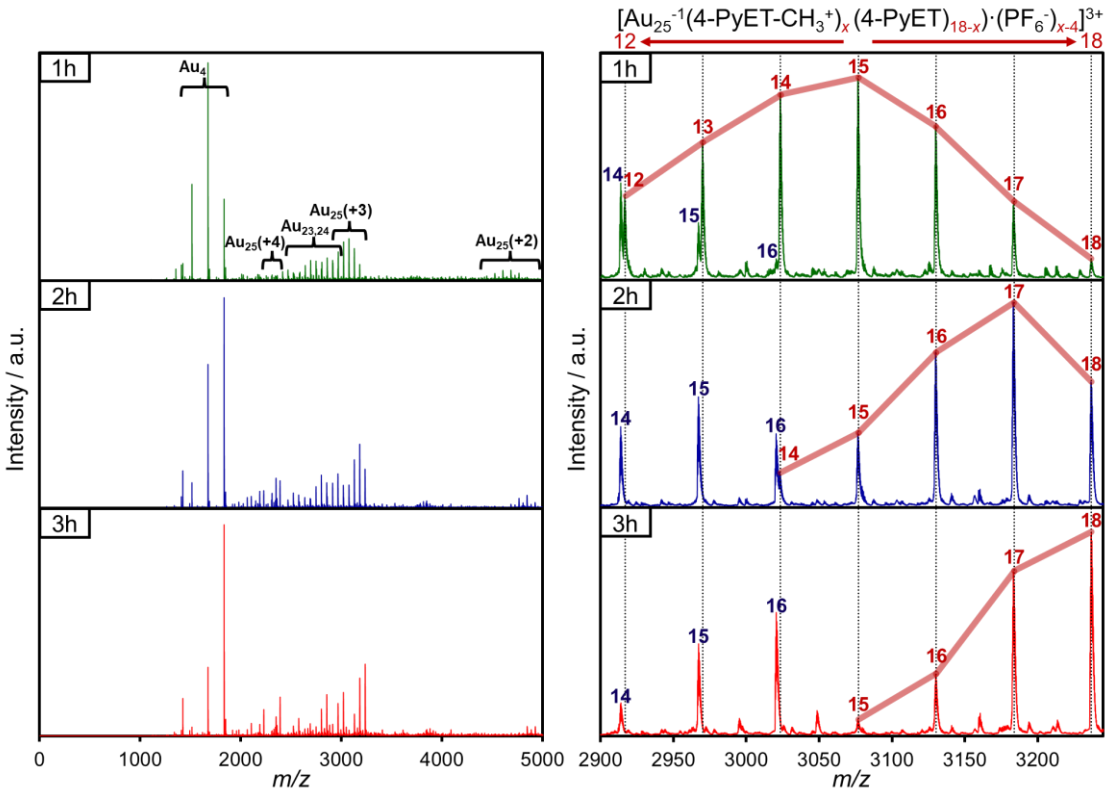

Figure 4.3 Positive-mode ESI-MS of the samples after different numbers of reaction cycles (left), and the expanded ESI-MS of group $Au_{25}(+3)$ (right). The red and blue numbers indicate the x values of $[Au_{25}^{-1}(4\text{-PyET-}CH_3^+)_x(4\text{-PyET})_{18-x}\cdot(PF_6^-)_{x-4}]^{3+}$ and fragmentation product $[Au_{24}^{0}(4\text{-PyET-}CH_3^+)_x(4\text{-PyET})_{16-x}\cdot(PF_6^-)_{x-3}]^{3+}$, respectively.

Table 4.1 The compositions and charge assignments of the observed Au_{25} cluster peaks.

x value	Composition	1h *m/z* (obs.)	2h *m/z* (obs.)	3h *m/z* (obs.)	*m/z* (calc.)
Total charge +2 : $Au_{25}^{-1}(4\text{-PyET-}CH_3^+)_x(4\text{-PyET})_{18-x}\cdot(PF_6^-)_{x-3}$					
11	$Au_{25}^{-1}(4\text{-PyET-}CH_3^+)_{11}(4\text{-PyET})_7(PF_6^-)_8$	4368.38	-	-	4368.40
12	$Au_{25}^{-1}(4\text{-PyET-}CH_3^+)_{12}(4\text{-PyET})_6(PF_6^-)_9$	4448.39	-	-	4448.40
13	$Au_{25}^{-1}(4\text{-PyET-}CH_3^+)_{13}(4\text{-PyET})_5(PF_6^-)_{10}$	4528.38	-	-	4528.38
14	$Au_{25}^{-1}(4\text{-PyET-}CH_3^+)_{14}(4\text{-PyET})_4(PF_6^-)_{11}$	4608.36	4608.36	-	4608.38
15	$Au_{25}^{-1}(4\text{-PyET-}CH_3^+)_{15}(4\text{-PyET})_3(PF_6^-)_{12}$	4688.37	4688.38	4688.31	4688.37
16	$Au_{25}^{-1}(4\text{-PyET-}CH_3^+)_{16}(4\text{-PyET})_2(PF_6^-)_{13}$	4768.35	4768.36	4768.37	4768.36
17	$Au_{25}^{-1}(4\text{-PyET-}CH_3^+)_{17}(4\text{-PyET})_1(PF_6^-)_{14}$	4848.33	4848.36	4848.36	4848.36
18	$Au_{25}^{-1}(4\text{-PyET-}CH_3^+)_{18}(PF_6^-)_{15}$	-	4928.34	4928.34	4928.35
Total charge +3 : $Au_{25}^{-1}(4\text{-PyET-}CH_3^+)_x(4\text{-PyET})_{18-x}\cdot(PF_6^-)_{x-4}$					
12	$Au_{25}^{-1}(4\text{-PyET-}CH_3^+)_{12}(4\text{-PyET})_6(PF_6^-)_8$	2917.30	-	-	2917.28
13	$Au_{25}^{-1}(4\text{-PyET-}CH_3^+)_{13}(4\text{-PyET})_5(PF_6^-)_9$	2970.62	-	-	2970.61
14	$Au_{25}^{-1}(4\text{-PyET-}CH_3^+)_{14}(4\text{-PyET})_4(PF_6^-)_{10}$	3023.94	3023.95	-	3023.94
15	$Au_{25}^{-1}(4\text{-PyET-}CH_3^+)_{15}(4\text{-PyET})_3(PF_6^-)_{11}$	3077.27	3077.28	3077.27	3077.27
16	$Au_{25}^{-1}(4\text{-PyET-}CH_3^+)_{16}(4\text{-PyET})_2(PF_6^-)_{12}$	3130.59	3130.60	3130.61	3130.60
17	$Au_{25}^{-1}(4\text{-PyET-}CH_3^+)_{17}(4\text{-PyET})_1(PF_6^-)_{13}$	3183.92	3183.92	3183.93	3183.92
18	$Au_{25}^{-1}(4\text{-PyET-}CH_3^+)_{18}(PF_6^-)_{14}$	3237.24	3237.25	3237.25	3237.25
Total charge +4 : $Au_{25}^{-1}(4\text{-PyET-}CH_3^+)_x(4\text{-PyET})_{18-x}\cdot(PF_6^-)_{x-5}$					
14	$Au_{25}^{-1}(4\text{-PyET-}CH_3^+)_{14}(4\text{-PyET})_4(PF_6^-)_9$	2231.72	-	-	2231.71
15	$Au_{25}^{-1}(4\text{-PyET-}CH_3^+)_{15}(4\text{-PyET})_3(PF_6^-)_{10}$	2271.71	2271.71	2271.71	2271.71
16	$Au_{25}^{-1}(4\text{-PyET-}CH_3^+)_{16}(4\text{-PyET})_2(PF_6^-)_{11}$	2311.70	2311.71	2311.70	2311.70
17	$Au_{25}^{-1}(4\text{-PyET-}CH_3^+)_{17}(4\text{-PyET})_1(PF_6^-)_{12}$	2351.70	2351.70	2351.69	2351.70
18	$Au_{25}^{-1}(4\text{-PyET-}CH_3^+)_{18}(PF_6^-)_{13}$	2391.69	2391.69	2391.69	2391.69

The weaker methylating reagent, Me_2SO_4 was also evaluated by varying the reaction time and number of reaction cycles; this gave clusters with various *x* values. Specifically, those with *x*=8.5, 9.7, 12.6, and 14.1 were formed by reactions with Me_2SO_4 for times of 2, 5, 15, and 60 min, respectively (see Figure S4.3 and Table S4.3). The abundance ratios of each cluster species with different *x* values, determined by the intensities of their ESI-MS peaks, are shown in Figure 4.4. Monitoring the reaction with Me_2SO_4 revealed that the absorption spectral changes (i.e., the structural change of Au_{25} core) were completed at 15 min, where the minimum *x* value of the contained Au clusters was 9 (Figure S4.12). These observations indicate that the structural changes are complete when approximately half number of the surface Py groups are cationized. To further understand the mechanisms of the spectral and structural changes caused by the dense surface charges, the isolation into each cluster species and their single-crystal X-ray structure analysis are now under progress.

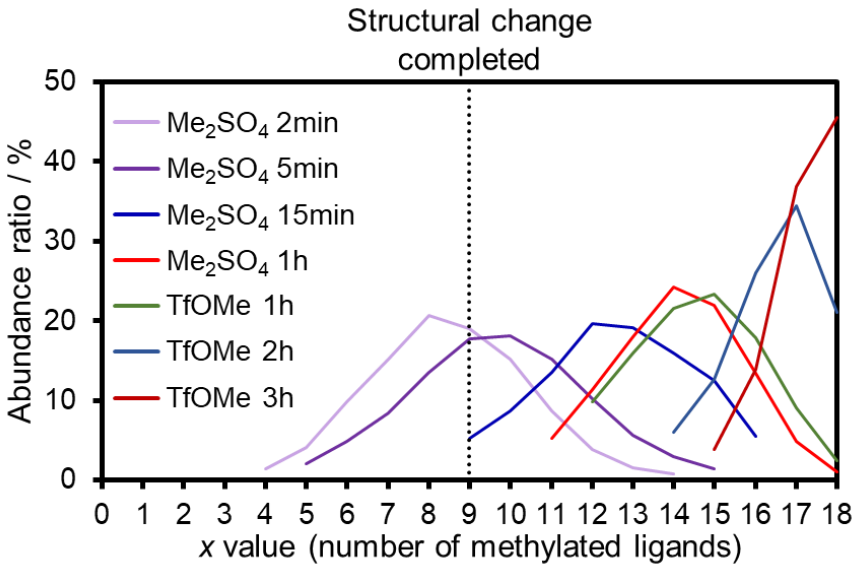

Figure 4.4 The abundance ratios of each cluster species with different *x* values under representative conditions.

4.4 Conclusion

This chapter have demonstrated a novel method for obtaining cationized Au clusters via the surface Menshutkin S_N2 reaction. By changing the methylating reagent, reaction time, and number of reaction cycles, the number of methylated ligands (*x*) was successfully controlled, and an *x* of approximately 18 (i.e., fully methylated Au_{25}(4-PyET-CH_3^+)$_{18}$) was obtained under the optimal condition. This work proposed not only a new synthetic pathway for cationized Au clusters, but also provides a novel idea for diversifying the R-groups of molecular metal clusters through the surface chemical reaction.

4.5 Supporting information

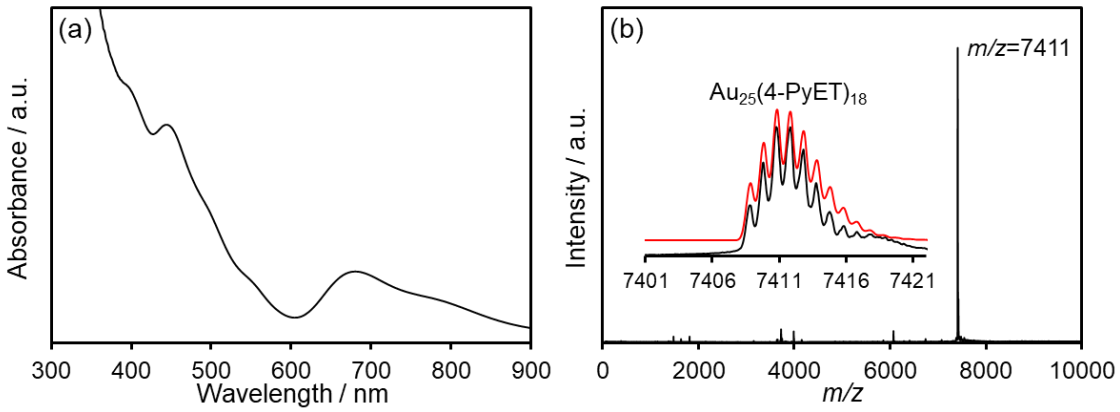

Figure S4.1 (a) UV-Vis absorption spectrum and (b) negative-mode ESI-MS of synthesized $Au_{25}(4\text{-PyET})_{18}$ clusters.

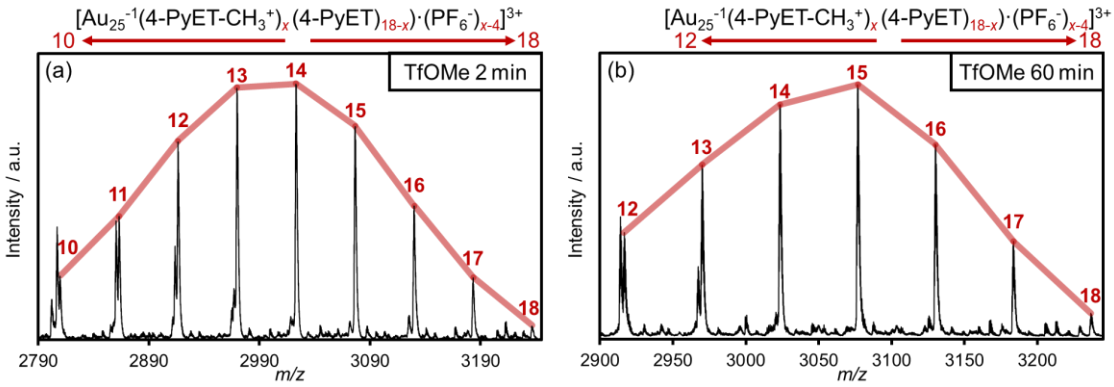

Figure S4.2 Positive-mode ESI-MS of the samples after (a) 2 min and (b) 60 min of reaction with TfOMe. The red numbers indicate the *x* values of $[Au_{25}^{-1}(4\text{-PyET-}CH_3^+)_x(4\text{-PyET})_{18-x}\cdot(PF_6^-)_{x-4}]^{3+}$.

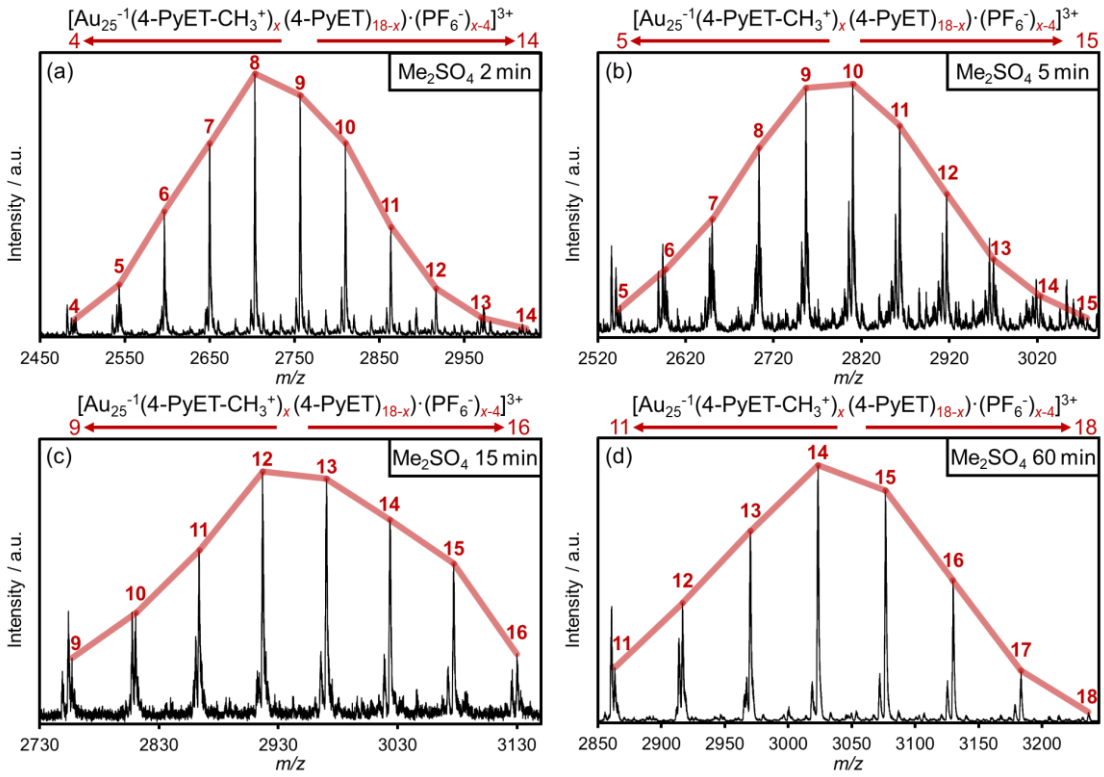

Figure S4.3 Positive-mode ESI-MS of the samples after (a) 2 min, (b) 5 min, (c) 15 min, and (d) 60 min of reaction with Me_2SO_4. The red numbers indicate the *x* values of $[Au_{25}{}^{-1}(4\text{-PyET-CH}_3{}^{+})_x(4\text{-PyET})_{18-x}\cdot(PF_6{}^{-})_{x-4}]^{3+}$.

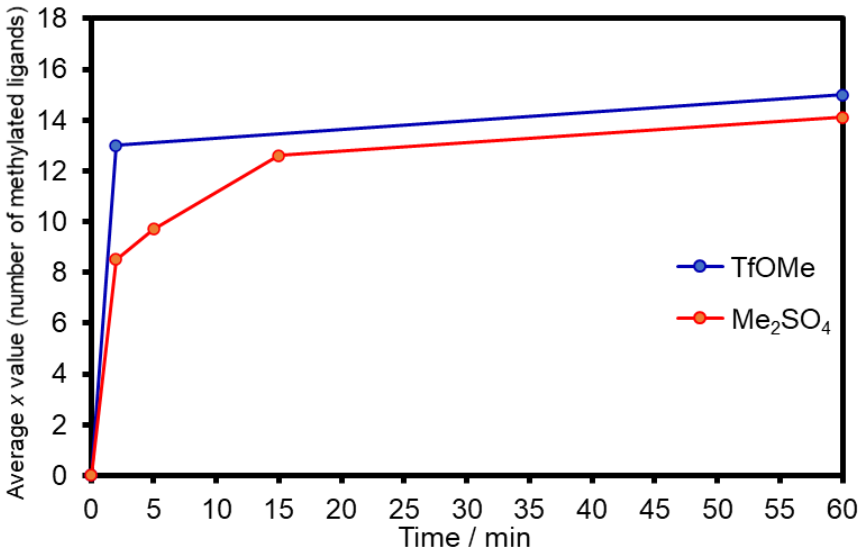

Figure S4.4 The change of *x* value after reaction with Me_2SO_4 (2, 5, 15, and 60 min) and TfOMe (2 and 60 min). The average *x* values are calculated from the ratio of mass spectral signal intensity.

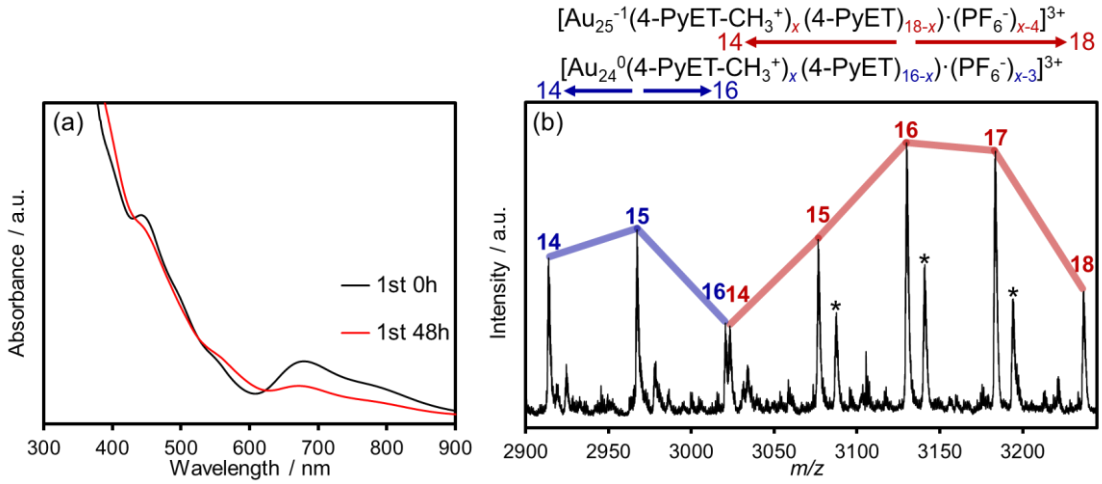

Figure S4.5 (a) UV-Vis absorption spectra (before (0h) and after reaction (48h)) and (b) positive-mode ESI-MS of the sample after 48h of reaction with TfOMe. The red and blue numbers indicate the *x* values of $[Au_{25}^{-1}(4\text{-PyET-}CH_3^+)_x(4\text{-PyET})_{18-x}\cdot(PF_6^-)_{x-4}]^{3+}$ and $[Au_{24}^{0}(4\text{-PyET-}CH_3^+)_x(4\text{-PyET})_{16-x}\cdot(PF_6^-)_{x-3}]^{3+}$, respectively. The peaks (*) are unassigned peaks.

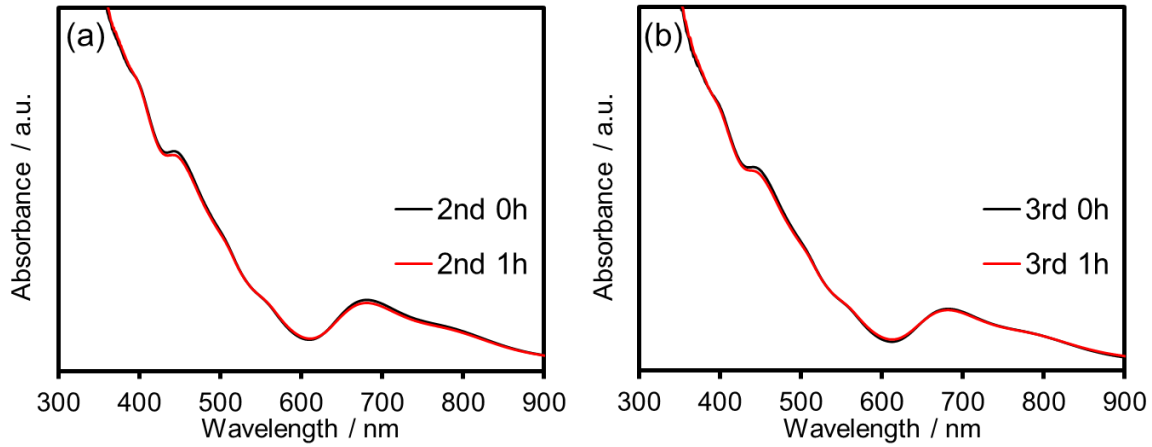

Figure S4.6 UV-Vis absorption spectra of the samples before (0h) and after reaction (1h) after different reaction cycles: (a) 2nd cycle, (b) 3rd cycle.

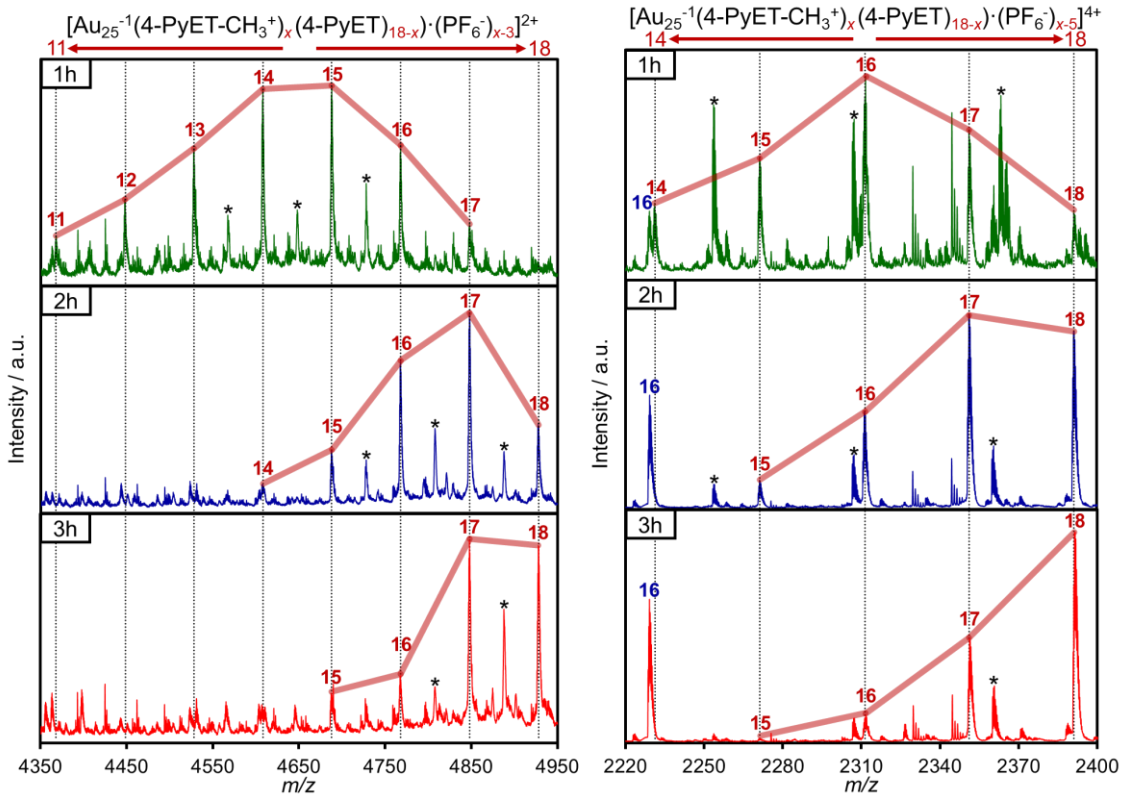

Figure S4.7 Expanded ESI-MS of group Au_{25}(+2) (left) and Au_{25}(+4) (right). The red numbers indicate the *x* values of $[Au_{25}^{-1}(4\text{-PyET-CH}_3^+)_x(4\text{-PyET})_{18-x}\cdot(PF_6^-)_{x-3}]^{2+}$ and $[Au_{25}^{-1}(4\text{-PyET-CH}_3^+)_x(4\text{-PyET})_{18-x}\cdot(PF_6^-)_{x-5}]^{4+}$. The peaks (*) are unassigned peaks.

Table S4.1 Detailed calculation for average number of methylated ligands from the mass spectral signal intensity ratio.

x value	1h		2h		3h		4h	
	Intensity	Intensity×*x*	Intensity	Intensity×*x*	Intensity	Intensity×*x*	Intensity	Intensity×*x*
Total charge +2 : $Au_{25}^{-1}(4\text{-PyET-}CH_3^+)_x(4\text{-PyET})_{18-x}\cdot(PF_6^-)_{x-3}$								
11	1672	18392	-		-		-	
12	2874	34488	-		-		-	
13	4548	59124	-		-		-	
14	6486	90804	1353	18942	-		-	
15	6621	99315	2934	44010	1851	27765	-	
16	4673	74768	7072	113152	2584	41344	-	
17	2069	35173	9267	157539	7772	132124	2286	38862
18	-		4155	74790	7578	136404	4070	73260
x value (ave.)	14.2		16.5		17.1		17.6	
Degree of cationization (ave.)	79.1 %		91.6 %		94.8 %		98.0 %	
Total charge +3 : $Au_{25}^{-1}(4\text{-PyET-}CH_3^+)_x(4\text{-PyET})_{18-x}\cdot(PF_6^-)_{x-4}$								
12	11181	134172	-		-		-	
13	18234	237042	-		-		-	
14	24553	343742	7834	109676	-		-	
15	26651	399765	16457	246855	4850	72750	1922	28830
16	20395	326320	34192	547072	17186	274976	5908	94528
17	10257	174369	45006	765102	46971	798507	22939	389963
18	2730	49140	27603	496854	58424	1051632	47631	857358
x value (ave.)	14.6		16.5		17.2		17.5	
Degree of cationization (ave.)	81.1 %		91.8 %		95.8 %		97.1 %	
Total charge +4 : $Au_{25}^{-1}(4\text{-PyET-}CH_3^+)_x(4\text{-PyET})_{18-x}\cdot(PF_6^-)_{x-5}$								
14	1340	18760	-		-		-	
15	2121	31815	3260	48900	740	11100	-	
16	3549	56784	10261	164176	4200	67200	2509	40144
17	2613	44421	21232	360944	15638	265846	7428	126276
18	1210	21780	19452	350136	31635	569430	25214	453852
x value (ave.)	16.0		17.0		17.5		17.6	
Degree of cationization (ave.)	89.0 %		94.7 %		97.2 %		98.0 %	

Average of Total charge +2 ~ +4				
x value (ave.)	**15.0**	**16.7**	**17.3**	**17.6**
Degree of cationization (ave.)	**83.1 %**	**92.7 %**	**95.9 %**	**97.7 %**

* It was assumed that mass spectral signal intensities are directly proportional to solution concentrations of the corresponding cluster species, and calculated the average number of methylated ligands (average *x* value).

* *X* value (ave.) and Cationization degree (ave.) are calculated from following formulas.

* *X* value (ave.) = (Total value of intensity×*x* (*x*=1~18)) / (Total value of intensity (*x*=1~18))

* Degree of cationization (ave.) = *x* (ave.) / 18×100 [%]

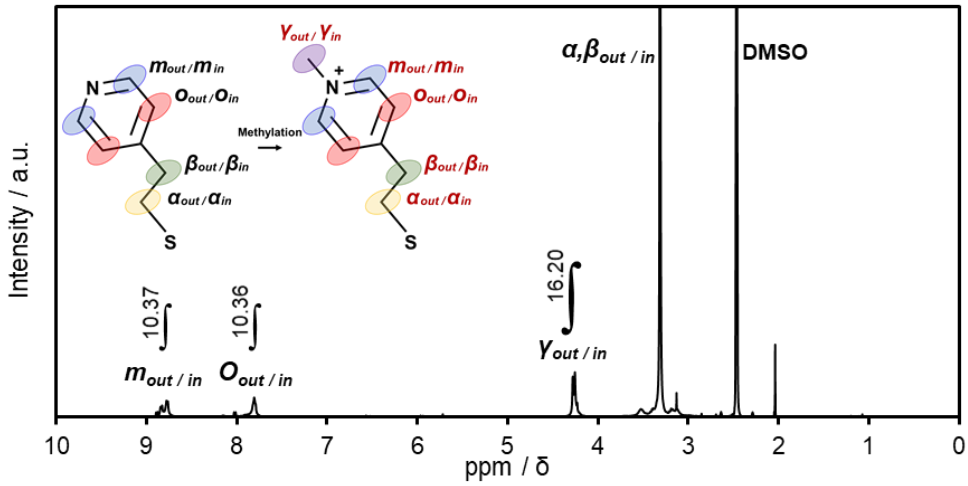

Figure S4.8 ^{1}H NMR spectrum of the sample after 3-cycle reaction in DMSO-d_6 at 400 MHz. The average x value (average number of methylated ligands) of 17.3 (96.0%) was calculated from the integral values of peak m_{out}/m_{in} and peak γ_{out}/γ_{in}.

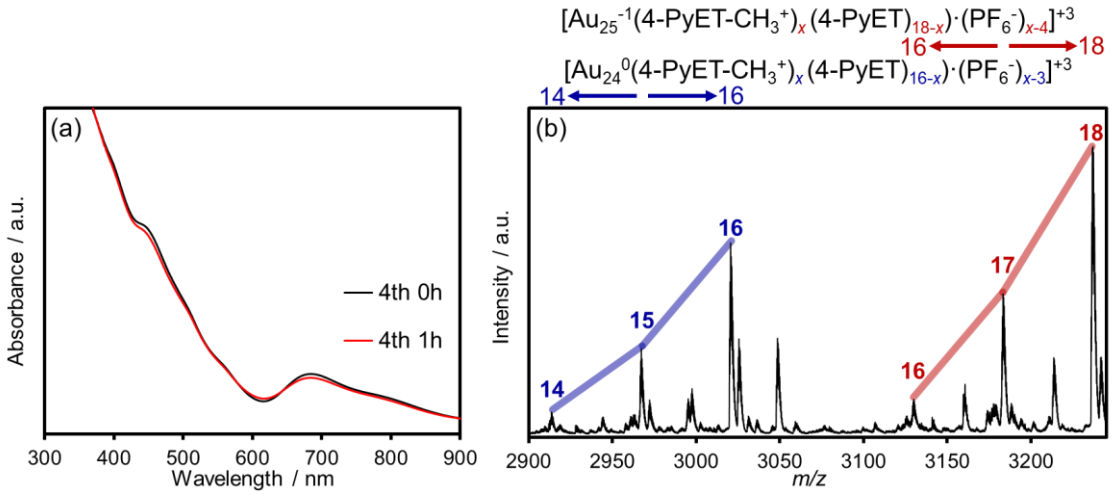

Figure S4.9 (a) UV-Vis absorption spectra before (0h) and after 4th reaction (1h), and (b) positive-mode ESI-MS of the sample after 1h of 4-cycle reaction with TfOMe. The red and blue numbers indicate the x values of $[Au_{25}^{-1}(4\text{-PyET-CH}_3^{+})_x(4\text{-PyET})_{18-x}\cdot(PF_6^{-})_{x-4}]^{3+}$ and $[Au_{24}^{0}(4\text{-PyET-CH}_3^{+})_x(4\text{-PyET})_{16-x}\cdot(PF_6^{-})_{x-3}]^{3+}$, respectively.

Main peaks : $Au_{25}(SR)_{18}$

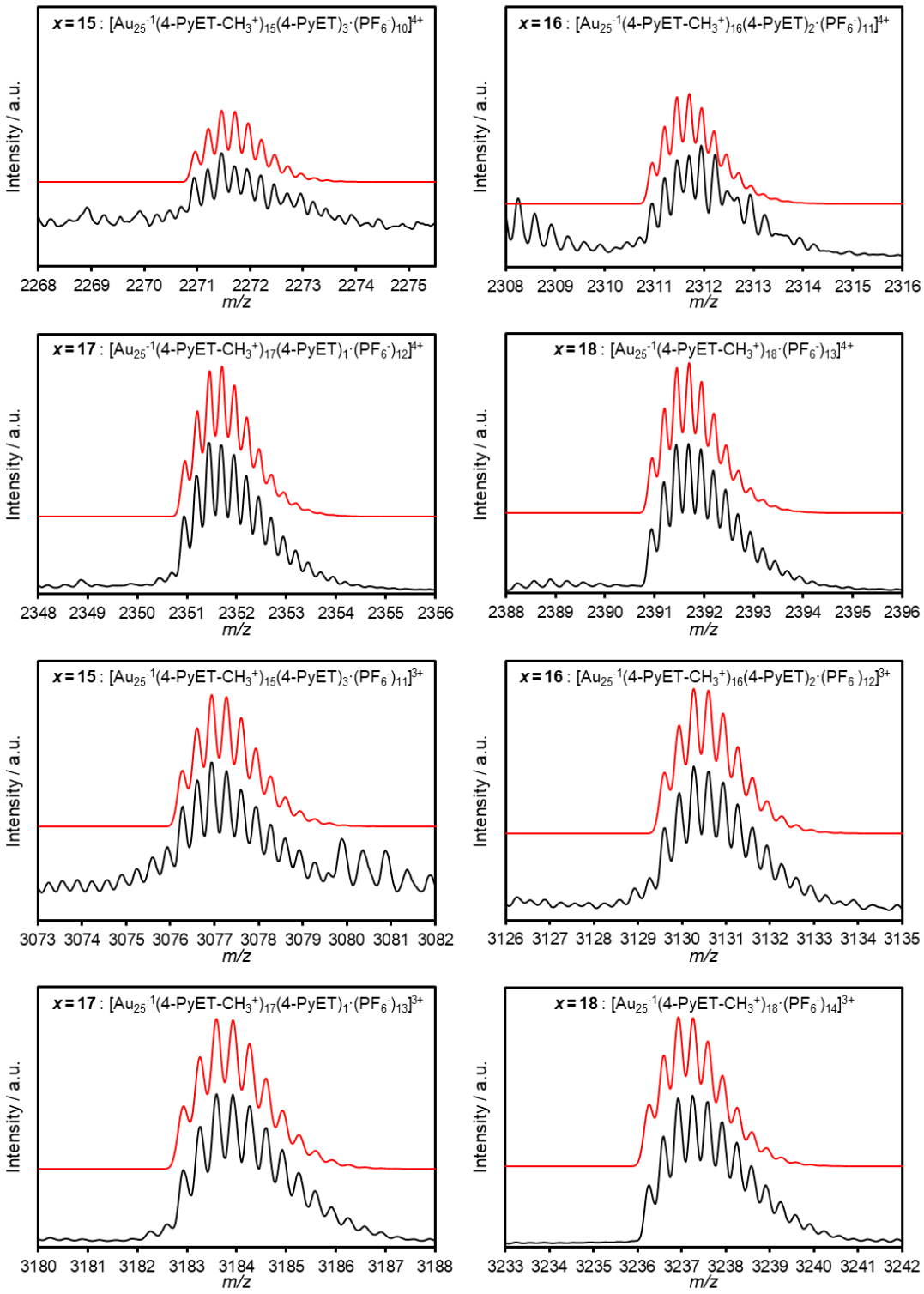

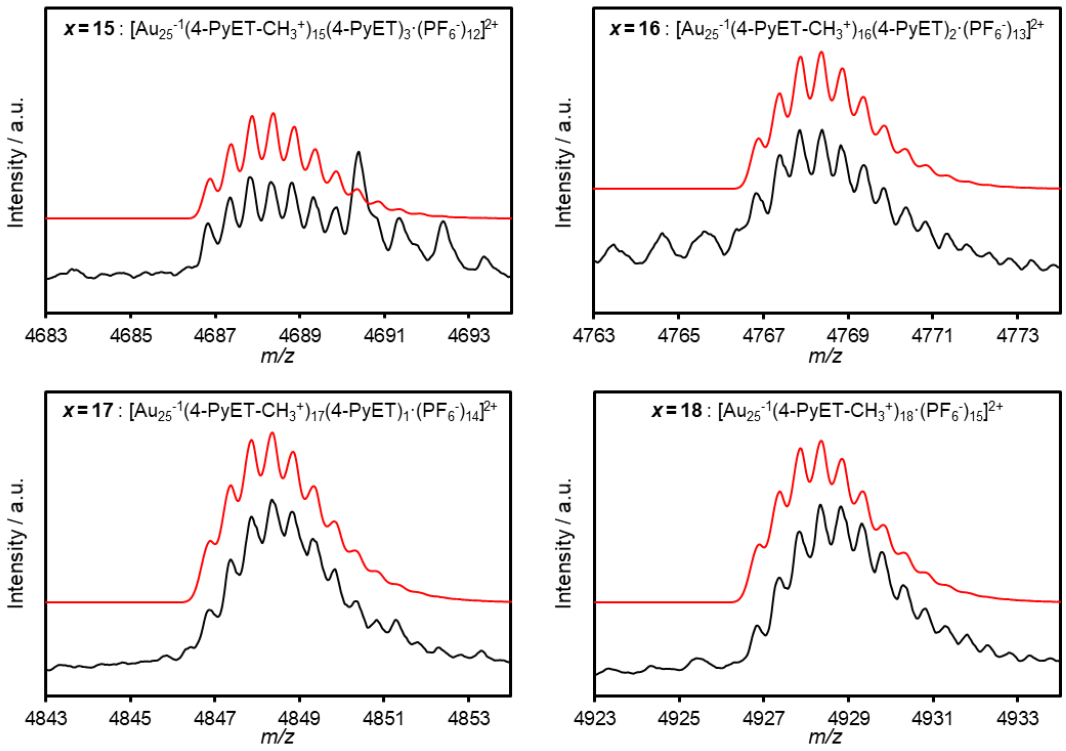
x = 15 : [Au25-1(4-PyET-CH3+)15(4-PyET)3·(PF6-)12]2+
x = 16 : [Au25-1(4-PyET-CH3+)16(4-PyET)2·(PF6-)13]2+
x = 17 : [Au25-1(4-PyET-CH3+)17(4-PyET)1·(PF6-)14]2+
x = 18 : [Au25-1(4-PyET-CH3+)18·(PF6-)15]2+
Intensity / a.u.
m/z
4683
4685
4687
4689
4691
4693
4763
4765
4767
4769
4771
4773
4843
4845
4847
4849
4851
4853
4923
4925
4927
4929
4931
4933

Fragment peaks : $Au_{24}(SR)_{16}$, $Au_{23}(SR)_{15}$, $Au_4(SR)_4$

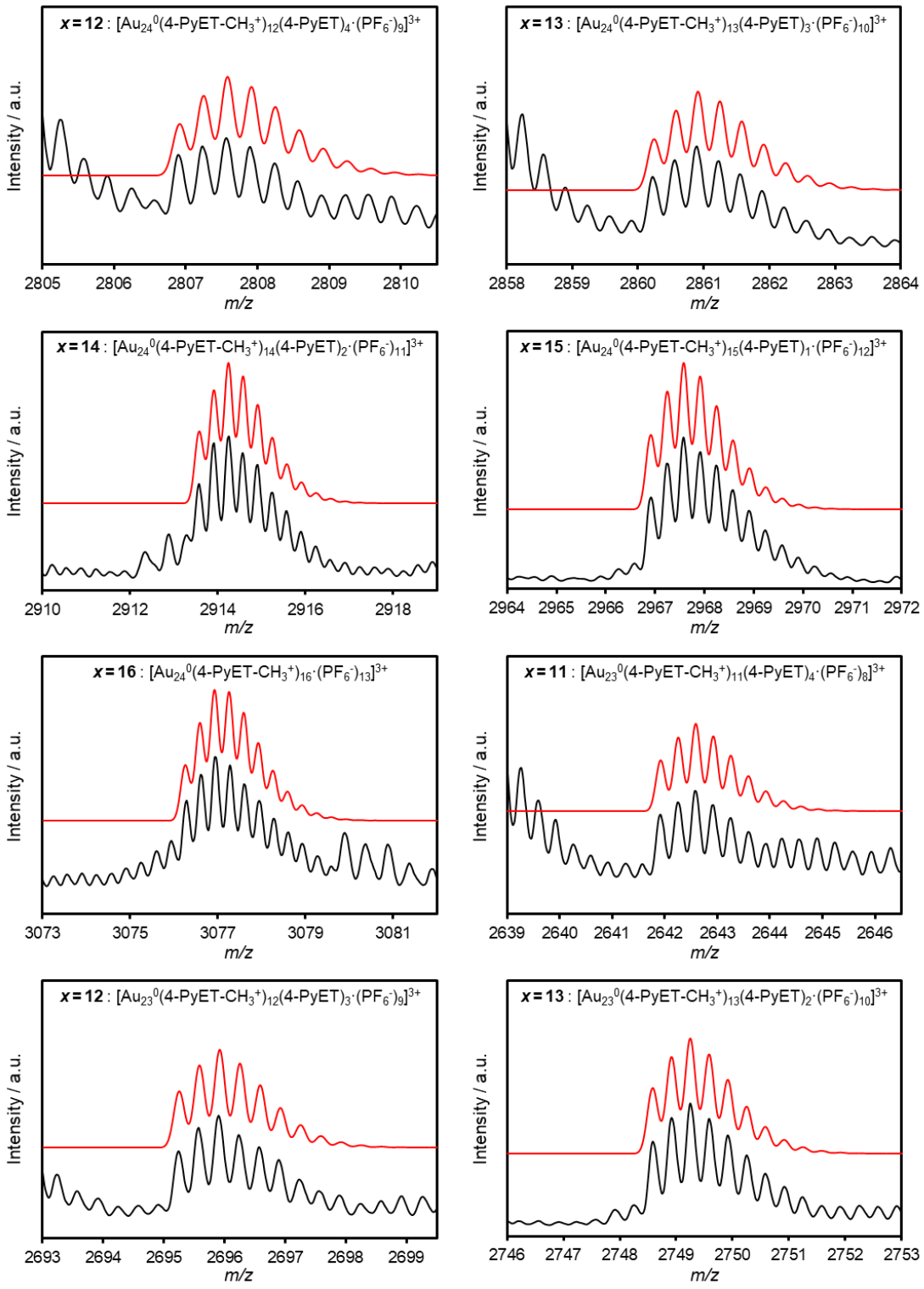

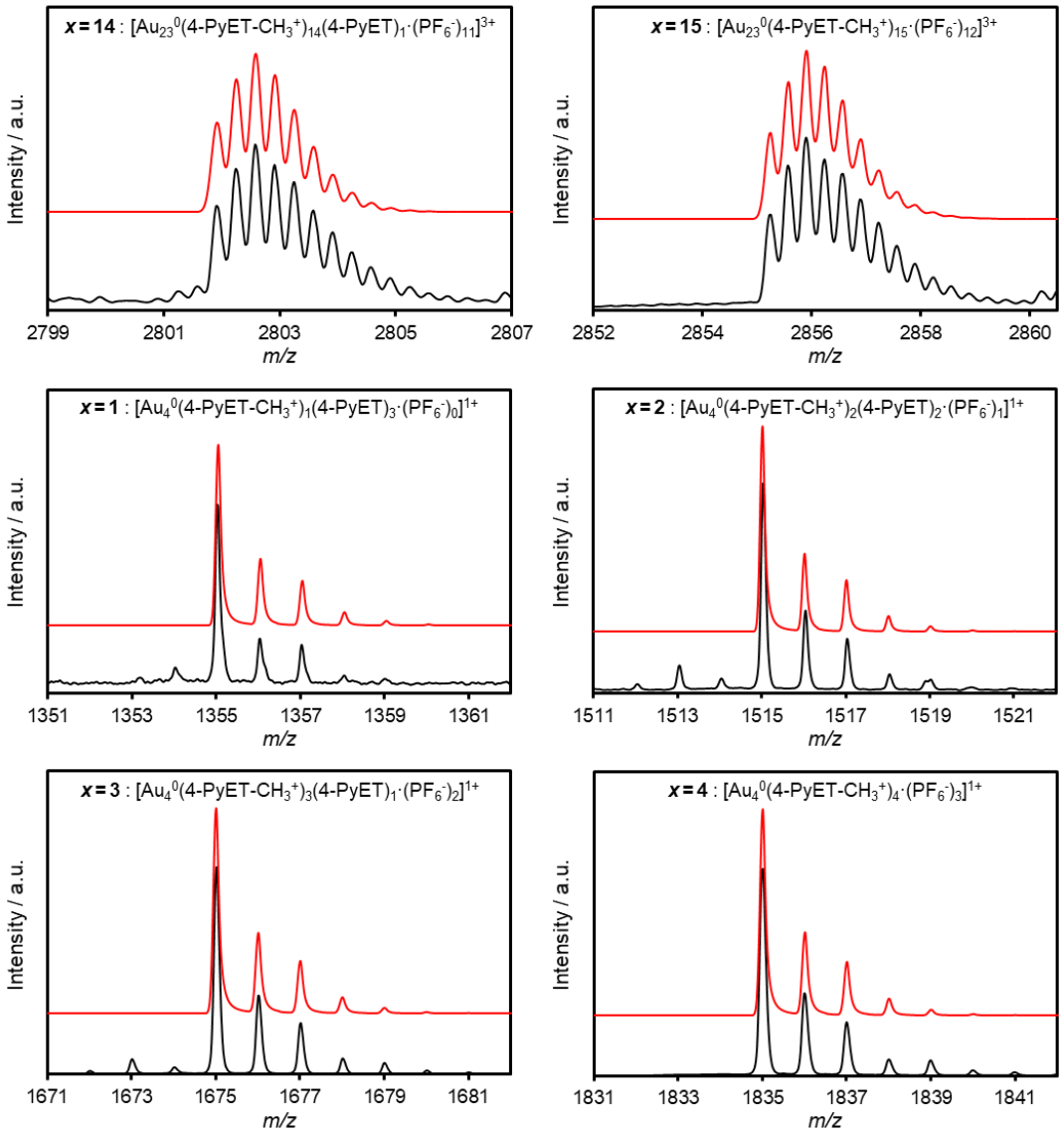

Figure S4.10 Expanded ESI-MS (black lines) and simulated isotope patterns (red lines) for the main peaks ($[Au_{25}^{-1}(4\text{-PyET-}CH_3^+)_x(4\text{-PyET})_{18-x}\cdot(PF_6^-)_{x-3}]^{2+}$, $[Au_{25}^{-1}(4\text{-PyET-}CH_3^+)_x(4\text{-PyET})_{18-x}\cdot(PF_6^-)_{x-4}]^{3+}$, and $[Au_{25}^{-1}(4\text{-PyET-}CH_3^+)_x(4\text{-PyET})_{18-x}\cdot(PF_6^-)_{x-5}]^{4+}$) and fragment peaks ($[Au_{24}^{0}(4\text{-PyET-}CH_3^+)_x(4\text{-PyET})_{16-x}\cdot(PF_6^-)_{x-3}]^{3+}$, $[Au_{23}^{0}(4\text{-PyET-}CH_3^+)_x(4\text{-PyET})_{15-x}\cdot(PF_6^-)_{x-3}]^{3+}$, and $[Au_4^{0}(4\text{-PyET-}CH_3^+)_x(4\text{-PyET})_{4-x}\cdot(PF_6^-)_{x-1}]^{1+}$).

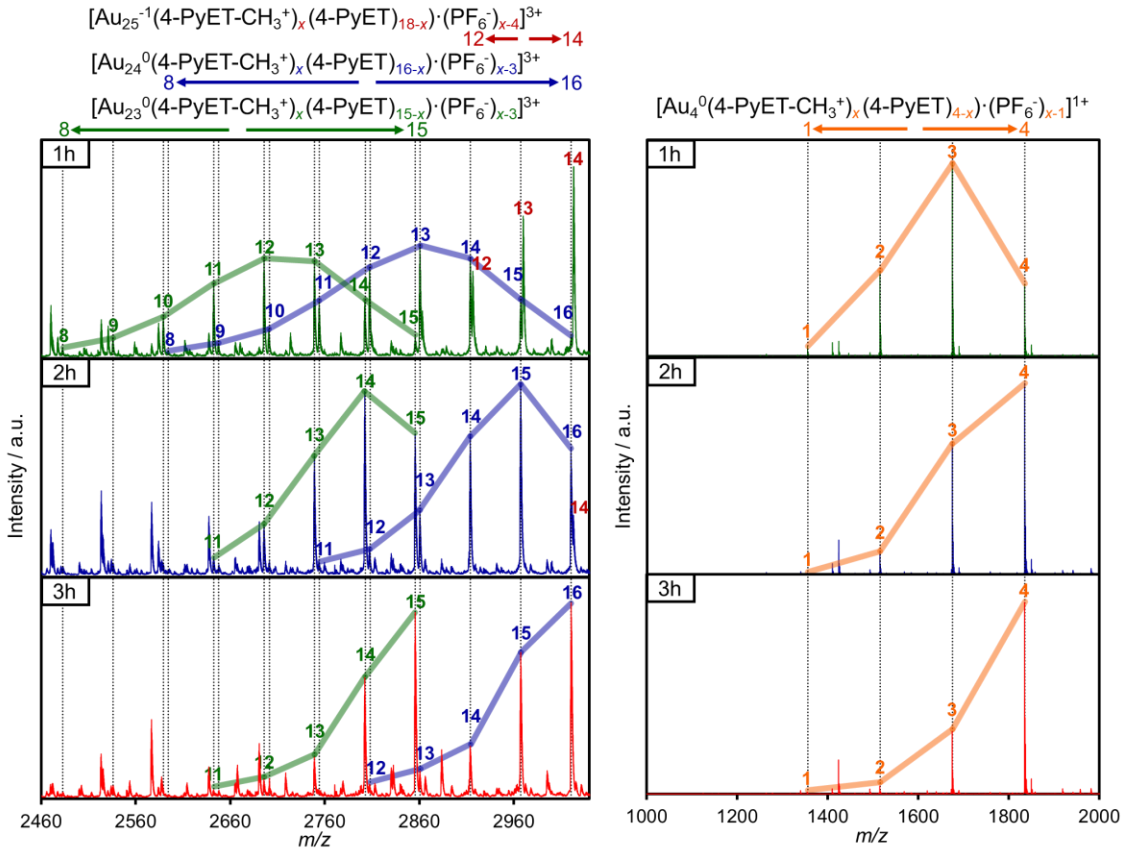

Figure S4.11 Expanded ESI-MS of group Au_4, Au_{23}, and Au_{24}. The red, blue, green and orange numbers indicate the *x* values of $[Au_{25}^{-1}(4\text{-PyET-CH}_3^+)_x(4\text{-PyET})_{18-x}\cdot(PF_6^-)_{x-4}]^{3+}$, $[Au_{24}^{0}(4\text{-PyET-CH}_3^+)_x(4\text{-PyET})_{16-x}\cdot(PF_6^-)_{x-3}]^{3+}$, $[Au_{23}^{0}(4\text{-PyET-CH}_3^+)_x(4\text{-PyET})_{15-x}\cdot(PF_6^-)_{x-3}]^{3+}$, and $[Au_4^{0}(4\text{-PyET-CH}_3^+)_x(4\text{-PyET})_{4-x}\cdot(PF_6^-)_{x-1}]^{1+}$, respectively.

Table S4.2 The compositions and charge assignments of observed fragment peaks (Au_4, Au_{23}, and Au_{24}).

x value	Composition	1h *m/z* (obs.)	2h *m/z* (obs.)	3h *m/z* (obs.)	*m/z* (calc.)
Total charge +3 : $Au_{24}^{0}(4\text{-PyET-CH}_3^{+})_x(4\text{-PyET})_{16-x}\cdot(PF_6^{-})_{x-3}$					
8	$Au_{24}^{0}(4\text{-PyET-CH}_3^{+})_8(4\text{-PyET})_8(PF_6^{-})_5$	2594.28	-	-	2594.26
9	$Au_{24}^{0}(4\text{-PyET-CH}_3^{+})_9(4\text{-PyET})_7(PF_6^{-})_6$	2647.61	-	-	2647.60
10	$Au_{24}^{0}(4\text{-PyET-CH}_3^{+})_{10}(4\text{-PyET})_6(PF_6^{-})_7$	2700.94	-	-	2700.93
11	$Au_{24}^{0}(4\text{-PyET-CH}_3^{+})_{11}(4\text{-PyET})_5(PF_6^{-})_8$	2754.27	2754.27	-	2754.26
12	$Au_{24}^{0}(4\text{-PyET-CH}_3^{+})_{12}(4\text{-PyET})_4(PF_6^{-})_9$	2807.59	2807.60	2807.56	2807.59
13	$Au_{24}^{0}(4\text{-PyET-CH}_3^{+})_{13}(4\text{-PyET})_3(PF_6^{-})_{10}$	2860.92	2860.93	2860.90	2860.92
14	$Au_{24}^{0}(4\text{-PyET-CH}_3^{+})_{14}(4\text{-PyET})_2(PF_6^{-})_{11}$	2914.24	2914.26	2914.26	2914.25
15	$Au_{24}^{0}(4\text{-PyET-CH}_3^{+})_{15}(4\text{-PyET})_1(PF_6^{-})_{12}$	2967.57	2967.58	2967.57	2967.58
16	$Au_{24}^{0}(4\text{-PyET-CH}_3^{+})_{16}(PF_6^{-})_{13}$	3020.88	3020.90	3020.90	3020.90
Total charge +3 : $Au_{23}^{0}(4\text{-PyET-CH}_3^{+})_x(4\text{-PyET})_{15-x}\cdot(PF_6^{-})_{x-3}$					
8	$Au_{23}^{0}(4\text{-PyET-CH}_3^{+})_8(4\text{-PyET})_7(PF_6^{-})_5$	2482.62	-	-	2482.60
9	$Au_{23}^{0}(4\text{-PyET-CH}_3^{+})_9(4\text{-PyET})_6(PF_6^{-})_6$	2535.95	-	-	2535.93
10	$Au_{23}^{0}(4\text{-PyET-CH}_3^{+})_{10}(4\text{-PyET})_5(PF_6^{-})_7$	2589.27	-	-	2589.26
11	$Au_{23}^{0}(4\text{-PyET-CH}_3^{+})_{11}(4\text{-PyET})_4(PF_6^{-})_8$	2642.60	2642.60	2642.58	2642.59
12	$Au_{23}^{0}(4\text{-PyET-CH}_3^{+})_{12}(4\text{-PyET})_3(PF_6^{-})_9$	2695.92	2695.92	2695.90	2695.92
13	$Au_{23}^{0}(4\text{-PyET-CH}_3^{+})_{13}(4\text{-PyET})_2(PF_6^{-})_{10}$	2749.24	2749.25	2749.25	2749.25
14	$Au_{23}^{0}(4\text{-PyET-CH}_3^{+})_{14}(4\text{-PyET})_1(PF_6^{-})_{11}$	2802.57	2802.58	2802.57	2802.58
15	$Au_{23}^{0}(4\text{-PyET-CH}_3^{+})_{15}(PF_6^{-})_{12}$	2855.89	2855.90	2855.90	2855.90
Total charge +1 : $Au_4^{0}(4\text{-PyET-CH}_3^{+})_x(4\text{-PyET})_{4-x}\cdot(PF_6^{-})_{x-1}$					
1	$Au_4^{0}(4\text{-PyET-CH}_3^{+})_1(4\text{-PyET})_3$	1355.06	1354.99	1355.03	1355.04
2	$Au_4^{0}(4\text{-PyET-CH}_3^{+})_2(4\text{-PyET})_2(PF_6^{-})_1$	1515.05	1515.05	1515.04	1515.03
3	$Au_4^{0}(4\text{-PyET-CH}_3^{+})_3(4\text{-PyET})_1(PF_6^{-})_2$	1675.02	1675.02	1675.02	1675.02
4	$Au_4^{0}(4\text{-PyET-CH}_3^{+})_4(PF_6^{-})_3$	1835.00	1835.00	1835.00	1835.00

Table S4.3 The *x* values of the clusters with different methylating reagent, reaction time, and number of reaction cycles.

x value (ave.)	Methylating reagent	Reaction time	Number of cycles
17.3	TfOMe	3h	3
16.7	TfOMe	2h	2
15.0	TfOMe	1h	1
13.0	TfOMe	2 min	1
14.1	Me_2SO_4	1h	1
12.6	Me_2SO_4	15 min	1
9.7	Me_2SO_4	5 min	1
8.5	Me_2SO_4	2 min	1

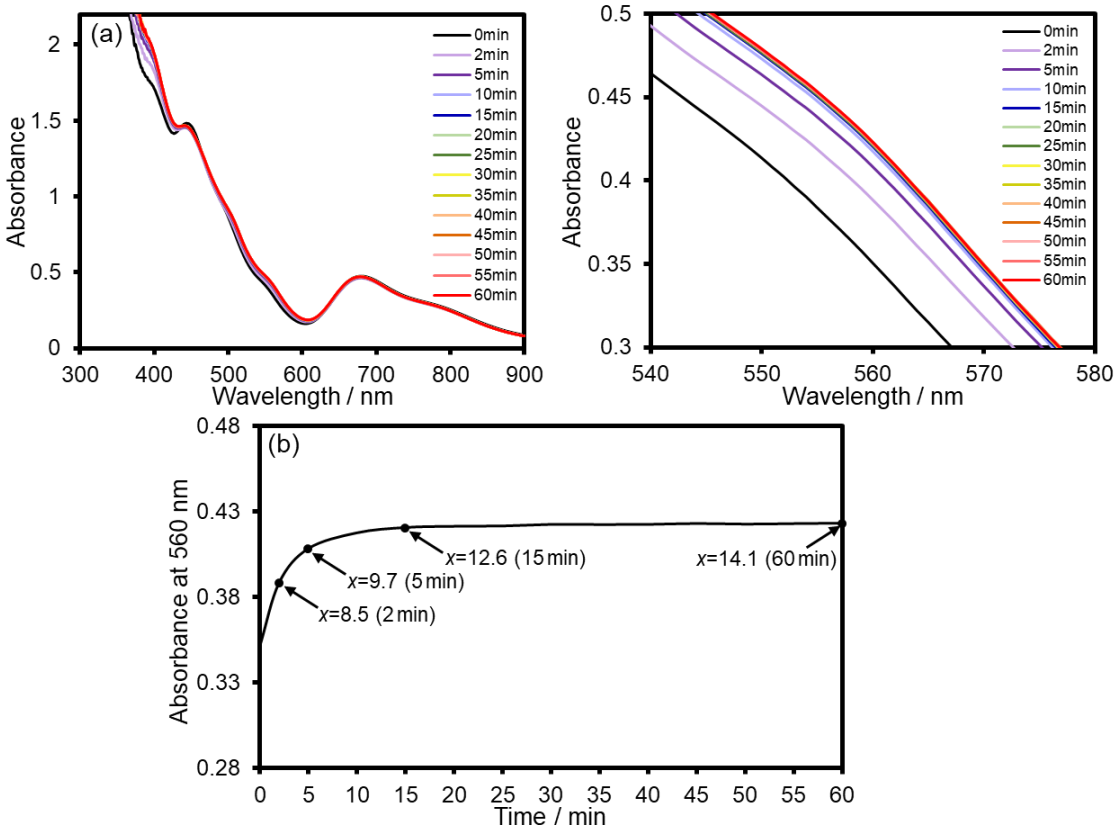

Figure S4.12 (a) UV-Vis absorption spectra of the samples after reaction with Me_2SO_4 for various time intervals and (b) the change of absorbance at 560 nm with reaction time and the corresponding *x* values.

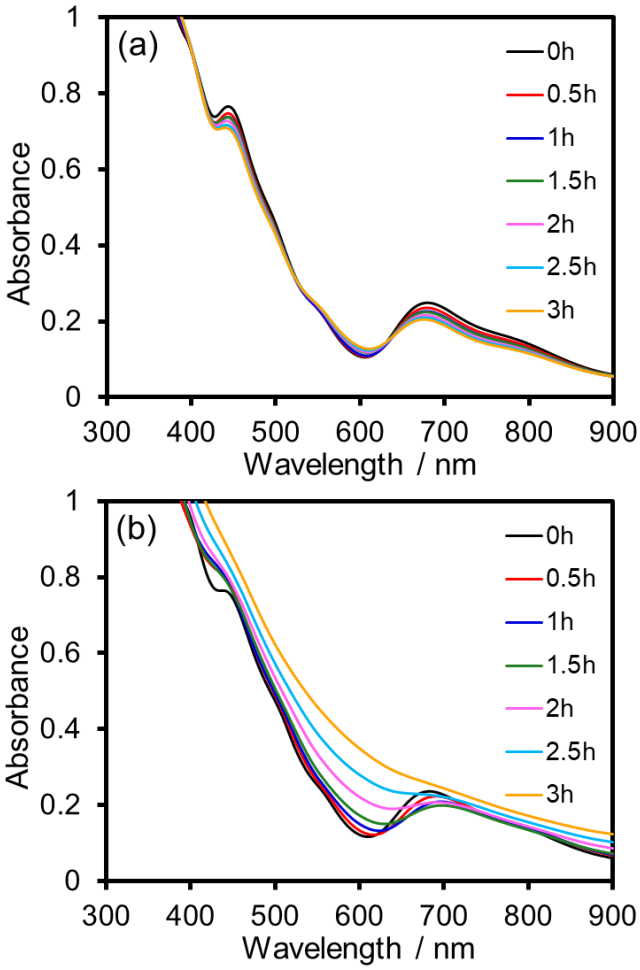

Figure S13. Time dependences of absorption spectra of (a) Au_{25}(4-PyET)$_{18}$ and (b) Au_{25}(4-PyET-CH_3^+)$_x$(4-PyET)$_{18-x}$ (x≈18, after 3-cycles reaction with TfOMe) in DMF solution (2×10^{-5} M, 1.0 mL) at 80 °C under stirring at 200 rpm.

4.6 References

(1) Li, G.; Jin, R. Atomically Precise Gold Nanoclusters as New Model Catalysts. *Acc. Chem. Res.* **2013**, *46*, 1749–1758.

(2) Wan, X. K.; Wang, J. Q.; Nan, Z. A.; Wang, Q. M. Ligand effects in catalysis by atomically precise gold nanoclusters. *Sci. Adv.* **2017**, *3*, e1701823.

(3) Guan, G.; Zhang, S. Y.; Cai, Y.; Liu, S.; Bharathi, M. S.; Low, M.; Yu, Y.; Xie, J.; Zheng, Y.; Zhang, Y. W., Han, M. Y. Convenient Purification of Gold Clusters by Co-Precipitation for Improved Sensing of Hydrogen Peroxide, Mercury Ions and Pesticides. *Chem. Commun.* **2014**, *50*, 5703–5705.

(4) Shen, R., Liu, P., Zhang, Y., Yu, Z., Chen, X., Zhou, L., Nie, B; Żaczek, A.; Chen, J; Liu, J. Sensitive Detection of Single-cell Secreted H_2O_2 by Integrating a Microfluidic Droplet Sensor and Au Nanoclusters. *Anal. Chem.* **2018**, *90*, 4478–4484.

(5) Zheng, K.; Setyawati, M. I.; Leong, D. T.; Xie, J. Surface Ligand Chemistry of Gold Nanoclusters Determines Their Antimicrobial Ability. *Chem. Mater.* **2018**, *30*, 2800–2808.

(6) Zheng, K.; Setyawati, M. I.; Leong, D. T.; Xie, J. Antimicrobial Gold Nanoclusters. *ACS Nano*, **2017**, *11*, 6904–6910.

(7) Chen, Y.; Zeng, C.; Kauffman, D. R.; Jin, R. Tuning the Magic Size of Atomically Precise Gold Nanoclusters via Isomeric Methylbenzenethiols. *Nano Lett.* **2015**, *15*, 3603–3609.

(8) Yan, J.; Teo, B. K.; Zheng, N. Surface Chemistry of Atomically Precise Coinage-Metal Nanoclusters: From Structural Control to Surface Reactivity and Catalysis. *Acc. Chem. Res.* **2018**, *51*, 3084–3093.

(9) Ackerson, C. J.; Jadzinsky, P. D.; Kornberg, R. D. Thiolate Ligands for Synthesis of Water-Soluble Gold Clusters. *J. Am. Chem. Soc.* **2005**, *127*, 6550–6551.

(10) Knoppe, S.; Bürgi, T. Chirality in Thiolate-protected Gold Clusters. *Acc. Chem. Res.* **2014**, *47*, 1318–1326.

(11) Yang, H.; Wang, Y.; Lei, J.; Shi, L.; Wu, X.; Makinen, V.; Lin, S.; Tang, Z.; He, J.; Hakkinen, H.; Zheng, L.; Zheng, N. Ligand-Stabilized $Au_{13}Cu_x$ (x = 2, 4, 8) Bimetallic Nanoclusters: Ligand Engineering to Control the Exposure of Metal Sites. *J. Am. Chem. Soc.* **2013**, *135*, 9568–9571.

(12) Yuan, X.; Goswami, N.; Chen, W.; Yao, Q.; Xie, J. Insights into the Effect of Surface Ligands on the Optical Properties of Thiolated Au_{25} Nanoclusters. *Chem. Commun.* **2016**, *52*, 5234–5237.

(13) Nel, A. E.; Mädler, L.; Velegol, D.; Xia, T.; Hoek, E. M.; Somasundaran, P.; Klaessig, F.; Castranova, V.; Thompson, M. Understanding biophysicochemical interactions at the nano-bio interface. *Nat. Mater.* **2009**, *8*, 543−557.

(14) Ishida, Y.; Narita, K.; Yonezawa, T.; Whetten, R. L. Fully Cationized Gold Clusters: Synthesis of $Au_{25}(SR^+)_{18}$. *J. Phys. Chem. Lett.* **2016**, *7*, 3718–3722.

(15) Narita, K.; Ishida, Y.; Yonezawa, T; Huang, Z. Super Polycationic Molecular Compounds: $Au_{144}(SR^+)_{60}$ Clusters. *J. Phys. Chem. C* **2019**, *123*, 21768−21773.

(16) Huang, Z.; Ishida, Y.; Narita, K.; Yonezawa, T. Kinetics of Cationic-Ligand-Exchange Reactions in Au_{25} Nanoclusters. *J. Phys. Chem. C* **2018**, *122*, 18142−18150.

(17) Fields-Zinna, C. A.; Sardar, R.; Beasley, C. A.; Murray, R. W. Electrospray Ionization Mass Spectrometry of Intrinsically Cationized Nanoparticles,

$[Au_{144/146}(SC_{11}H_{22}N(CH_2CH_3)_3{}^{3+})_X\text{-}(S(CH_2)_5CH_3)_Y]^{X+}$. *J. Am. Chem. Soc.* **2009**, *131*, 16266−16271.

(18) Gunawardene, P. N.; Corrigan, J. F.; Workentin, M. S. Golden Opportunity: A Clickable Azide-Functionalized $[Au_{25}(SR)_{18}]^-$ Nanocluster Platform for Interfacial Surface Modifications, *J. Am. Chem. Soc.* **2019**, *141*, 11781−11785.

(19) Cui, X.; Wang, J.; Liu, B.; Ling, S.; Long, R.; Xiong, Y. Turning Au Nanoclusters Catalytically Active for Visible-Light-Driven CO_2 Reduction through Bridging Ligands, *J. Am. Chem. Soc.* **2018**, *140*, 16514−16520.

(20) Menschutkin, N. Beiträge zur Kenntnis der Affinitätskoeffizienten der Alkylhaloide und der organischen Amine. *Z. Phys. Chem.* **1890**, *5*, 589−600.

(21) Huang, Z.; Ishida, Y.; Yonezawa, T. Basic $[Au_{25}(SCH_2CH_2Py)_{18}]^- \cdot Na^+$ Clusters: Synthesis, Layered Crystallographic Arrangement, and Unique Surface Protonation. *Angew. Chem., Int. Ed.* **2019**, *58*, 13411–13415.

(22) Negishi, Y.; Chaki, N. K.; Shichibu, Y.; Whetten, R. L.; Tsukuda, T. Origin of Magic Stability of Thiolated Gold Clusters: a Case Study on $Au_{25}(SC_6H_{13})_{18}$. *J. Am. Chem. Soc.* **2007**, *129*, 11322–11323.

(23) Zhu, M.; Aikens, C. M.; Hollander, F. J.; Schatz, G. C.; Jin, R. Correlating the Crystal Structure of a Thiol-Protected Au_{25} Cluster and Optical Properties. *J. Am. Chem. Soc.* **2008**, *130*, 5883–5885.

(24) Zhu, M.; Chan, G.; Qian, H.; Jin, R. Unexpected Reactivity of $Au_{25}(SCH_2CH_2Ph)_{18}$ Nanoclusters with Salts, *Nanoscale*, **2011**, *3*, 1703–1707.

Chapter 5

Unique Kinetics of Cationic-Ligand-Exchange Reactions on $Au_{25}(SR)_9(SR^+)_9$ Clusters

5.1 Introduction

Thiolate-protected gold clusters ($Au_m(SR)_n$) have potential applications in diverse fields, such as catalysis,[1,2] sensing,[3,4] and bio-applications,[5,6] because of their interesting physicochemical properties. Up-to-date, many thiolate-protected Au clusters with different core size and thiolate ligands have been synthesized;[7-10] however the cationized Au clusters protected by cationic thiolate ligands had not been synthesized, due to the difficulty in handling the positive charges of cationic groups.[11-13] The cationized Au clusters are desirable as they widen the applications of bioimaging and sensing.[14]

Recently, for the first time, our group successfully synthesized the fully cationized Au clusters using size-focusing method by preventing the formation of $[Au(I)]^-–SR^+$ ionic polymer complexes that hinder the homogeneous reduction of Au precursors (i.e. $Au_{25}(S(CH_2)_{11}N(CH_3)_3^+)_{18}$, $Au_{144}(S(CH_2)_{11}N(CH_3)_3^+)_{60}$).[11,12] Furthermore, our group successfully synthesized the fully cationized Au clusters as main product using surface reaction method, in which the neutral Au_{25}(4-PyET)$_{18}$ clusters (4-PyET=SCH_2CH_2Py) were cationized to Au_{25}(4-PyET-$CH_3^+)_x$(4-PyET)$_{18-x}$ (x≈18) via surface Menshutkin reaction.[15] Thus, the fully cationized Au clusters have been successfully synthesized using several method so far; however the ligand-exchange method synthesizing the fully cationized Au clusters (exchange ratio: 100%) has not been developed yet. The ligand-

exchange method can produce not only the Au clusters with bi- (or tri-) thiolate ligands,[16,17] but also the new Au clusters with different core size that have not been obtained using normal size-focusing method through a ligand-exchange-induced size/structure transformation (LEIST) process.[18,19]

Murray group reported for the first time the neutral-to-cationic ligand-exchange reaction on hexanethiolate (HSC_6H_{13})-protected neutral Au_{140} clusters with the cationic ligand, $HS(CH_2)_{11}N(CH_2CH_3)_3^+$.[20] Two types of size-transformed Au clusters, $Au_{144}(SR)_{60}$ and $Au_{146}(SR)_{59}$, were obtained with the ligand-exchange ratio of ca. 20%. Recently, our group reported the neutral-to-cationic ligand-exchange reaction on the $Au_{25}(PET)_{18}$ clusters (PET=$S(CH_2)_2C_6H_5$) with the cationic ligand ($HS(CH_2)_{11}N(CH_3)_3^+$), preserving the Au_{25} core structure, and the reaction kinetics was investigated.[13] The reaction was suppressed by two types of coulombic repulsions (i) between the attached cationic ligands and incoming cationic ligands in solution, and (ii) among the surface cationic ligands on the cluster surface. Similar with the case by Murray group, the ligand-exchange ratio was ca. 20%, due to the two types of repulsion.

In this study, the cationized $Au_{25}(4\text{-PyET-}CH_3^+)_x(4\text{-PyET})_{18-x}$ ($x\approx9$) clusters, which containing both of neutral and cationic ligands at the nearly equivalent amount, were ligand-exchanged with the cationic ligand ($HS(CH_2)_{11}N(CH_3)_3^+$), and the reaction kinetics was investigated by comparison between neutral and cationic ligands. My expectation was that the cationic ligands are infrequently exchanged, due to the coulombic repulsion between the attached cationic ligands and incoming cationic ligands. However, ESI-MS results exhibited the opposite phenomenon that the cationic ligands were dominantly exchanged (Scheme 5.1). This study is the first case of the cationic-to-cationic ligand-exchange reaction, and the revealed unique reaction kinetics would be

contributed to improve the exchange ratio up to 100% in the neutral-to-cationic ligand-exchange reaction.

Scheme 5.1 Ligand-exchange reaction on $Au_{25}(4\text{-PyET-CH}_3^+)_x(4\text{-PyET})_{18-x}$ ($x\approx9$) clusters with cationic ligands ($HS(CH_2)_{11}N(CH_3)_3^+$).

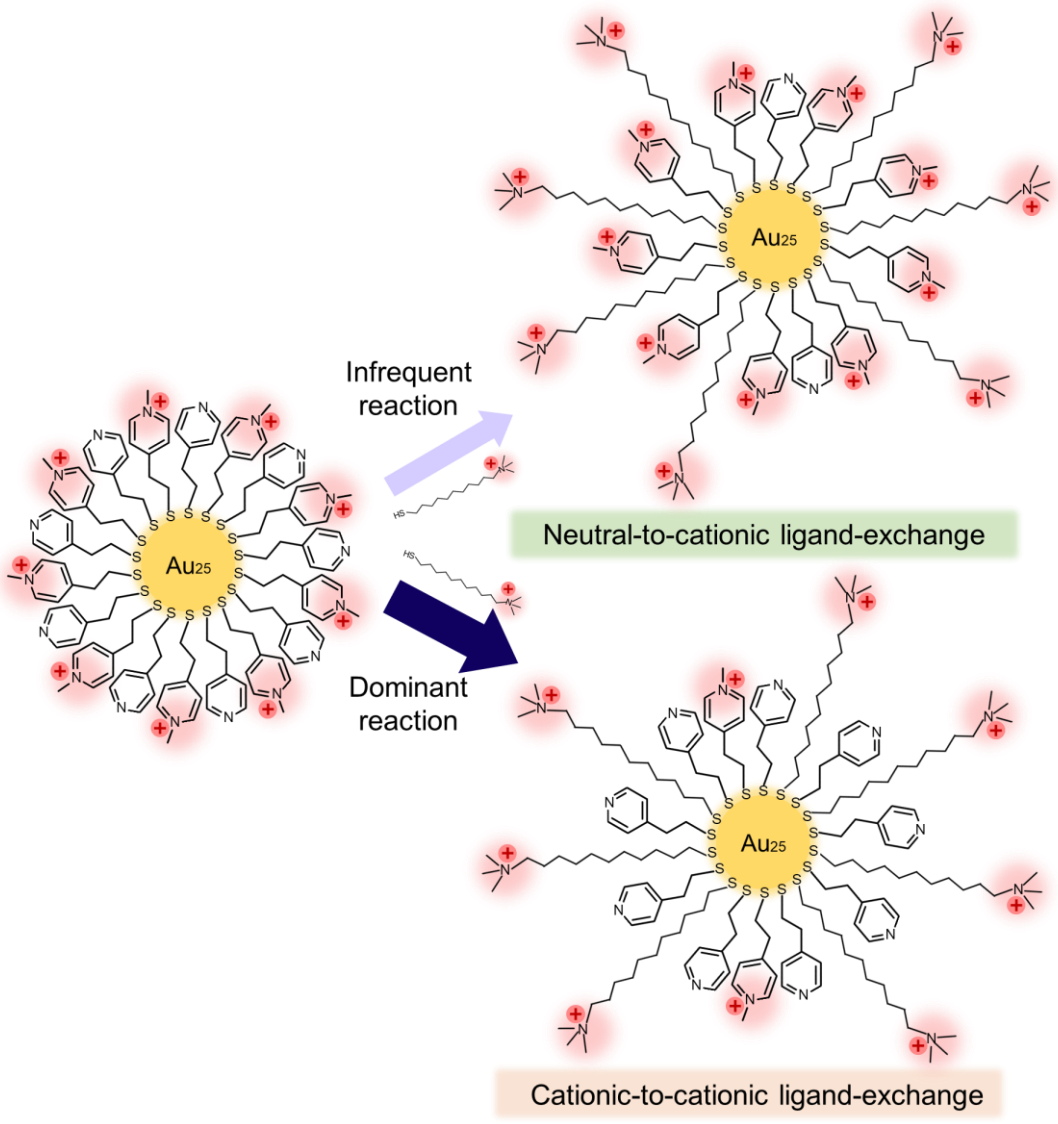

5.2 Experimental section

5.2.1 Chemicals

Hydrogen tetrachloroaurate (III) Tetrahydrate ($HAuCl_4 \cdot 4H_2O$, > 99%, Wako), 4-pyridineethanethiol hydrochloride (4-PyET·HCl, $C_7H_9NS \cdot HCl$, > 97%, TCI), sodium borohydride ($NaBH_4$, > 92%, Kanto), hydrochloric acid (HCl, 35~37%, Kanto), sodium hydroxide (NaOH, > 97%, Kanto), dimethyl sulfate ($C_2H_6O_4S$, > 98%, TCI), potassium hexafluorophosphate (KPF_6, > 95%, TCI), (11-mercaptoundecyl)-*N*,*N*,*N*-trimethylammonium bromide ($SR^+ \cdot Br^-$, 99%, Aldrich). Tetrahydrofuran (THF, > 99.5%, Junsei), methanol (MeOH, > 99.6%, Junsei), dichloromethane (DCM, > 99%, Wako), *N,N*-dimethylformamide, super dehydrated (dehydrated DMF, > 99.5%, Kanto), diethyl ether, super dehydrated (> 99.5%, Wako), Acetonitrile (> 99.9%, RCI labscan). Deioized pure water (> 18.2 MΩ) was prepared by an Organo/ELGA purelab system.

5.2.2 Synthesis of Au_{25}(4-PyET)$_{18}$ clusters

The $Au_{25}(4\text{-PyET})_{18}$ clusters were synthesized by following the recently reported works.[21] In brief, 8 mL of 4-PyET solution (MeOH, 100 mM) was added dropwise into 24 mL of $HAuCl_4$ solution (THF, 6.7 mM; 4-PyET:Au = 5:1 in molar ratio). The mixture changed into light reddish cloudy suspension, and then into white cloudy suspension during 4-PyET dropping. After overnight stirring, 1.6 mL of the fresh-made $NaBH_4$ solution (1.6 mmol, $NaBH_4$:Au = 5:1 in molar ratio; prepared by dissolving 189.2 mg of $NaBH_4$ in 5 mL of cold pure water) was rapidly added to the suspension under vigorous stirring. The color of the solution immediately turned black after addition of $NaBH_4$. Finally, the etching process was allowed to continue for at least 48h. Over the long time of etching process, the solution color would become dark brown slowly, suggesting the

formation of monodisperse Au_{25}(4-PyET)$_{18}$. The crude samples were purified based on the protonated states of the pendant Py moiety on Au_{25} cluster.

5.2.3 Synthesis of Au_{25}(4-PyET-CH_3^+)$_x$(4-PyET)$_{18-x}$ (x≈9) clusters through surface Menshutkin reaction on Au_{25}(4-PyET)$_{18}$ clusters

The Au_{25}(4-PyET-CH_3^+)$_x$(4-PyET)$_{18-x}$ (x≈9) clusters were synthesized through surface Menshutkin reaction on Au_{25}(4-PyET)$_{18}$ clusters described in chapter 4.[15] The Au_{25}(4-PyET)$_{18}$ clusters (1 mg, ~0.13 μmol) were dissolved in dehydrated DMF (1 mL). In this solution, liquid dimethyl sulfate (23 μL, ~240 μmol) and KPF_6 (4.5 mg, ~24 μmol) were added in the mole ratio of methyl trifluoromethanesulfonate:KPF_6:4-PyET = 100:10:1. The solution was stirred at 200 rpm for 2min. The obtained Au_{25}(4-PyET-CH_3^+)$_x$(4-PyET)$_{18-x}$ clusters were precipitated by adding KPF_6 aqueous solution (0.1 M, 5 mL) and washed by water and DCM.

5.2.4 Ligand-exchange reaction on Au_{25}(4-PyET-CH_3^+)$_x$(4-PyET)$_{18-x}$ (x≈9) clusters with cationic ligands

Prior to the ligand-exchange reaction, the Br^- counteranion of the cationic ligand ((11-mercaptoundecyl)-*N*,*N*,*N*-trimethylammonium) was replaced with hexafluorophosphate (PF_6^-). $SR^+ \cdot PF_6^-$ was prepared by dissolving $SR^+ \cdot Br^-$ (82 mg, 0.25 mmol) in pure water, followed by precipitation through the addition of KPF_6 (55 mg, 0.3 mmol). The white precipitate was collected by centrifugation, washed three times with pure water, and dried overnight under vacuum.

The Au_{25}(4-PyET-CH_3^+)$_x$(4-PyET)$_{18-x}$ (x≈9) clusters were dissolved in dehydrated DMF (1.0 mL). KPF_6 (12.2 mg, 12 μmol) and $SR^+ \cdot PF_6^-$ (4.7 mg, 12 μmol,)

in a 1:5 molar ratio (based on the exchangeable surface ligands (18 per cluster)) were added, and the reaction was arrowed for 1, 3, 5h under stirring at 300 rpm. The obtained clusters were precipitated by adding KPF_6 aqueous solution (0.1 M, 5 mL) and washed by water and DCM.

5.2.5 Characterization

UV-Vis absorption spectra of samples were recorded using a JASCO V-630 spectrophotometer using a quartz cuvette with a 1 nm optical path. Electrospray Ionization Mass Spectrometry (ESI-MS) was performed using a Bruker Daltonics micrOTOF-HS mass spectrometer. The purified sample, dissolved in acetonitrile (~100 μg/mL), was directly infused at 4 mL/min. The nebulizer pressure was set to 1.5 bar, and the sheath gas was set to 4.0 L/min. The dry temperature was kept at 180 °C. The electrospray emitter potential was held at 4500 V (positive mode). The capillary exit, skimmer 1, hexapole 1, skimmer 2 voltage settings were 200, 50, 25, and 28 V, respectively. The lens 1 transfer and lens 1 pre puls storage were set at 160, and 30 μs, respectively.

5.3 Results and discussion

5.3.1 Optical absorption spectroscopy

The Au_{25}(4-PyET-CH_3^+)$_x$(4-PyET)$_{18-x}$ (x=8.5) clusters were synthesized by the surface Menshutkin reaction method described in chapter 4, and characterized by ESI-MS and UV-Vis absorption spectrum (Figure S5.1). Figure 5.1 shows the UV-Vis absorption spectra before (0h) and after ligand-exchange reaction (1h, 2h, 3h, 4h, 5h). Note that the Br^- counteranion of the purchased cationic ligand was replaced with PF_6^- before the ligand-exchange reaction, which is important because Br^- causes the rapid decomposition of the Au_{25} clusters by oxidation.[12,14,22] The characteristic Au_{25} cluster peaks[8,23] at 400, 450, and 670 nm gradually decreased by prolonging the reaction time, indicating that the Au_{25} clusters gradually decomposed by the ligand-exchange reaction with the cationic ligand. This observation is different from the neutral-to-neutral ligand-exchange reaction on Au_{25} clusters, in which the Au_{25} cluster did not decompose for long time even in the high-temperature reaction.[24-27] The stability of the Au_{25} clusters was affected by the incoming cationic ligands and decreased due to the densely distributed positive charges on the small cluster surface, as discussed the recent report by our group.[12,14]

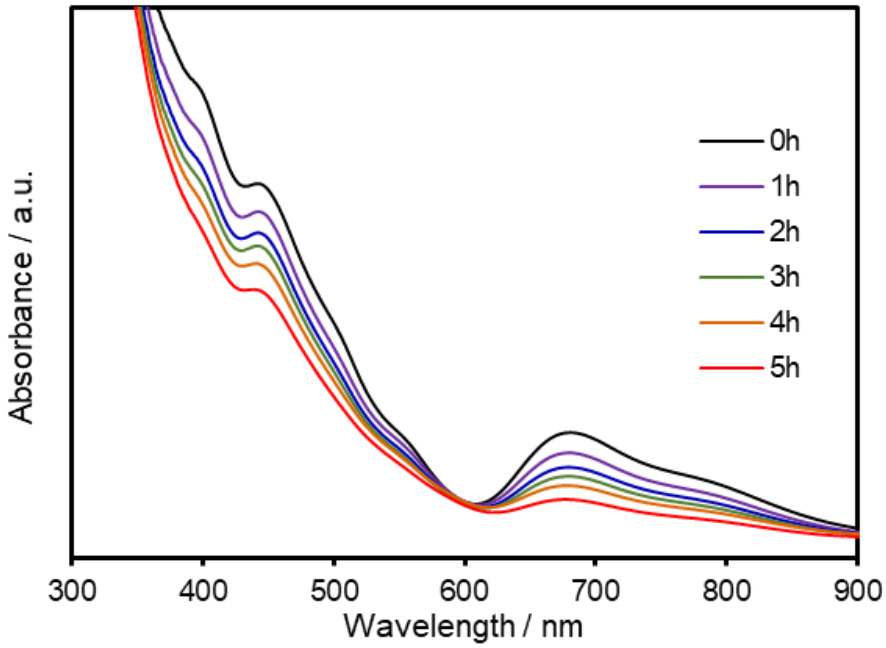

Figure 5.1 UV-Vis absorption spectra before (0h) and after the cationic-ligand-exchange reaction (1h, 2h, 3h, 4h, 5h).

5.3.2 ESI-MS

The positive-mode ESI-MS of the Au_{25} clusters after the ligand-exchange reaction for 1h, 3h, 5h (Figure 5.2) showed the ligand-exchanged Au_{25} clusters, which containing 3 types of ligands ($S(CH_2)_2C_5H_4$ (PyET), $S(CH_2)_2C_5H_4\text{-}CH_3^+$ (PyET-Me), and $S(CH_2)_{11}N(CH_3)_3^+$ (MUTA)). Specifically, $Au_{25}(PyET)_{5\text{-}14}(PyET\text{-}Me)_{1\text{-}8}(MUTA)_{1\text{-}9}$ (1h), $Au_{25}(PyET)_{5\text{-}12}(PyET\text{-}Me)_{1\text{-}5}(MUTA)_{3\text{-}10}$ (3h), $Au_{25}(PyET)_{5\text{-}11}(PyET\text{-}Me)_{1\text{-}3}(MUTA)_{4\text{-}12}$ (5h) were observed (total number of PyET, PyET-Me, and MUTA is 18), indicating that more number of the ligands (PyET or PyET-Me) were exchanged with MUTA by prolonging the reaction time. The compositions and charge assignments of the observed Au_{25} cluster peaks are summarized in Table S5.1. Moreover, one average composition was determined from the peak intensity ratio in ESI-MS for each reaction time (1h, 3h, 5h), assumed that mass spectral intensities are directly proportional to the solution concentrations of the corresponding cluster species (see Table S5.1 for the detailed calculation method). Figure 5.3 shows the average numbers of each 3 ligands (average composition of the Au_{25} clusters) at the each reaction time (Figure 5.3(A)), and their changes during the ligand-exchange reaction (Figure 5.3(B)). Neutral PyET ligands were slowly exchanged with cationic MUTA ligands, whereas cationic PyET-Me were quickly exchanged. This observation was different from my expectation that the cationic ligands are infrequently exchanged, due to the coulombic repulsion between the attached cationic ligands and incoming cationic ligands. This is because the cationic ligands, that would cause the decrease of cluster stability due to the repulsion on the cluster surface, are dominantly exchanged to keep the energy level of whole Au_{25} clusters low.

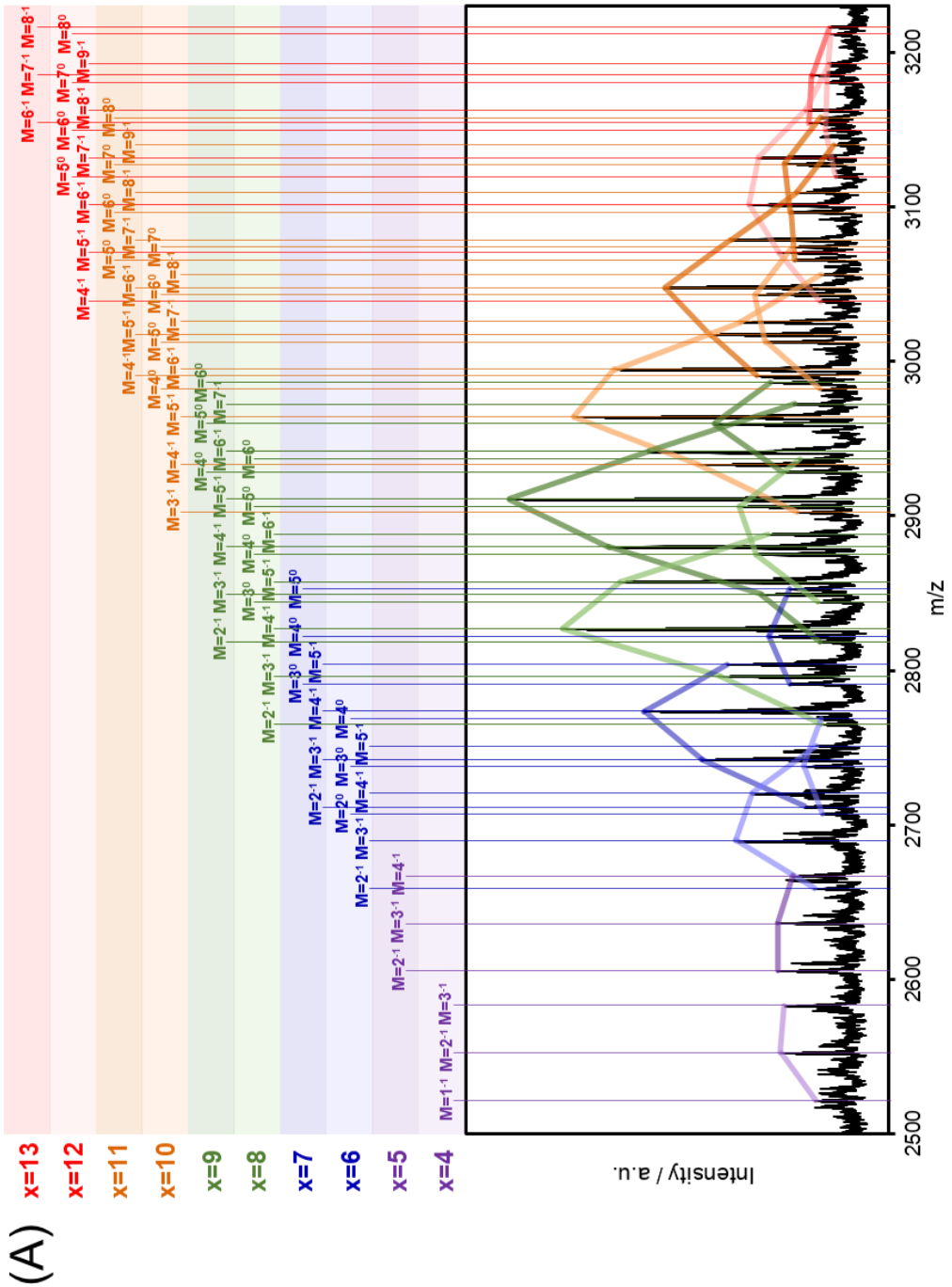
(A)
x=13
x=12
x=11
x=10
x=9
x=8
x=7
x=6
x=5
x=4
M=6-1 M=7-1 M=8-1
M=50 M=60 M=70 M=80
M=4-1 M=5-1 M=6-1 M=7-1 M=8-1 M=9-1
M=50 M=60 M=70 M=80
M=4-1 M=5-1 M=6-1 M=7-1 M=8-1 M=9-1
M=40 M=50 M=60 M=70
M=3-1 M=4-1 M=5-1 M=6-1 M=7-1 M=8-1
M=40 M=50 M=60
M=2-1 M=3-1 M=4-1 M=5-1 M=6-1 M=7-1
M=30 M=40 M=50 M=60
M=2-1 M=3-1 M=4-1 M=5-1 M=6-1
M=30 M=40 M=50
M=2-1 M=3-1 M=4-1 M=5-1
M=20 M=30 M=40
M=2-1 M=3-1 M=4-1 M=5-1
M=2-1 M=3-1 M=4-1
M=1-1 M=2-1 M=3-1
Intensity / a.u.
2500
2600
2700
2800
2900
3000
3100
3200
m/z

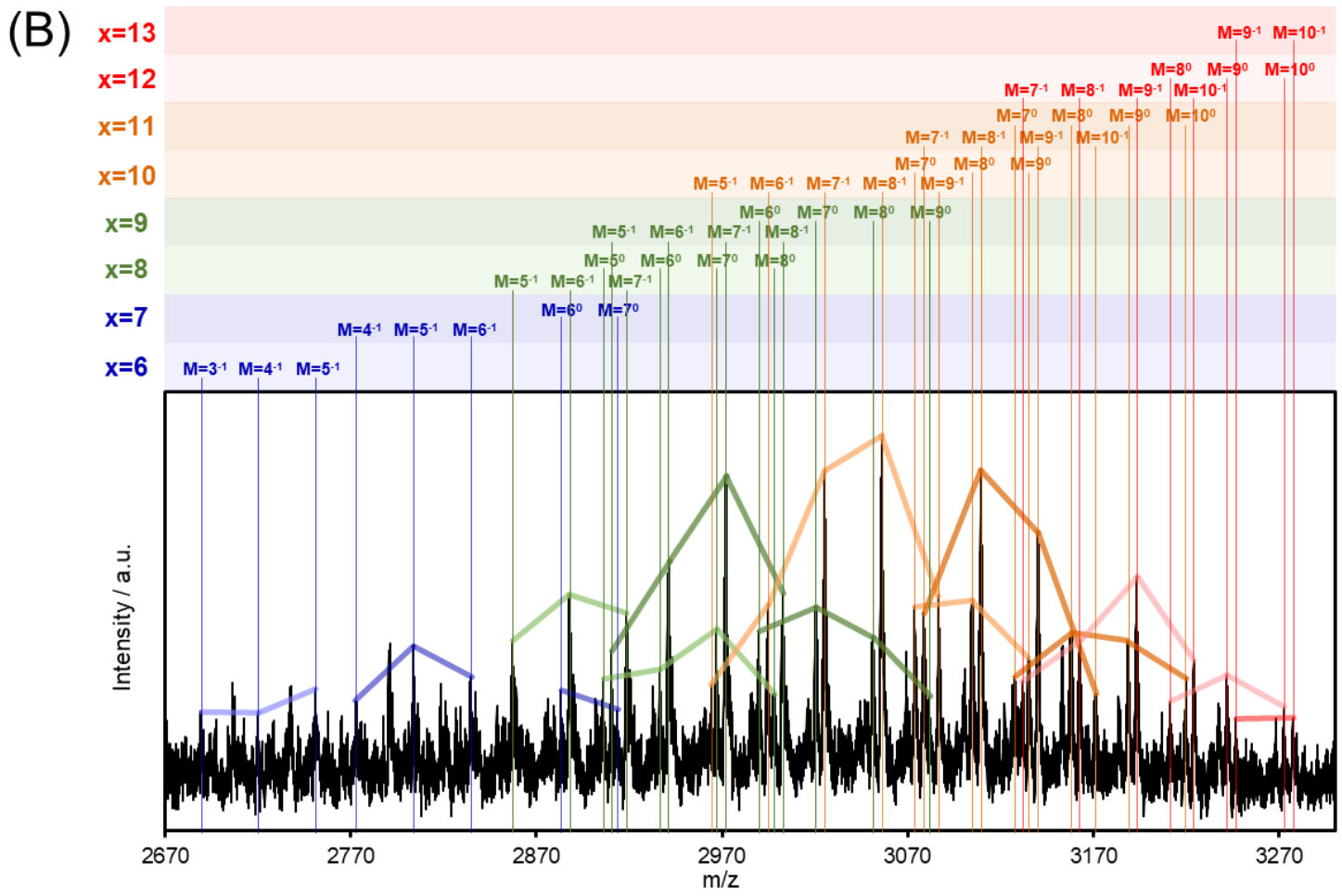
(B)
x=13
x=12
x=11
x=10
x=9
x=8
x=7
x=6
M=3-1 M=4-1 M=5-1
M=4-1 M=5-1 M=6-1
M=5-1 M=6-1 M=7-1
M=6-1 M=7-1 M=8-1
M=5-1 M=6-1 M=7-1 M=8-1 M=9-1
M=6-1 M=7-1 M=8-1 M=9-1 M=10-1
M=7-1 M=8-1 M=9-1 M=10-1
M=8-1 M=9-1 M=10-1
M=9-1 M=10-1
M=60 M=70
M=50 M=60 M=70 M=80
M=60 M=70 M=80 M=90
M=70 M=80 M=90
M=70 M=80 M=90 M=100
M=80 M=90 M=100
M=90 M=100
Intensity / a.u.
2670
2770
2870
2970
3070
3170
3270
m/z

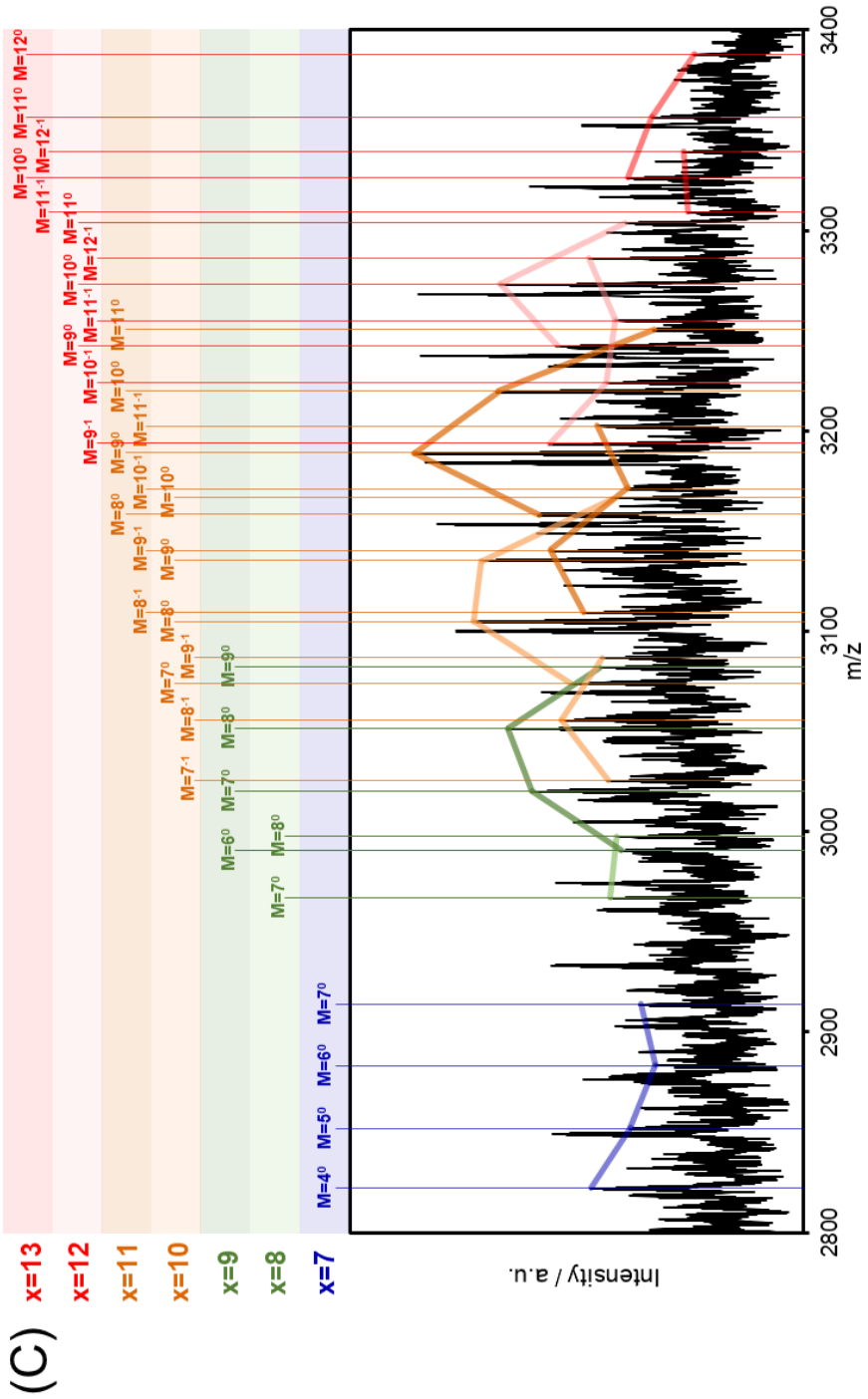

Figure 5.2 The positive-mode ESI-MS of the Au_{25} clusters with core charge 0 or -1 after the ligand-exchange reaction for (A) 1h, (B) 3h, (C) 5h. M indicates the number of MUTA ligands and *x* indicates the total number of cationic ligand (PyET-Me or MUTA). For example, (*x*=13, M=10^0) indicates the $Au_{25}^0(PyET)_5(PyET\text{-}Me)_3(MUTA)_{10}$.

(A)

	PyET	PyET-Me	MUTA
0h	9.50	8.50	0
1h	9.09	4.06	4.86
3h	8.29	2.40	7.30
5h	7.38	1.56	9.06

(B)

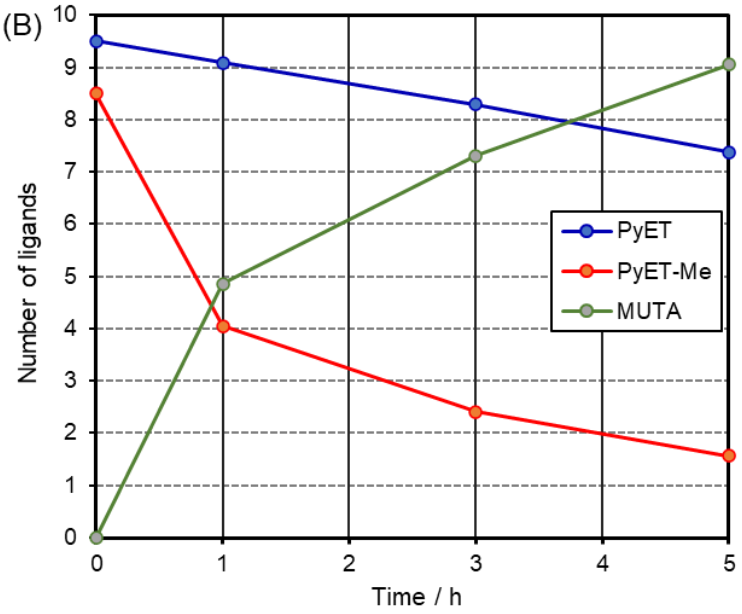

Figure 5.3 (A) the average numbers of the 3 types of ligands (average composition of the Au_{25} clusters) at the each reaction time calculated from the ESI-MS results, and (B) their changes during the ligand-exchange reaction.

5.4 Conclusion

The cationized $Au_{25}(4\text{-PyET-}CH_3^+)_x(4\text{-PyET})_{18-x}$ ($x \approx 8.5$) clusters (4-PyET = $S(CH_2)_2C_5H_4N$), which containing both of neutral and cationic ligands at the nearly equivalent amount, were ligand-exchanged with the cationic ligands ($HS(CH_2)_{11}N(CH_3)_3^+$), and the reaction kinetics was investigated by comparison neutral and cationic ligands. ESI-MS results showed that the cationic 4-PyET-CH_3^+ ligands were dominantly exchanged to keep the energy level of whole Au_{25} clusters low.

5.5 Supporting information

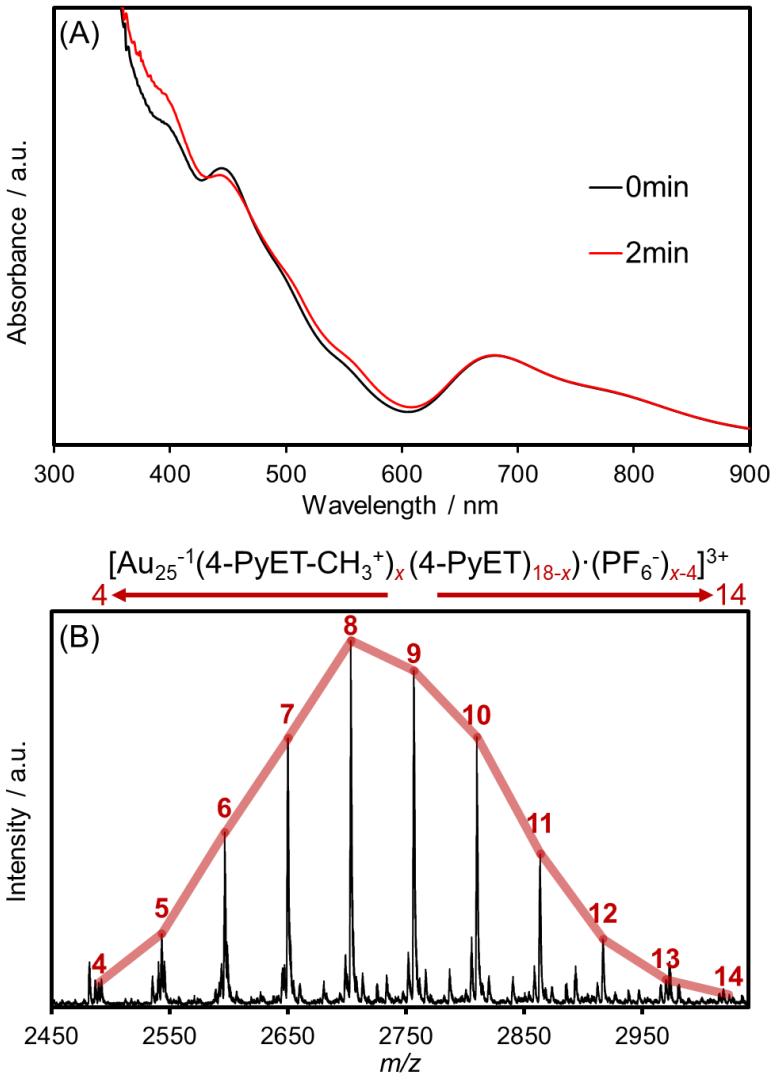

Figure S5.1 (A) UV-Vis absorption spectra and (B) positive-mode ESI-MS of the synthesized $Au_{25}(4\text{-PyET-}CH_3^+)_x(4\text{-PyET})_{18-x}$ (x=8.5) clusters.

Table S5.1 The compositions and charge assignments of the observed Au_{25} cluster peaks.

1h						
Core charge	PyET	PyET-Me	MUTA	m/z (calc.)	m/z (obs.)	Intensity
x=4						
-1	14	3	1	2521.45	2521.46	208
-1	14	2	2	2552.19	2552.20	307
-1	14	1	3	2582.93	2582.90	295
x=5						
-1	13	3	2	2605.52	2605.50	315
-1	13	2	3	2636.26	2636.24	316
-1	13	1	4	2667.00	2667.04	272
x=6						
0	12	4	2	2707.17	2707.21	191
0	12	3	3	2737.92	2737.94	240
0	12	2	4	2768.66	2768.59	196
-1	12	4	2	2658.85	2658.82	214
-1	12	3	3	2689.59	2689.55	435
-1	12	2	4	2720.34	2720.29	388
-1	12	1	5	2751.08	2751.19	204
x=7						
0	11	4	3	2791.25	2791.35	283
0	11	3	4	2821.99	2821.99	340
0	11	2	5	2852.73	2852.64	283
-1	11	5	2	2712.19	2712.18	237
-1	11	4	3	2742.93	2742.92	532
-1	11	3	4	2773.67	2773.68	695
-1	11	2	5	2804.41	2804.40	459
x=8						
0	10	5	3	2844.58	2844.57	203
0	10	4	4	2875.32	2875.32	377
0	10	3	5	2906.07	2906.05	426
0	10	2	6	2936.81	2936.83	254
-1	10	6	2	2765.52	2765.37	191
-1	10	5	3	2796.26	2796.32	481
-1	10	4	4	2827.00	2827.09	926
-1	10	3	5	2857.74	2857.81	762
-1	10	2	6	2888.49	2888.41	345
x=9						
0	9	5	4	2928.66	2928.65	302
0	9	4	5	2959.40	2959.38	493
0	9	3	6	2990.14	2990.16	378
-1	9	7	2	2818.85	2818.87	195
-1	9	6	3	2849.59	2849.58	363
-1	9	5	4	2880.34	2880.34	796
-1	9	4	5	2911.08	2911.09	1077
-1	9	3	6	2941.82	2941.79	683
-1	9	2	7	2972.56	2972.54	271
x=10						
0	8	6	4	2981.99	2982.03	198
0	8	5	5	3012.73	3012.72	351
0	8	4	6	3043.47	3043.49	380
0	8	3	7	3074.22	3074.17	277
-1	8	7	3	2902.93	2902.82	261
-1	8	6	4	2933.67	2933.75	540
-1	8	5	5	2964.41	2964.45	895
-1	8	4	6	2995.15	2995.17	778
-1	8	3	7	3025.89	3025.81	422
-1	8	2	8	3056.64	3056.67	193
x=11						
0	7	6	5	3066.06	3066.08	269
0	7	5	6	3096.81	3096.80	279
0	7	4	7	3127.55	3127.81	293
0	7	3	8	3158.29	3158.02	195
-1	7	7	4	2987.00	2986.91	337
-1	7	6	5	3017.74	3017.78	506
-1	7	5	6	3048.49	3048.44	637
-1	7	4	7	3079.23	3079.17	449
-1	7	3	8	3109.97	3109.92	262
-1	7	2	9	3140.71	3140.89	157
x=12						
0	6	7	5	3119.40	3119.69	154
0	6	6	6	3150.14	3149.89	180
0	6	5	7	3180.88	3180.63	178
0	6	4	8	3211.62	3211.82	165
-1	6	8	4	3040.33	3039.96	197
-1	6	7	5	3071.08	3071.12	313
-1	6	6	6	3101.82	3102.04	398
-1	6	5	7	3132.56	3132.59	371
-1	6	4	8	3163.30	3163.39	237
-1	6	3	9	3194.04	3194.04	171
x=13						
-1	5	7	6	3155.15	3155.00	226
-1	5	6	7	3185.89	3185.95	218
-1	5	5	8	3216.64	3216.72	171

3h						
Core charge	PyET	PyET-Me	MUTA	m/z (calc.)	m/z (obs.)	Intensity
			x=6			
-1	12	3	3	2689.59	2689.61	153
-1	12	2	4	2720.34	2720.29	152
-1	12	1	5	2751.08	2751.10	176
			x=7			
0	11	1	6	2883.48	2883.49	174
0	11	0	7	2914.22	2914.20	155
-1	11	3	4	2773.67	2773.59	164
-1	11	2	5	2804.41	2804.39	218
-1	11	1	6	2835.15	2835.27	188
			x=8			
0	10	3	5	2906.07	2906.02	186
0	10	2	6	2936.81	2936.58	196
0	10	1	7	2967.55	2968.09	236
0	10	0	8	2998.29	2998.04	171
-1	10	3	5	2857.74	2857.58	224
-1	10	2	6	2888.49	2888.58	270
-1	10	1	7	2919.23	2919.31	252
			x=9			
0	9	3	6	2990.14	2990.01	233
0	9	2	7	3020.88	3020.99	258
0	9	1	8	3051.63	3051.79	227
0	9	0	9	3082.37	3082.22	168
-1	9	4	5	2911.08	2911.08	214
-1	9	3	6	2941.82	2941.83	303
-1	9	2	7	2972.56	2972.61	386
-1	9	1	8	3003.30	3003.24	270
			x=10			
0	8	3	7	3074.22	3074.13	258
0	8	2	8	3104.96	3105.06	265
0	8	1	9	3135.70	3135.68	208
-1	8	5	5	2964.41	2964.65	181
-1	8	4	6	2995.15	2995.33	259
-1	8	3	7	3025.89	3025.78	392
-1	8	2	8	3056.64	3056.47	427
-1	8	1	9	3087.38	3087.22	269
			x=11			
0	7	4	7	3127.55	3127.62	188
0	7	3	8	3158.29	3158.33	231
0	7	2	9	3189.03	3188.92	223
0	7	1	10	3219.77	3219.78	187
-1	7	4	7	3079.23	3079.10	251
-1	7	3	8	3109.97	3109.82	393
-1	7	2	9	3140.71	3140.69	330
-1	7	1	10	3171.45	3171.74	171
			x=12			
0	6	4	8	3211.62	3211.67	163
0	6	3	9	3242.37	3242.34	190
0	6	2	10	3273.11	3273.10	157
-1	6	5	7	3132.56	3132.64	183
-1	6	4	8	3163.30	3163.33	224
-1	6	3	9	3194.04	3194.01	287
-1	6	2	10	3224.79	3224.73	204
			x=13			
-1	5	4	9	3247.38	3247.24	146
-1	5	3	10	3278.12	3278.25	147

5h						
Core charge	PyET	PyET-Me	MUTA	m/z (calc.)	m/z (obs.)	Intensity
x=7						
0	11	3	4	2821.99	2822.56	202
0	11	2	5	2852.73	2852.80	180
0	11	1	6	2883.48	2882.87	165
0	11	0	7	2914.22	2914.18	174
x=8						
0	10	1	7	2967.55	2967.49	191
0	10	0	8	2998.29	2998.35	187
x=9						
0	9	3	6	2990.14	2990.59	185
0	9	2	7	3020.88	3020.86	236
0	9	1	8	3051.63	3051.47	250
0	9	0	9	3082.37	3082.10	197
x=10						
0	8	3	7	3074.22	3074.19	213
0	8	2	8	3104.96	3104.98	269
0	8	1	9	3135.70	3135.59	265
0	8	0	10	3166.44	3166.54	190
-1	8	3	7	3025.89	3026.03	193
-1	8	2	8	3056.64	3056.55	219
-1	8	1	9	3087.38	3087.32	196
x=11						
0	7	3	8	3158.29	3158.19	232
0	7	2	9	3189.03	3188.98	303
0	7	1	10	3219.77	3219.87	256
0	7	0	11	3250.52	3250.57	166
-1	7	3	8	3109.97	3109.71	206
-1	7	2	9	3140.71	3140.47	225
-1	7	1	10	3171.45	3171.56	182
-1	7	0	11	3202.20	3202.60	198
x=12						
0	6	3	9	3242.37	3242.49	222
0	6	2	10	3273.11	3273.10	254
0	6	1	11	3303.85	3303.72	182
-1	6	3	9	3194.04	3193.97	226
-1	6	2	10	3224.79	3224.72	194
-1	6	1	11	3255.53	3255.54	188
-1	6	0	12	3286.27	3286.39	203
x=13						
0	5	3	10	3326.44	3326.53	181
0	5	2	11	3357.18	3356.80	167
0	5	1	12	3387.92	3388.22	143
-1	5	2	11	3308.86	3308.98	146
-1	5	1	12	3339.60	3339.49	149

Calculation method to determine the average composition (PyET, PyET-Me, MUTA)

$$\text{PyET} = \frac{18 \times \text{Total value of (Number of PyET} \times \text{Intensity) for all peaks}}{\text{Total value of (Number of PyET} \times \text{Intensity) for all peaks} + \text{Total value of (Number of PyET-Me} \times \text{Intensity) for all peaks} + \text{Total value of (Number of MUTA} \times \text{Intensity) for all peaks}}$$

$$\text{PyET-Me} = \frac{18 \times \text{Total value of (Number of PyET-Me} \times \text{Intensity) for all peaks}}{\text{Total value of (Number of PyET} \times \text{Intensity) for all peaks} + \text{Total value of (Number of PyET-Me} \times \text{Intensity) for all peaks} + \text{Total value of (Number of MUTA} \times \text{Intensity) for all peaks}}$$

$$\text{MUTA} = \frac{18 \times \text{Total value of (Number of MUTA} \times \text{Intensity) for all peaks}}{\text{Total value of (Number of PyET} \times \text{Intensity) for all peaks} + \text{Total value of (Number of PyET-Me} \times \text{Intensity) for all peaks} + \text{Total value of (Number of MUTA} \times \text{Intensity) for all peaks}}$$

5.6 References

(1) Li, G.; Jin, R. Atomically Precise Gold Nanoclusters as New Model Catalysts. *Acc. Chem. Res.* **2013**, *46*, 1749–1758.

(2) Wan, X. K.; Wang, J. Q.; Nan, Z. A.; Wang, Q. M. Ligand effects in catalysis by atomically precise gold nanoclusters. *Sci. Adv.* **2017**, *3*, e1701823.

(3) Guan, G.; Zhang, S. Y.; Cai, Y.; Liu, S.; Bharathi, M. S.; Low, M.; Yu, Y.; Xie, J.; Zheng, Y.; Zhang, Y. W., Han, M. Y. Convenient Purification of Gold Clusters by Co-Precipitation for Improved Sensing of Hydrogen Peroxide, Mercury Ions and Pesticides. *Chem. Commun.* **2014**, *50*, 5703–5705.

(4) Shen, R., Liu, P., Zhang, Y., Yu, Z., Chen, X., Zhou, L., Nie, B; Żaczek, A.; Chen, J; Liu, J. Sensitive Detection of Single-cell Secreted H_2O_2 by Integrating a Microfluidic Droplet Sensor and Au Nanoclusters. *Anal. Chem.* **2018**, *90*, 4478–4484.

(5) Zheng, K.; Setyawati, M. I.; Leong, D. T.; Xie, J. Surface Ligand Chemistry of Gold Nanoclusters Determines Their Antimicrobial Ability. *Chem. Mater.* **2018**, *30*, 2800–2808.

(6) Zheng, K.; Setyawati, M. I.; Leong, D. T.; Xie, J. Antimicrobial Gold Nanoclusters. *ACS Nano*, **2017**, *11*, 6904–6910.

(7) Negishi, Y.; Chaki, N. K.; Shichibu, Y.; Whetten, R. L.; Tsukuda, T. Origin of Magic Stability of Thiolated Gold Clusters: a Case Study on $Au_{25}(SC_6H_{13})_{18}$. *J. Am. Chem. Soc.* **2007**, *129*, 11322−11323.

(8) Tsukuda, T. Toward an Atomic-Level Understanding of Size-Specific Properties of Protected and Stabilized Gold Clusters. *Bull. Chem. Soc. Jpn.* **2012**, *85*, 151−168.

(9) Alvarez, M. M.; Chen, J.; Plascencia-Villa, G.; Black, D. M.; Griffith, W. P.; Garzon, I. L.; Jose-Yacaman, M.; Demeler, B.; Whetten,´ R. L. Hidden Components in Aqueous "Gold-144" Fractionated by PAGE: High-Resolution Orbitrap ESI−MS Identifies the Gold-102 and Higher All-Aromatic Au-pMBA Cluster Compounds. *J. Phys. Chem. B* **2016**, *120*, 6430−6438.

(10) Kumar, S.; Jin, R. Water-Soluble $Au_{25}(Capt)_{18}$ Nanoclusters: Synthesis, Thermal Stability, and Optical Properties. *Nanoscale* **2012**, *4*, 4222−4227.

(11) Ishida, Y.; Narita, K.; Yonezawa, T.; Whetten, R. L. Fully Cationized Gold Clusters: Synthesis of $Au_{25}(SR^{+})_{18}$. *J. Phys. Chem. Lett.* **2016**, *7*, 3718–3722.

(12) Narita, K.; Ishida, Y.; Yonezawa, T; Huang, Z. Super Polycationic Molecular Compounds: $Au_{144}(SR^{+})_{60}$ Clusters. *J. Phys. Chem. C* **2019**, *123*, 21768−21773.

(13) Huang, Z.; Ishida, Y.; Narita, K; Yonezawa, T. Kinetics of Cationic-Ligand-Exchange Reactions in Au_{25} Nanoclusters. *J. Phys. Chem. C* **2018**, *122*, 18142−18150.

(14) Nel, A. E.; Mädler, L.; Velegol, D.; Xia, T.; Hoek, E. M.; Somasundaran, P.; Klaessig, F.; Castranova, V.; Thompson, M. Understanding biophysicochemical interactions at the nano-bio interface. *Nat. Mater.* **2009**, *8*, 543−557.

(15) Narita, K.; Ishida, Y.; Nukui, S.; Huang, Z.; Yonezawa, T. Surface Menshutkin SN2 Reaction on Basic Gold Clusters Provides Novel Opportunities for the Cationization and Functionalization of Molecular Metal Clusters, *J. Phys. Chem. Lett.* **2021**, *12*, 11761-11765.

(16) Tracy, J. B.; Crowe, M. C.; Parker, J. F.; Hampe, O.; Fields-Zinna, C. A.; Dass, A.; Murray, R. W. Electrospray ionization mass spectrometry of uniform and mixed monolayer nanoparticles: $Au_{25}[S(CH_2)_2Ph]_{18}$ and $Au_{25}[S(CH_2)_2Ph]_{18-x}(SR)_x$. *J. Am.*

Chem. Soc. **2007**, *129,* 16209–16215.

(17) Dass, A.; Stevenson, A.; Dubay, G. R.; Tracy, J. B.; Murray, R. W. Nanoparticle MALDI-TOF mass spectrometry without fragmentation: $Au_{25}(SCH_2CH_2Ph)_{18}$ and mixed monolayer $Au_{25}(SCH_2CH_2Ph)_{18-x}(L)_x$. *J. Am. Chem. Soc.* **2008**, *130*, 5940–5946.

(18) Zhu, M.; Lanni, E.; Garg, N.; Bier, M. E.; Jin, R. Kinetically controlled, high-yield synthesis of Au_{25} clusters. *J. Am. Chem. Soc.* **2008**, *130*, 1138−1139.

(19) Zeng, C.; Liu, C.; Pei, Y.; Jin, R. Thiol ligand-induced transformation of $Au_{38}(SC_2H_4Ph)_{24}$ to $Au_{36}(SPh\text{-}t\text{-}Bu)_{24}$. *ACS Nano* **2013**, *7,* 6138–6145.

(20) Fields-Zinna, C. A.; Sardar, R.; Beasley, C. A.; Murray, R. W. Electrospray Ionization Mass Spectrometry of Intrinsically Cationized Nanoparticles, $[Au_{144/146}(SC_{11}H_{22}N(CH_2CH_3)_3^{3+})_X\text{-}(S(CH_2)_5CH_3)_Y]^{X+}$. *J. Am. Chem. Soc.* **2009**, *131*, 16266−16271.

(21) Huang, Z.; Ishida, Y.; Yonezawa, T. Basic $[Au_{25}(SCH_2CH_2Py)_{18}]^- \cdot Na^+$ Clusters: Synthesis, Layered Crystallographic Arrangement, and Unique Surface Protonation. *Angew. Chem., Int. Ed.* **2019**, *58*, 13411–13415.

(22) Zhu, M.; Chan, G.; Qian, H.; Jin, R. Unexpected reactivity of $Au_{25}(SCH_2CH_2Ph)_{18}$ nanoclusters with salts. *Nanoscale* **2011**, *3*, 1703−1707.

(23) Zhu, M.; Aikens, C. M.; Hollander, F. J.; Schatz, G. C.; Jin, R. Correlating the Crystal Structure of a Thiol-Protected Au_{25} Cluster and Optical Properties. *J. Am. Chem. Soc.* **2008**, *130*, 5883–5885.

(24) Meng, X.; Xu, Q.; Wang, S.; Zhu, M. Ligand-exchange synthesis of selenophenolate-capped Au_{25} nanoclusters. *Nanoscale* **2012**, *4*, 4161−4165.

(25) Dass, A.; Holt, K.; Parker, J. F.; Feldberg, S. W.; Murray, R. W. Mass Spectrometrically Detected Statistical Aspects of Ligand Populations in Mixed Monolayer $Au_{25}L_{18}$ Nanoparticles. *J. Phys. Chem. C* **2008**, *112*, 20276−20283.

(26) Fernando, A.; Aikens, C. M. Ligand Exchange Mechanism on Thiolate Monolayer Protected $Au_{25}(SR)_{18}$ Nanoclusters. *J. Phys. Chem. C* **2015**, *119*, 20179−20187.

(27) Niihori, Y.; Hossain, S.; Sharma, S.; Kumar, B.; Kurashige, W.; Negishi, Y. Understanding and Practical Use of Ligand and Metal Exchange Reactions in Thiolate-Protected Metal Clusters to Synthesize Controlled Metal Clusters. *Chem. Rec.* **2017**, *17*, 473−484.

Chapter 6

General Conclusion

Up-to-date, the Au clusters with various types of surface thiolate ligands have been synthesized; however, the cationic-ligand-protected Au clusters have never been synthesized with atomic precision. This thesis aims to establish the synthesis method of atomically pure cationized Au clusters by using several synthetic approach.

Chapter two reports the first successful synthesis of atomically precise fully cationized Au clusters using size-focusing method. By preventing the formation of $[Au(I)]^-$–SR^+ ionic polymer complexes that hinder the homogeneous reduction of Au precursors and the formation of atomically pure clusters, $Au_{25}(S(CH_2)_{11}N(CH_3)_3^+)_{18}$ clusters were successfully synthesized.

Chapter three reports the successful synthesis of atomically pure fully cationized $Au_{144}(S(CH_2)_{11}N(CH_3)_3^+)_{60}$ clusters, which is the largest size in the most stable and studied Au clusters. The similar sized quasi-stable compounds of Au_{144}, such as Au_{142}, Au_{143}, and Au_{146}, etc., which make the size-focusing into a single Au_{144} structure difficult. Through the thermal etching in the optimized condition and selective precipitation, atomically pure $Au_{144}(SR^+)_{60}$ clusters were successfully synthesized.

Chapter four demonstrates the surface Menshutkin reaction on the $Au_{25}(S(CH_2)_2C_5H_4N)_{18}$ clusters to transform them into the cationized $Au_{25}(S(CH_2)_2$ $C_5H_4N\text{-}CH_3^+)_x(S(CH_2)_2$ $C_5H_4N)_{18-x}$ clusters. This method proposed not only a new synthetic pathway for cationized Au clusters, but also provides a novel idea for diversifying the R-groups of molecular metal clusters through the surface chemical

reaction.

Chapter five investigated the cationic-ligand-exchange reaction on the cationized $Au_{25}(4\text{-PyET-}CH_3^+)_x(4\text{-PyET})_{18-x}$ ($x\approx9$) clusters (4-PyET = $S(CH_2)_2C_5H_4N$), which containing both of neutral and cationic ligands at the nearly equivalent amount. MS results revealed the unique reaction kinetics that the cationic-to-cationic ligand exchange reaction was dominantly proceeded than the neutral-to-cationic ligand-exchange reaction.

In this study, the synthesis methods of atomically pure cationized Au clusters have been investigated, wherein: (a) the fully cationized Au clusters, $Au_{25}(SR^+)_{18}$ and $Au_{144}(SR^+)_{60}$, were synthesized using size-focusing method, (b) the cationized Au clusters, $Au_{25}(SR^+)_x(SR)_{18-x}$ ($x\approx18$), were synthesized using surface reaction method, and (c) the unique reaction kinetics of cationic-to-cationic ligand-exchange method was revealed.

ACKNOWLEDGEMENTS

I would like to express my great appreciation towards various people whom had provided me with great assistance, during these three years of my PhD degree research. The dissertation would have been impossible without the contributions from many people.

A special note of thanks dedicated to my professor, Professor Yonezawa Tetsu, for giving me a chance to conduct my research under his supervision and guidance. Researching in his laboratory for six years has been my great honor. A special appreciation dedicated to my supervisor, assistant professor Dr. Ishida Yohei for his guidance and advice throughout the whole period of my research. Thanks to the deep discussion with him on my research, I have grown a lot. I would also like to express my gratitude towards assistance professor Dr. Nguyen Thanh Mai, for her advice on my research during seminar meetings. She also gave me great motivation to improve my English communication skill. Great thanks are also given to associate professor Dr. Sakairi Masatoshi for his helpful advice on my research, and Mr. Tsukamoto Hiroki for his experimental assistance. I would also like to thank Prof. Okino Tatsufumi for his helps on ESI-MS measurement. I would also like to thank my comrade in PhD program, Ms. Saw Min Jia for her supports and technical discussion on my research, and other members of the laboratory for their companionship.

I would like to particularly grateful to my parents, Mr. Narita Tokuaki and Mrs. Narita Michiyo, my brother Mr. Narita Tomohiro for their understanding and long lasting support.

LIST OF JOURNAL PUBLICATIONS

1. Y. Ishida, **K. Narita**, T. Yonezawa, R. L. Whetten, "Fully Cationized Gold Clusters: Synthesis of $Au_{25}(SR^{+})_{18}$". *J. Phys. Chem. Lett.* **2016**, *7*, 3718–3722.

2. **K. Narita**, Y. Ishida, T. Yonezawa, Z. Huang, "Super Polycationic Molecular Compounds: $Au_{144}(SR^{+})_{60}$ Clusters". *J. Phys. Chem. C* **2019**, *123*, 21768−21773.

3. **K. Narita**, Y. Ishida, S. Nukui, Z. Huang, T. Yonezawa, "Surface Menshutkin S_N2 Reaction on Basic Gold Clusters Provides Novel Opportunities for the Cationization and Functionalization of Molecular Metal Clusters". *J. Phys. Chem. Lett.* **2021**, 12, 11761-11765.

4. **K. Narita**, Y. Ishida, T. Yonezawa, "Unique Kinetics of Cationic-Ligand-Exchange Reactions on $Au_{25}(SR)_9(SR^{+})_9$ Clusters". (*to be submitted*)

RELATED PUBLICATIONS

1. Y. Ishida, Y. L. Huang, T. Yonezawa, **K. Narita**, "Charge Neutralization Strategy: A Novel Synthetic Approach to Fully Cationized Thiolate−Protected $Au_{25}(SR^{+})_{18}$ Clusters with Atomic Precision". *ChemNanoMat* **2017**, *3*, 298−302.

2. Z. Huang, Y. Ishida, **K. Narita**, T. Yonezawa, Kinetics of Cationic-Ligand-Exchange Reactions in Au_{25} Nanoclusters. *J. Phys. Chem. C* **2018**, *122*, 18142−18150.

LIST OF CONFERENCES

K. Narita, Y. Ishida, T. Yonezawa, "Super Polycationic Molecular Compounds: $Au_{144}(SR^{+})_{60}$ Clusters", The 3rd A3 Foresight Symposium on Organic/Inorganic Nanohybrid Platforms for Precision Tumor Imaging and Therapy, 2019, China, Oral presentation. (**The Best Poster Award**)

K. Narita, Y. Ishida, T. Yonezawa, "Super Polycationic Molecular Compounds: $Au_{144}(SR^{+})_{60}$ Clusters", The 8th International Doctoral Symposium on Advanced Materials, 2019, Japan, Oral presentation. (**Outstanding Presentation Award**)

K. Narita, Y. Ishida, T. Yonezawa, "Cationization of Neutral Ligands on Au_{25} Cluster Surface Through Menshutkin Reaction", The 19th Annual Meeting of the Society of Nano Science and Technology, 2021, online ZOOM meeting, Oral presentation.